Effect of furnace design on atomic absorption and emission signals in spectrochemical analysis
by Stephen Richard Lawson

A thesis submitted in partial fulfillment of the requirements for the degree of . . DOCTOR OF PHILOSOPHY in CHEMISTRY
Montana State University
© Copyright by Stephen Richard Lawson (1981)

Abstract:
An examination has been made of several new furnace designs and applications for both atomic absorption and emission. Problems with current furnace designs are analyzed and experimental data from three new alternate designs are presented. These alternate furnace designs were developed specifically to increase the thermal energy available to analyte molecules before they diffused from the optical path.

A two pronged support furnace was developed in which electric current passed across both ends of an 18mm long graphite tube. The tube center, where the sample was placed, heated by thermal conduction from the ends. Thus the analyte vapor always encountered walls hotter than the surface it left as it diffused toward the furnace ends. This heating mode resulted in ten-fold improvements in lead recoveries from some chloride salts compared to the CRA-63 atomizer. The dependence of lead recoveries on interferent/analyte ratios was also established for lead in magnesium chloride solutions.

A double-walled furnace was also examined and compared to the twopronged support furnace. The heating of this furnace was spatially uniform during the atomization of lead and cobalt. Despite this, recoveries for lead and cobalt were equal or superior to those obtained with the two-pronged furnace. Recoveries for lead in ZnSO4, however, were lower in the double-walled design. Possible mechanisms for these differences are discussed.

Studies on a third design which involved switching of heating modes during atomization were initiated. A graphite furnace was held by four supports which were electrically insulated from one another. A switching circuit changed the polarity of two diagonally opposite electrical supports during the atomization cycle. This changes the electric current direction from across both furnace ends to a lengthwise flow. The switching can be varied to occur at any point in the atomization cycle. The furnace design and circuit schematic are presented.

Generation of electric discharges in a constant temperature Woodriff furnace was explored as a means of creating new emission sources. The long, hot graphite tube provides both long residence times and sufficient thermal energy to decompose and atomize even large solid samples. A d.c. arc, radio-frequency discharge and a microwave discharge were studied. The rf plasma appeared to be the most promising route. Evidence is presented which indicates that thermionic emission from the hot graphite walls aids formation and maintenance of a plasma.

EFFECT OF FURNACE DESIGN ON ATOMIC ABSORPTION AND EMISSION SIGNALS IN SPECTROCHEMICAL ANALYSIS

by

Stephen Richard Lawson

A thesis submitted in partial fulfillment
of the requirements for the degree

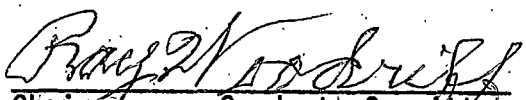
of

DOCTOR OF PHILOSOPHY

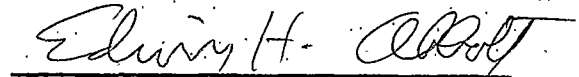
in

CHEMISTRY

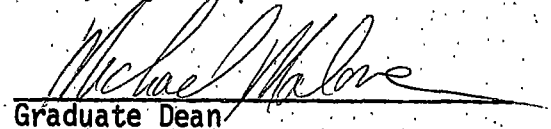
Approved:



Chairperson, Graduate Committee



Head, Major Department



Graduate Dean

MONTANA STATE UNIVERSITY
Bozeman, Montana

October, 1981

ACKNOWLEDGMENT

I wish to thank my advisor Ray Woodriff for his constant support and cookies. May a quantum mechanist find your zwitters. I also wish to thank the permanent residents of Ray's lab; Gary, Clint, Mary, Chris, Donna, Twink and Jim who entertained me during my scholastic struggles. Finally, I must thank Bridger Bowl for showing me that there is more to do during Montana winters than research.

TABLE OF CONTENTS

	Page
List of Figures	vi
List of Tables	vii
Chapter 1: Furnace Designs for Atomic Absorption Spectroscopy	1
Introduction	1
1. Parameters Influencing Atomic Absorption Analysis	1
1.1 The Temporal Characteristics of an Absorption Peak	2
1.2 Chemical Reactions	12
1.3 Length, Temperature and Pressure	24
2. Designs of Commercial Pulse-Heated Electrothermal Atomizers	28
2.1 Massmann and HGA Atomizers	28
2.2 CRA Atomizers	32
2.3 The IL-455 and IL-555 Atomizers	34
3. Alternate Designs for Pulse-Heated Electrothermal Atomizers	37
3.1 The L'vov Platform	38
3.2 Capacitive Discharge Heating	39
3.3 Combination Atomizers	41
3.4 The Fastac Autosampler	41
3.5 Forked Supports	43
3.5.1 Apparatus and Techniques	43
3.5.2 Results and Discussion	50
3.6 Double-Walled Furnace	70
3.6.1 Apparatus and Procedure	73
3.6.2 Results and Discussion	79
3.7 Dual - Pulse-Heated Furnace	100
3.7.1 Experimental	100
Conclusions	106

TABLE OF CONTENTS

	Page
Chapter 2: Multielement Atomic Absorption Spectroscopy	107
1. Introduction	107
2. Experimental	108
2.1 Apparatus	108
2.2 Procedure	110
3. Results and Discussion	111
3.1 Dual Element Analysis in Solids	111
3.1.1 Analysis of Major and Minor Constituents in Unweighed Samples	112
1. Determination of Trace Zinc In Cadmium Samples	112
2. Use of Iron in Hemoglobin as the Internal Standard in Blood	118
3.2 General Analysis	122
Chapter 3: Graphite Furnaces as Sources for Atomic Emission Spectroscopy	124
Introduction	124
1. Electrical Plasmas for Emission Spectroscopy	124
1.1 D. C. Arcs	128
1.2 Radiofrequency Plasmas	131
1.3 Microwave Plasmas	135
Experimental	135
2. Stabilization of Plasmas by Confinement in a Constant Temperature Furnace	136
2.1 D. C. Arc in a Closed Tube	137
2.2 Radiofrequency Plasma in a Constant Temperature Furnace	141
2.3 Microwave Plasma Confined in a Constant Temperature Furnace	154

LIST OF TABLES

Table		Page
1.	Characteristic Parameters for Three Pulse-Heated Commercial Atomizers	36
2.	Percent Recovery Obtained for 480 pg Pb in Three Chloride Matrices	51
3.	Percent Recovery Obtained for 480 pg Pb in Four Different Matrices	52
4.	Summary of Data for 480 pg Pb in Several Chloride Matrices	59
5.	Effect of Increasing the Amount of Pb at a Constant Interferent Level	64
6.	Effect of Constant Interferent/Analyte Ratios	65
7.	Effect of Atomizer Length on Peak Height	66
8.	Comparison of Recoveries Obtained for 480 pg Pb Measured in Three Different Furnaces	81
9.	Correlation of ΔT_d Values with Percent Recovery	89
10.	Comparison of Recoveries Obtained for 960 pg Co Measured in Three Different Furances	96
11.	Sample Results for Simultaneous Determination of Cu and Zn in Mineral Feed and NBS Orchard Leaves	113
12.	Simultaneous Determination of Zinc and Cadmium In NBS Coal Fly Ash (SRM 1633)	114
13.	Calculation of Zinc Concentration in an Unweighed Sample	119
14.	Summary of Peak Areas Obtained for Various Electrode Configurations	147

LIST OF FIGURES

Figure		Page
1.	(A) CRA-63 atomizer with center heating supports (B) 18 mm tube with two-pronged supports	45
2.	Oscilloscope traces of the temperature profiles of end-heated 18 mm atomizers heated at two different power levels	56
3.	Oscilloscope traces of the Pb absorption curves for 480 pg Pb with 2.4 µg $ZnSO_4$ and 480 pg Pb as the nitrate	58
4.	Cross-sectional views of the double-walled furnace	72
5.	Relative temperature profiles of double-walled furnace operated at 0.4K/ms	78
6.	Comparison of Pb signals with and without $FeCl_3$ present in 18 mm ordinary graphite double-walled and end-heated furnace	87
7.	Comparison of Pb signals with and without $FeCl_3$ in 18 mm pyrohytically coated graphite double-walled and end-heated furnace	92
8.	Schematic drawing of the electrical switching network used to change current direction in the dual-pulse heated furnace	103
9.	Diagram of the dual-pulse heated furnace	105
10.	Plot of peak width at fixed height versus weight of cadmium	117
11.	Plot of the weight of lead against the ratio of absorbances measured simultaneously for iron and lead in each of nine blood samples	121
12.	Top view of the d.c. arc confined in a boron nitride tube	139

LIST OF FIGURES

Figure		Page
13.	Diagram of two electrode arrangements used to couple rf power to a constant temperature graphite furnace	143
14.	Illustration of an overlapping electrode arrangement used to couple rf power to a constant temperature graphite furnace	144
15.	Plot of emission intensity versus concentration of cadmium	151
16.	Plot of emission intensity versus weight of cadmium in NBS coal fly ash	153
17.	Schematic drawing of the apparatus used to couple 2.45 GHZ microwaves to a constant temperature furnace	156

ABSTRACT

An examination has been made of several new furnace designs and applications for both atomic absorption and emission. Problems with current furnace designs are analyzed and experimental data from three new alternate designs are presented. These alternate furnace designs were developed specifically to increase the thermal energy available to analyte molecules before they diffused from the optical path.

A two pronged support furnace was developed in which electric current passed across both ends of an 18mm long graphite tube. The tube center, where the sample was placed, heated by thermal conduction from the ends. Thus the analyte vapor always encountered walls hotter than the surface it left as it diffused toward the furnace ends. This heating mode resulted in ten-fold improvements in lead recoveries from some chloride salts compared to the CRA-63 atomizer. The dependence of lead recoveries on interferent/analyte ratios was also established for lead in magnesium chloride solutions.

A double-walled furnace was also examined and compared to the two-pronged support furnace. The heating of this furnace was spatially uniform during the atomization of lead and cobalt. Despite this, recoveries for lead and cobalt were equal or superior to those obtained with the two-pronged furnace. Recoveries for lead in $ZnSO_4$, however, were lower in the double-walled design. Possible mechanisms for these differences are discussed.

Studies on a third design which involved switching of heating modes during atomization were initiated. A graphite furnace was held by four supports which were electrically insulated from one another. A switching circuit changed the polarity of two diagonally opposite electrical supports during the atomization cycle. This changes the electric current direction from across both furnace ends to a lengthwise flow. The switching can be varied to occur at any point in the atomization cycle. The furnace design and circuit schematic are presented.

Generation of electric discharges in a constant temperature Woodriff furnace was explored as a means of creating new emission sources. The long, hot graphite tube provides both long residence times and sufficient thermal energy to decompose and atomize even large solid samples. A d.c. arc, radio-frequency discharge and a microwave discharge were studied. The rf plasma appeared to be the most promising route. Evidence is presented which indicates that thermionic emission from the hot graphite walls aids formation and maintenance of a plasma.

CHAPTER I

INTRODUCTION

Furnace Designs for Atomic Absorption Spectroscopy

1. Parameters Influencing Atomic Absorption Analysis

Electrothermal atomizers for atomic absorption spectroscopy have increased considerably since their analytical use was first proposed and studied by L'vov (1) and Woodriff (2). This growth was most pronounced after the introduction of several commercial pulse-heated models in the late 1960's and early 1970's. The individual models and their characteristics will be reviewed later. The furnaces which have evolved during this time are all designed to vaporize and ultimately atomize the sample elements to be determined into a relatively small volume compared to flame techniques (3). The higher gas phase analyte concentrations and longer residence times produced by furnaces result in greater sensitivities and correspondingly lower limits of detection than is attainable with flame atomization. However, the magnitude of furnace sensitivities and the accuracy of a determination are dependent upon the chosen furnace design. This is because the rate of analyte supply into the light path must at least be equal to its rate of removal to achieve the greatest sensitivities (1). The absorbance peak area must also be independent of the sample chemistry for a given amount of analyte. These requirements are not always attained in many

present-day furnace designs (3,4). This is partially due to the needs for simplicity of operation, compactness, component reliability, minimal development and fabrication costs, etc. which commercial production requires. Thus research among several groups including ours has concentrated on alternative furnace designs during the last five years (5-11) in an attempt to meet all the above requirements.

1.1 The Temporal Characteristics of an Absorption Peak

The shape of an absorbance peak generated in any furnace is the result of two basic time constants: τ_1; the time to transfer all the analyte atoms present into the analytical volume (atomization time) and τ_2; the mean length of time spent by an atom within the light path (residence time). Both time constants are determined and altered by parameters of the atomizer design such as heating rate, furnace length, pressure, heating mode (pulsed or constant), inert gas flow, temporal and spatial temperature distribution and physico-chemical properties of the furnace material. i.e. tantalum, molybdenum, tungsten, graphite (ordinary or pyrolytic), vitreous carbon, etc. The sample matrix chemistry can also profoundly alter the atomization time (12,13). The relative importance of these parameters in the various designs available will be considered in detail later.

The accurate measurement of τ_1 and τ_2 from experimental absorption curves should be emphasized. The mathematical model

developed by L'vov (14) defines τ_1 as the time elapsed from the moment atomization begins to the point where N_t, the total number of atoms of the analyte within the analytical volume at any time, t, is a maximum. Since the model assumes that the decay of the absorbance signal is independent of the atomization process and atom loss is due to diffusion only, τ_2 can be defined from:

$$N_{t \geq \tau_1} = N_{\tau_1} \exp (\tau_1 - t)/\tau_2 \quad (1.1)$$

where, N_{τ_1}, the number of atoms in the analytical volume at the peak maximum is equal to:

$$N_{\tau_1} = 2 N_o \tau_2^2/\tau_1^2 (\tau_1/\tau_2 - 1) + \exp(-\tau_1/\tau_2) \quad (1.2)$$

Thus, from this model, the time required for the absorbance signal to increase from the first detectable absorbance to the peak maximum can be used to obtain τ_1. τ_2 can be calculated from the slope of a log A_o/A_t versus time plot. However, the assumptions of this model ($\tau_2 \geq \tau_1$) are seldom attained in pulse-heated furnaces. Only the constant temperature furnaces of L'vov and Woodriff have sufficiently long residence times to prevent loss of atoms from the analytical volume before atomization is complete. Even for these furnaces, the model does not account for diffusion complicated by carbide formation. Woodriff, et. al. (15) developed a more thorough model to account for those elements which react with the graphite walls. For such cases,

two time constants are required:

$$M_t = M_o C \exp(-t/T_a) + M_o (1-c) \exp(-t/T_b) \quad (1.3)$$

where M_t is the mass of analyte vapor at time, t, M_o is the initial weight of analyte, t is the time elapsed after the sample is vaporized, T_a and T_b are time constants which depend upon the graphite (T_2) and gas phase (T_1) diffusion time constants respectively and the equilibrium constant for analyte distribution between graphite and the gas phase. C, the concentration of analyte in the graphite walls, is a function of the equilibrium constant, K, time, wall thickness,(a), tube diameter (x), tube length (l) and Z (Z = x + a).

$$C = BK \sin((\pi Z/a)(T_2/T_a)^{\frac{1}{2}}) \sin(n\pi x/l) \exp(-t/T_a) \quad (1.4)$$

The decay portion of the absorbance curve can be accurately described by this model even when analyte - wall reactions are present. The two time constants, T_a and T_b, can thereby be obtained from this portion of the curve.

Interpretation of the absorbance curves generated from small, pulse-heated furances is more complicated. Fuller (16) used a simple two-exponential model to describe the rate of atomization and loss of copper atoms from a Perkin-Elmer HGA-70 graphite furnace:

$$\text{Absorbance (Cu)} = k_1/(k_2-k_1)\, p\, [Cu]_o (\exp(-k_1 t) - \exp(-k_2 t)) \quad (1.5)$$

where k_1 is the rate constant of atomization, k_2 is the rate constant

of atom removal and p is a temperature dependent constant which relates the measured abosrbance to the number of copper atoms in the furnace. k_1 was evaluated by plotting log absorbance against time and obtaining k_1 from the slope. Enough copper was deposited in the furance to ensure constant temperature conditions were attained well before complete atomization had occurred. k_2 was then obtained mathematically by a method of successive approximations. An important conclusion resulting from his work was that the rate of atom loss was 3-20 times the rate of atomization depending on the temperature. These measurements were conducted under standard operating conditions for the HGA-70. i.e. an internal gas flow through the furnace of argon. The forced flow removal of atoms from this furnace assures that the majority of absorbance peak shape is determined by the atomization process alone.

An excellent study by Broek and de Galan (4) confirmed the findings of Fuller on the HGA furnace and drew a similar conclusion for the Varian CRA-63 minifurnace. They developed a model to describe the time dependence of the atom population in a furnace using a convolution of a supply function S(t) and removal function R(t):

$$N(t) = \int_0^t S(t') R(t-t') dt' \qquad (1.6)$$

where N(t) is the atom number at time, t, and R(t) is the normalized response when an infinitely rapid atom pulse is supplied. The time constant of the supply function is defined as:

$$\tau_s = \int_0^\infty S(t)\, dt/S_{max} = No/S_{max} \qquad (1.7)$$

If S(t) is slow in comparison to R(t) (which was confirmed valid experimentally) then T_s can be obtained from the normalized peak area:

$$\tau_s = \frac{\int_0^t A(t)\, dt}{A_{max}} \qquad (1.8)$$

However, experimentally, one must verify that the removal function is indeed sufficiently rapid to obtain an accurate τ_s. Broek and de Galan did this by forcing a high flow (0.5 to 2.0 l/min) of inert gas through the furnace. The peak height continuously decreased as the flow rate increases but the peak shape then represents the supply function. Using silver, lead and manganese, atomizing temperatures between 1000 and 2000K and heating rates between 0.1 and 1.0K/ms, they concluded that τ_s is about 1s in both the CRA-63 and HGA-72 furnaces. They also found the supply function is determined by the furnace temperature and the activation energy and frequency factor of the dominate atom forming process on the furnace surface. This is in agreement with work by Torsi and Tessari (17-19) who used an open graphite rod and Sturgeon, et. al. (20) who used an HGA-2100 furnace. However, the supply function could not be completely modeled by a simple first order Arrhenius - type rate constant. This also agrees with the work of Torsi and Tessari (19). The experimental absorbance curves always exhibited a prolonged tailing compared to the theoretical supply functions.

Broek and de Galan suggested this effect was due to unequal absorption site energies which held the analyte in the graphite matrix until sufficient heat was applied. Gas-phase reactions such as dissociation of dimers and adsorption - redesorption along the furnace wall were considered as possible secondary atom supplies. The high flow rates through the furnaces, however, should have minimized such sources. The fact that experimental - theoretical agreement was better for all three cases (silver, lead and manganese) in the CRA-63 than the HGA-72 suggests the pyrolytic coating on the CRA-63, which reduces solution soaking into the furnace walls, is the cause of the reduced tailing observed in this furnace.

The removal function, R(t), is described by a combination of three transport processes: diffusion, expansion and convection. Approximation of the three processes by an exponential decay allows the net response function to be written as a simple exponential:

$$R(t) = N(t)/N(t_o) = N(t_o) \exp(-t/\tau_R) \qquad (1.9)$$

Experimental measurement of T_R from the absorbance curve requires $S(t) > R(t)$. Since atomization from the furnace wall was too slow for this purpose, an alternate experiment was carried out. Mercury vapor was rapidly injected into the furnace using an injection syring at varying times during the atomization cycle. The sample could thereby be introduced in less than 10 ms. The time constant, τ_s, was thus

obtained as the slope of a log absorbance as time plot. Once τ_s and its dependence on temperature and heating rate was found, comparison to mathematical descriptions of diffusive, expansive and convective time constants allowed an estimation of the relative contribution each process to the overall removal function.

The time constant for diffusion can be expressed by:

$$\tau_d = \frac{0.125L^2}{D} \qquad (1.10)$$

where L is the furance length in centimeters and D is the mass diffusivity of the analyte in cm^2/sec. For comparison, τ_d for a length of 0.9 cm (CRA-63) and D = 1.8 cm^2/sec. is equal to 56 ms while τ_d = 544 ms for a 2.8 cm furnace (HGA-72).

The time constant due to expansion of the gas phase as the furnace temperature increases during atomization can be approximated by:

$$\tau_e = T(t_o)/(dT/dt)_{to} \qquad (1.11)$$

where $T(t_o)$ and $(dT/dt)_{to}$ are the temperature and heating rate of the gas at the moment, t_o, that a particular atom is introduced. For a temperature of 1000K and a heating rate of 1K/ms, τ_e = 1s.

For larger furnaces like the HGA-72 where a constant internal flow of inert gas induces convective loss of vapor, a third time constant, τ_c, must be considered:

$$\tau_c = K\ (V/F)\ (300/T) \qquad (1.12)$$

where F is the cold gas flow rate, V is the cell volume, T is the furnace temperature and K is a proportionality factor dependent on the flow pattern through the furnace. The authors found K difficult to estimate but felt τ_c = 50-100 ms for V equal to a few cm^3, F = 1l/min and T = 1000K.

Experimentally, τ_R was between 100 and 30 ms for mercury in a CRA-63 furnace which led the authors to conclude that diffusion was the dominant removal process in this furnace.

The HGA-72 furnace operated under forced convection conditions had removal time constants between 90 and 150 ms for temperatures between 2500 and 500K respectively indicating forced convection as the dominant removal process. Although these times are longer than Broek and de Galan predicted from equation (1.10), they argue that the flow of argon through the furnace is uncertain. It enters through holes drilled in the wall so that some unknown fraction of the total measured flow flushes the furance vapors. A fraction of 0.5 would account for the difference between experiment and theory. Another possible cause is the gas-wall temperature (up to several hundred K (21)) lag created by the flowing gas. However, this has been reduced in later HGA models by introducing the gas from the furnace ends rather than the center (21).

When operating under static conditions (i.e. stop flow), the removal function of the HGA is dominated by both diffusive and

expansive time constants. At lower temperatures (i.e. 800-1300K) expansion and diffusion are fairly comparable process for atom removal although diffusion tends to be faster. However, at higher temperatures and heating rates, diffusion increases faster than expansion and removal becomes dominated by the diffusion process. The net time constant, τ_R, varied between 1.00 and 1.96 s for temperatures and heating rates between 2300K (1.25K/ms) and 800K (1.15/ms) respectively.

In the above model, no element-specific losses such as recombination in the gas phase (22), diffusion through the graphite walls (15), intercalation or carbide formation (15), and condensation at the cooler furnace ends (20,23) were considered. Since the theoretical model used overestimated the observed removal rates, this was apparently justified for the specific cases studied. The authors noted that elements were chosen which minimized such possibilities. However, in general chemical losses must be considered. Formation of carbides, and reactions with the sample matrix to form monochloride, monocyanides, sulfides, etc. can, in some cases, dominate the removal process. In addition, Sturgeon and Chakrabarti (24) were able to demonstrate that the major loss of analyte at atmospheric pressure in the HGA-2100 was diffusion to the cooled furnace ends where condensation occurred. Mercury was detected on the quartz end windows, their brass receptacles and graphite cones following atomization of mercury in the furnace.

However, if no significant revaporization occurred, this finding would not be in conflict with the model of Broek and de Galan.

1.2 Chemical Reactions

1.2.1 Influence of the Furnace Surface

The chemistry of both the furnace and the sample matrix can have a strong influence on the recorded absorbance trace. In fact, either the furnace itself or more commonly, the furnace surface is sometimes altered to reduce matrix interferences. The range of possible materials which are suitable for electrothermal atomizers is fairly limited. Those with sufficiently high melting points and chemical inertness include metal oxides, metals and some allotropes of carbon.

Several metal oxides have been studied in our laboratory because of an interest in using furnaces which were stable toward oxidizing, inert and reducing atmospheres in connection with MHD (magnetohydrodynamics) potassium vapor pressure studies in a constant temperature furnace (24). Beryllium oxide is a good ceramic but is unstable in the presence of water vapor above 1500K (25) and too toxic to be considered. Thorium oxide, although the highest melting of the ceramic oxides (3600K) (26) and very inert to metals at high temperatures, is radioactive and expensive and therefore not practical. Zirconium oxide tubes cracked when heated due to inadequate resistance to thermal stress (24).

Metals were more useful than ceramics as choices for furnace materials. A platinum - rhodium alloy (10% Rh) was very useful for the

MHD work since temperatures above 2069 K were not required. The addition of rhodium increases the hardness and doubles the electrical resistivity of the furnace tube (27). It is sufficiently inert toward oxidizing atmospheres to be run in air and water vapor at elevated constant temperatures. Unfortunately, the limited temperature range and high cost limit its use outside special applications.

Tungsten has the highest melting point (3710K) of all metals and a low thermal coefficient of expansion (26). It is useful for the determination of high boiling, carbide-forming metals. However, its high electrical conductivity, poor machinability and low stability to oxidizing atmospheres limit its use. Tungsten tubes can be run in a hydrogen atmosphere but tend to become brittle with age.

Tantalum (M.P. 3296K) and molybdenum (M.P. 2917K) (26) have been the metals most frequently used as atomizers. Both should be operated in reducing atmospheres. Thus, except for the tantalum strip (28), the majority of work utilizing these metals has been as linings or coatings inside graphite furnaces. L'vov used tantalum foil to line a graphite furnace to prevent diffusion through the walls (3). Fuller found that the rate of copper atomization in a tantalum lined furnace was greater than atomization from a graphite furnace (16). He concluded that the rate-determining step, reduction of copper oxide, was more rapid using tantalum due to the greater free energy change. Henn

(29) decreased interferences on selenium in industrial effluent samples by adding a molybdenum solution to an HGA-2100 furnace. Apparently molybdenum binds to the selenium which allows ashing up to 1700^{o}K without loss of analyte. Hodges (30) used orthophosphoric acid as a matrix modifier to prevent interferences on lead in urine samples. However, excessive molecular background resulted from this treatment. Alkali metal chlorides were converted to the corresponding phosphates which lead to the molecular absorption during atomization. He discovered that a molybdenum coating (or more likely Mo_2C) on a graphite furnace significantly reduced this background by the Mo or Mo_2C catalyzed reduction of alkali metal phosphates to phosphides which absorb in the far UV. Zatka (31) soaked HGA-74 furnaces in a 6% tantalum solution to form a uniform layer of TaC (MP 4270K) (26) over the entire furnace. The purpose was to increase the overall inertness of the furnace to oxidative attack. He concluded that, except for carbide formation, possible interferences remained the same as those encountered in untreated graphite furnaces. Stiefel, et. al. (32) coated an HGA-72 furnace with a ZrC layer to obtain increases in sensitivity for beryllium determinations in digested biological tissue. The ZrC layer probably inhibits the formation of Be_2C since greater signal enhancement were obtained for beryllium in aqueous extracts than for benzene solutions. Apparently carbonaceous residues remaining after the dry

and ash cycles of benzene solutions resulted in beryllium carbide formation. Lanthanum solutions were used to coat furnaces for lead analyses in non-saline waters (33) and fertilizers (34). Thompson, et. al. suggested that the LaC_2 surface may cause a shift in the appearance temperature of lead. Such a shift can decrease the temporal overlap between analyte and interfering salts thereby increasing recovery (35). Sturgeon et. al. (20), concluded that atomic lead is formed by reduction of the oxide to the metal by graphite then subsequent vaporization into the gas phase. However, in the absence of reducing agents, $PbO_{(s)}$ sublimes to $PbO_{(g)}$ (36) which lends support to the above hypothesis.

All of the furnace materials and coatings mentioned thus far suffer from a reduced range of general application compared to furnaces coated with pyrolytic graphite. While a metal carbide layer may reduce formation of analyte carbides, the furnace is no longer useful for the determination of the element used for the coating or any other elements which may be present as trace impurities in the coat. Pyrolytic graphite layers are easily grown on a graphite surface by the pyrolysis of methane in argon at $\sim$ 1400 K (37). Sturgeon and Chakrabarti (38) have presented a thorough review of the properties of graphite and pyrolytic graphite. It should be stressed here, however, that pyrolytic graphite provides the impermeability and inertness to carbide

formation and oxidation for which metal carbides have been used buy without the disadvantages. For those situations where the carbide layer was used to modify the sample matrix to prevent interferences, we argue that a correct furnace design using pyrolytic graphite would obviate such a need. By a correct design we are referring to atomization into an isothermal environment, sufficiently high temperatures for complete atomization and long residence times (i.e. $\tau_2 \geq \tau_1$).

Vitreous (or glassy) carbon is also a possible material for furnaces. It has graphite - like sheets in layers with some SP^3 bonding between layers and an overall more amorphous structure than graphite (39). This results in a 3-8 times greater electrical resistance than graphite but it is also 6-7 harder (40). It has about the same gas permeability as hard glass. Although inert to oxidation and most carbide forming metals, it is readily attacked by alkali metals (41). However, it can be heated in air up to 900 K without weight loss (24). Studies in this lab on 15 cm long furnace tubes in a constant temperature furnace found vitreous carbon tubes had a lifetime twice that of a pyrolytically coated graphite tube at 2300K (24). Thus vitreous carbon appears to be the superior furnace material. Unfortunately, it is expensive, difficult to machine due to its hardness (W_2C or diamond drills) and has a slightly higher coefficient of thermal expansion than graphite. Cups of vitreous carbon shattered when rapidly heated in a

CRA-63 atomizer. The spring tension on the supports required to maintain good electrical contact was too large for the cup during heating. In general, pyrolytic graphite is equally effective at a lower cost and can be produced in the lab for any shape part with simple apparatus.

1.2.2 Analyte - Matrix Interactions

Ideally, variations in the chemical composition among different samples will have no effect on the integrated absorbance measured for a given amount of analyte and therefore aqueous solutions of simple metal salts can be used to calibrate the AA system. However, as most AA users have discovered, this is often not the case. In fact, in many commercial labs, results are not considered reliable unless the method of standard additions has been applied. Considering the number of matrix interferences reported in the literature such an approach is certainly reasonable. However, caution is advised when using this method since studies conducted in this lab on the Pb-$MgCl_2$ system demonstrated that the degree of signal supression can be dependent on the matrix/analyte ratio (7). Lead recoveries obtained for $MgCl_2$/Pb ratios less than 2000 varied substantially with increasing amounts of lead. Obviously, standard additions would not be useful in this situation, but at ratios of 2500 to 10,000, lead recoveries are constant for a fixed amount of magnesium chloride (Table 5).

The sample matrix can affect the atomization process in three

ways: (1) A change in the appearance temperature of the analyte. This can be due to a change in the chemical form in which the analyte is bound on the furnace surface relative to the calibration standard. The change in temperature therefore reflects a change in the activation energy, Ea, of the atomization process (20). The earlier appearance temperature can also be caused by the "carrier distillation effect" often observed and utilized in emission spectroscopy (42, 43). In this case, all or part of the matrix carries the analyte into the gas phase as it volatilizes. Entry of analyte into the gas phase at lower temperatures can result in loss of analyte in molecular form due to insufficient temperatures for atomization. (2) Higher or lower appearance temperatures can also result in increased or decreased atomization rates. Changes in atomization rates can also be due to a change in the rate determining step of atomization or a shift in the equilibrium involved in the atomization process. (3) The matrix can bond to the analyte on the atomizer surface or in the gas phase. Analyte thereby leaves the optical path in molecular form causing an absorbance decrease. The most widely reported interferences of this type are due to the formation of metal monochlorides (44,45), monocyanides (46), and sulfides (47).

Matrix interferences can be suppressed by two means: (1) Alteration of the analyte-matrix chemistry. This can be accomplished by a

wide variety of methods (29-36). The particular choice often being dependent on both the analyte to be determined and the chemical composition of the sample. This restrictive applicability hinders the practical utilization of multielement AAS to complex samples when such methods are employed. However, they can be effective for limited situations. The use of metal carbide or pyrolytic graphite coatings on the furnace covered in the previous section (1.2.1) is one class of pre-treatments which reduce interferences. The resulting inert layer forms a physical barrier between the analyte and the underlying graphite. Matrix-generated carbonaceous material can still form carbides but generally to a lesser degree. (2) The more widely encountered pre-treatments involve addition of reagents which change the molecular form in which the analyte is bound (29,30,48-50) and/or form a strong bond to the interfering anion (35,44,52). Reagents such as orthophosphoric acid (30,48-50) and molybdenum salts (29,48) form compounds with the analyte which are less volatile than the original form (e.g., chloride salts). A higher ashing temperature can thereby be used to volatilize the interfering matrix without loss of analyte. Chloride salts can be removed at lower ashing temperatures by adding ascorbic acid (53-55). oxalic acid (53) or hydrogen gas (51) prior to or during the ash stage. The chloride is thereby bound as HCl which is easily vaporized. This technique has been especially useful for the

determination of lead which can be lost as the volatile chloride at ashing temperatures below 900K (51). The mechanism by which ascorbic and oxalic acids reduce interferences on Pb, Mn, Cu and Co from seawater and other matrices is still uncertain. Regan and Warren (54) proposed that pyrolysis of ascorbic acid left a carbon residue which aided in the reduction of analyte oxides during the atomization step. However, Hydes (53) obtained the same improvements in Cu sensitivity using oxalic acid which does not leave a carbon residue. Although McLaren and Wheeler (55) showed that ascorbic acid changed the type of lead oxide formed when lead nitrate was pyrolyzed from red litharge to thermally unstable massicot, the mechanism does not account for sensitivity improvements obtained for other elements using this reagent. Early atomization of lead as a less stable oxide may decrease the analyte - matrix temporal overlap but loss of significant amounts of chloride as HCl gas during asking probably plays the dominate role in reducing interferences. Another effect proposed by Hydes (53) may also contribute to the observed improvements. He noticed that the surface tension of the sample drop was reduced when the ascorbic or oxalic acid was added. No visible salt crystals remained after drying although they were observable in the absence of the acids. The improved thermal contact between sample and furnace created by the finer salt crystals may accelerate decomposition of the matrix. Recent experiments

by Kahn, et. al. (10) using an autosampler on an IL555 furnace provide support for this mechanism. Interferences on lead and gold were reduced by simply aspirating a solution of the sample through a pneumatic nebulizer and spraying the resulting aerosol into the furnace which is preheated to approximately 450K. The solution dries on contact and leaves a uniform layer of very fine crystals on the graphite surface. The authors suggested that this technique prevented interferences associated with solutions soaking into the porous graphite and those caused by formation of large crystals during sample drying (52). However, the technique also reduced gas phase interferences (e.g., chloride interferences). This suggests that a change in heat transfer to the sample and/or a change in the physical contact between sample and the graphite surface caused by this uniform layer of fine crystals reduces the formation of analyte compounds during the atomization cycle. Thus the physical nature of the dried sample can also exert an influence upon the measured atomic absorbance signal. It would be interesting to compare these results with those from similar experiments run on a furnace coated with pyrolytic graphite or tantalum. This would provide a qualitative measure of the importance of surface/sample contact changes to the observed interference reductions.

The use of hydrogen in the sheath gas during ashing and atomization has been demonstrated to be an effective means of eliminating the

interference from chloride salts on lead. French and Cedergren (51) compared the magnitude of interferences on lead in steel samples dissolved in hydrochloric and nitric acids when analyzed in both the CRA-63 and HGA-72 furnaces. They found that the HGA-72, because it was constructed of ordinary graphite, produced enough hydrogen from traces of water left after the drying stage to remove all the chlorine present (as $FeCl_2$) and thus prevent an interference on lead. The CRA-63, which is constructed of pyrolytic graphite, generates five times less hydrogen during the ashing stage than the HGA-72. Insufficient amounts of chlorine were removed to prevent interferences. However, addition of hydrogen to the argon gas which shields the graphite parts from oxygen eliminated the remaining chlorine provided an ashing temperature of at least 775K was utilized. An optimum ashing temperature between 900 and 1000K was required for the HGA-72 because of the smaller amount of hydrogen present.

Strong acids remove interferences from halide salts by a mechanism similar to hydrogen (35,52). Phosphoric, sulfuric and nitric acid all helped to remove chlorine through formation and vaporization of HCl in the ashing step. However, the volatility and anion of the acid were also important. Phosphoric and sulfuric acid were more effective in eliminating interferences on lead and nickel from copper chloride than nitric acid. Phosphoric and sulfuric acid are also less volatile and

form pyrophosphates and sulfates of the interferents. Thus sufficient acid is present at elevated temperatures to react with the chloride salt. The pyrophosphate and sulfate salts have very low molecular absorbances and therefore background absorbance is also reduced.

Finally, we stress the importance of atomizer design as the means of eliminating the influence of chemical reactions on the atomic absorbance signal. Matrix-induced variations in the appearance temperature and/or atomization rate will not affect the integrated absorbance signal if the furnace tube is held at a constant temperature during the entire volatilization and atomization of the sample. A constant temperature eliminates variations in the diffusion and convection rates of atom removal during the absorption pulse. If the furnace is sufficiently long (or the sample sufficiently small) such that $\tau_2 \gg \tau_1$, then the absorbance peak will not be affected either. Gas phase interferences are eliminated by providing sufficient thermal energy and residence times to assure complete atomization before any analyte leaves the optical path. Knowledge of the furnace temperature prior to the beginning of volatilization is therefore valuable. When the above conditions have been met, the upper limit of matrix which can be tolerated may then be determined by the background absorbance level. However, to some extent, this too can be minimized using higher atomization temperatures.

1.3 Length, Temperature and Pressure

The relationship of length, temperature and pressure to peak height and peak area has been developed by L'vov (3) for a constant temperature furnace. The conditions of diffusion-controlled atom loss and $\tau_2 \gg \tau_1$ are required to prevent forced convection and slow atomization rates from dominating the absorbance peak shape. When these requirements are fulfilled, the absorbance peak height can be expressed as:

$$A_{peak} \simeq (f/AwS\,\Delta\nu_s)\,M \qquad (1.13)$$

and the peak area by:

$$A_{area} \simeq (f_2/Aw\,\Delta\nu s)\,M \qquad (1.14)$$

where f is the oscillator strength of the atomic absorption line, τ_2 is the mean residence time of an atom in the optical path, Aw is the atomic weight of the element concerned and M its mass in grams, S is the transverse cross-sectional area of the furnace and $\Delta\nu_s$ is the displacement of the frequency maximum of a line relative to its initial position as a result of a change in pressure of a foreign gas and/or temperature. For a furnace operated at atmospheric pressure (eg. the furnace design by Woodriff) the Lorentz contribution to $\Delta\nu_s$ is usually small. The measured absorbance terms can then be expressed by the following furnace parameters:

$$A_{peak} \simeq (T^{0.7}/S)\ M \qquad (1.15)$$

and,

$$A_{area} \simeq (l^2P/ST^{0.9})\ M \qquad (1.16)$$

Where the temperature dependence of $\Delta\nu_s$ and the temperature and pressure dependence of τ_2 has been inserted. Note that peak height does not depend on the furnace length (provided $\tau_1 \ll \tau_2$) but only on the cross sectional area. Thus small diameter furnaces are preferable where physical possible (i.e. factors such as light throughput must also be considered). The peak area varies directly with P and the square of the furnace length. Both terms are a result of the τ_2 dependence on these parameters:

$$\tau_2 = 10^3 l^2 P/D_o T^{1.6} \qquad (1.17)$$

where D_o is the analyte differsion coefficient at standard conditions (STP). The furnace length is therefore very important for sensitivity, especially relative sensitivity, under these conditions.

The furnace used by L'vov (1) was operated at several atmospheres pressure of argon. The line profile is then governed almost entirely by the Lorentz effect. When the pressure dependance of $\Delta\nu_s$ is added, the absorbance expressions become:

$$A_{peak} \simeq (T^{0.7}/SP)\ M \qquad (1.18)$$

and,

$$A_{area} \simeq (l^2/ST^{0.9})\ M \qquad (1.19)$$

the peak height now has an inverse dependance on pressure but the pressure dependance of peak area has been eliminated.

For pulsed atomizers, τ_2 is usually smaller than τ_1. Therefore, heating rate can have a large influence on peak height. Chakrabarti, et. al. demonstrated this influence using capacitive discharge heating of an anisotropic pyrolytic graphite tube (56). The authors expressed the temperature dependance of the rate constant for the evaporation of an analyte element into the analytical volume by an Arrhenius expression:

$$k(T) = A\exp(-\Delta H/RT) \qquad (1.20)$$

where A is a frequency factor, H is the heat of vaporization of the element, R is the gas constant and T is the temperature in degree Kelvin. This equation can also be expressed as a function of time by substituting $T_o + \alpha t$ for T where T_o is the furnace temperature immediately before the start of the atomization cycle (usually the temperature at the end of the ash cycle; 500-900K), α is the furnace heating rate in K/ms and t is the time in ms. When $\alpha t \gg T_o$, the rate constant expression becomes:

$$k(t) \simeq A\exp(-\Delta H/R\alpha t) \qquad (1.21)$$

When $\alpha t \ll T_o$:

$$k(t) = A\exp(-\Delta H/RT_o)\exp(\Delta H/RT_o^2)\alpha t \qquad (1.22)$$

In either case, k varies exponentially with the heating rate. Since extremely rapid heating rates were used (up to 60K/ms), a steady state temperature was usually reached before the first appearance of atoms in the gas phase. Therefore, assuming first order kinetics and steady state temperatures, k is inversely proportional to the atomization time τ_1. Using L'vov's (14) model for the relation between the analyte population when time $t = \tau_1$ (i.e. the absorbance maximum) and the time constants τ_1 and τ_2 under accelerated vaporization rates:

$$N_{peak} = 2N_o\tau_2^2/\tau_1^2(\tau_1/\tau_2 - 1 + \exp(-\tau_1/\tau_2)) \qquad (1.23)$$

where N_o is the total number of analyte atoms and N peak the number at $t = \tau_1$, one can see that the absorbance maximum will increase exponentially with the heating rate, α, since τ_1 decreased exponentially with k and α. It is also assumed that τ_2 remains constant with increasing α. This valid as long as a steady state temperature is reached before the first appearance of analyte atoms in the gas phase. When heating rates become sufficiently large to satisfy the condition, $\tau_2 \gg \tau_1$, then

$$N_{peak} = N_o \qquad (1.24)$$

and L'vov's model for temperature, length and pressure influences on absorbance peak height and peak area apply. Sensitivity enhancements up to 27-fold were observed using capacitive discharge heating (56).

2. Designs of Commercial Pulse - Heated Electrothermal Atomizers

2.1 Massmann and HGA Atomizers

The pulse-heated furnace originally introduced by Massmann (57) was 55 mm long, and 6.5 mm internal diameter. Electrical contact was made at both ends. The tube center, which contained the sample, heated first and remained hotter than the ends by several hundred degrees throughout the atomization cycle. The Perkin - Elmer Corp. adopted the Massmann design for commercial production and use. The first model, HGA-72, 2000, had a larger internal diameter, 8.6 mm, but a similar length, 53 mm. Removable quartz lenses fitted as windows of the furnace housing and capped both ends of the furnace tube. The furnace was therefore semienclosed with ports to allow a flow of argon or nitrogen to shield the graphite furnace parts. Part of this flow flushed the internal portion of the furance. This internal purge gas flowed from the sample port at the center to the ends and its magnitude was a fixed fraction of the total gas flow.

This design had several drawbacks. (1) The large internal diameter results in lower peak height and peak area sensitivities because of the larger cross sectional area which is inversely proportional to both methods of measuring sensitivity (44). Larger diameters are also more difficult to fully illuminate with the light source which can decrease the integrated absorbance more than the peak maximum. (2)

Large gas-wall temperature differences have been observed for this furnace (up to several hundred degrees) (58,59) and the later HGA-2100 model (60). This was the result of both the large internal diameter of the furnace (which was decreased to 6 mm in the HGA-2100) and the internal purge gas. Broek, et. al. (21) concluded that in the absence of internal gas flow (stopped-flow conditions) this temperature difference was at most 100K. They also concluded that preheating the gas before entering the furnace would also significantly reduce this problem. (3) L'vov (44) compared theoretical estimates of sensitivities for the HGA-2100 to experimental values measured by Sturgeon, et. al. (60). He found good agreement only for elements of low volatility (Cd, Sn and Zn). The sensitivities obtained for Cu, Mo and V were less than one third of the predicted values. L'vov attributed the poor correlation to the non-uniform temperature distribution along the furnace length. Findlay et. al. (61) recorded a temperature of 600K at the ends of an HGA-2000 when the center was only 1100K. Low volatility elements condense at the furnace ends where they are re-evaporated very slowly or not at all. As a result, the effective length of the furnace is decreased which decreases the residence time ($\tau_2 \propto \ell^2$). Long, broad tailing of the absorption pulse was observed for the HGA furnace which was not apparent for the uniformly heated CRA-63 (62). This drawn out tailing was difficult to fully integrate

and therefore part of the absorption pulse was left unrecorded. (4) The power applied to the furnace tube was determined by that required to maintain the final temperature. This sets an upper limit on the heating rate and therefore prevents optimization of peak absorbance sensitivity. Higher applied power increases the heating rate but also results in higher temperatures during the absorbance pulse. Consequently, the diffusivity increases and lowers the average residence time, τ_2. Sturgeon et. al. (60) found that the integrated absorbance decreased with higher atomization temperatures except for elements which were difficult to atomize (eg. Al and Cu). This can be explained by the equivalence of τ_1 and τ_2 observed for most elements under the stopped-flow conditions used by the authors. The decreases in τ_2 are more important and although peak absorbance initially increases with temperature, further increases cause a decline in both peak and integrated absorbance. However, for those elements for which $\tau_1 > \tau_2$ initially, increases in atomization temperature increase both peak and integrated absorbance. The decrease in τ_1 continually increases the gas phase atom concentration faster than lower τ_2 values can decrease it.

All of the above disadvantages have been solved with varying degrees of success over the last decade. The HGA-2200 model has been reduced in size to a 6 mm internal diameter and 28 mm length. The

internal purge gas flows from the ends toward the center at a rate independent of the external gas sheath. This substantially reduces the gas-wall temperature difference during atomization. Electronic valves have also been added to shut off the purge gas during atomization which increases τ_2 and also lowers the gas-wall temperature difference. A temperature feedback loop utilizing a photodiode has been added to allow variation of the heating rate independent of the final atomization temperature reached. The power level is automatically reduced when a predetermined temperature has been reached. The increased heating rates now available result in improved peak and integrated absorbances particularly for the more refractory metals. Some interferences are also reduced by the faster heating because the condition $\tau_2 \gg \tau_1$ is more nearly fulfilled than in earlier models. The HGA-2100 and HGA-2200 models are also pyrolytically coated to prevent carbide formation and diffusion through the walls. Slavin et. al. (63) solved the problem of non-uniform heating along the furnace length with a contoured tube. The ends of a conventional HGA-2200 tube were tapered so that they heated slightly faster than the center. This reduced the temperature difference between the center and ends from 1000K to 100K when the center temperature was 2800K. Unfortunately, up to 50% more power was required to heat the contoured tube. The center heated more slowly than in the conventional tube which resulted

in lower peak absorbances for some elements. No improvements were obtained for elements like vanadium which had produced absorbances far below theoretical in the conventional design.

2.2 CRA Atomizers

The CRA model atomizers were developed by Varian Techtron, Inc. in the early 1970's. They are the smallest tubular electrothermal atomizers in commercial use. The original CRA-61 model had an inside diameter of only 1.5 mm and a length of 4.5 mm. The small diameter was excellent for sensitivities in terms of atom density however the full potential of such a low cross sectional area was lost by the small τ_2 values resulting from the short length. Focusing of the light source also became a problem with such a small diameter. Therefore, when the length was increased to 9 mm in the CRA-63, the diameter was also widened to 3 mm. Both models were relatively open furnaces. Electrical contact was made at the tube center by two pyrolytically coated graphite support rods. The furnace itself was also constructed of pyrolytically coated graphite. The graphite parts were protected from atmospheric oxygen by a flow of nitrogen or argon moving upwards from rows of corrugated steel located directly below the furnace. This small, compact system does not suffer from the non-uniform temperature distribution and gas-wall temperature differences which plagued the earlier HGA models. The principal disadvantage of these atomizers is

the short residence times (~20 - 100 ms) compared to the relatively long atomization times (~1 sec) (4). Sturgeon et. al. (60, 62) performed a thorough comparison of the CRA-63 and HGA-2100 atomizers. The average of sensitivities obtained for three elements (Cd, Sn and Zn) in each furnace revealed the HGA-2100 produced 3.3 times larger peak absorbance values than the CRA-63 but only 0.6 times the integrated absorbance value. Both values agreed well with the theoretical estimates of L'vov: 4.0 and 0.40 respectively (44). The large difference in peak absorbances reflects the difference in τ_2 values (about a factor of 10 larger in the HGA-2100). A much smaller fraction of the total analyte atoms occupy the CRA-63 furnace at any moment compared to the HGA. However, the larger integrated absorbances in the CRA are a result of the higher atom densities created by its smaller cross sectional area.

The larger τ_1/τ_2 ratios observed in the CRA furnaces also affect the manner in which increasing atomization temperatures alter the peak and integrated absorbances. The power applied to the CRA-61 and CRA-63 furnaces was also, like the HGA-2000 and HGA-2100, determined by the required final temperature. However, unlike the HGA furnaces, increasing the final atomization temperature resulted in steadily increasing peak absorbances while the integrated absorbance remained unchanged (62). Since only 5-10% of the analyte atoms introduced are contained

in the furnace at the absorbance maximum (4), substantial increases in the heating rates would be required before the peak absorbance decreased. Apparently, the decreases in τ_2 caused by the higher temperatures offsets the increases in peak absorbance so that integrated absorbance remains unchanged. Although the effect of higher atomization temperatures is not as deleterious in the CRA's as in the HGA furnaces, peak and integrated abosrbance would increase if heating rates were independent of the final temperature.

The major changes incorporated into the latest model, the CRA-90, have been the addition of a temperature feedback control circuit and an optional hydrogen diffusion flame which is part of the sheath gas. The advantages of ashing and atomizing in the presence of hydrogen gas were covered earlier. The addition of this feature has significantly increased the amounts of chloride salts which can be tolerated in a sample without interference.

Several parameters characteristic of both the CRA and HGA furnaces are summarized in Table 1.

2.3 The IL-455 and IL-555 Atomizers

A more recent manufacturer of electrothermal atomizers for AA is Instrumentation Laboratory, Inc.. Their furnace is growing in popularity and have some features which deserve mention. Both the IL-455 and IL-555 furnaces are constructed of pyrolytically coated graphite with

dimensions of 4.5 mm inside diameter and a 38 mm length. Thus these furnaces have an average residence time greater than either the CRA or HGA furnaces and a cross sectional area intermediate between them. Theoretically, the IL furnaces should have the highest sensitivities among the three types of atomizers considered. Table 1 lists the sensitivities for five elements in each furnace. Except for cadmium, the IL has better sensitivities.

Electrical contact is made at both ends of the furnace and the center heats first as in the CRA and HGA models. However, no detailed measurements have been reported on any temperature non-uniformity or its effects. The IL-555 is equipped with a temperature feedback control circuit utilizing a tungsten resistance thermometer to decouple the heating rate from the final atomization temperature.

Two features on the IL-555 which are unique to commercial electrothermal atomizers are the Fastac auto-sampling system and a pressurized atomization chamber. The Fastac auto-sampler was mentioned briefly in section 1.2.2 and will be discussed in detail in the next section. Pressurization is achieved by enclosing the furnace in a chamber with an automatic or manually controlled access door. Pressures up to four atmospheres argon are possible. The principal advantage of pressurization is the resulting increase in residence time. Thus $\tau_2 \gg \tau_1$ may be attained although this has not been

Table 1

Characteristic Parameters for Three Pulse-Heated Commercial Atomizers

Atomizer	Inner Diam. (mm)	Length (mm)	(ms)	S^a (cm^{-2})	Q/N_2 [b] (s/cm^2)	Experimental Sensitivities [c] Cd	Cu	V	Sn	Mo
HGA-2100	6	28	200	.29	0.7	3.5E-13	2.1E-11	4.0E-10	2.9E-10	8.8E-11
CRA-63	3	9	20	.071	.28	9.5E-14	2.7E-12	3.1E-11	9.1E-12	7.5E-12
IL-555	4.75	38	361	.18	2.0	4E-13	8E-13	1/5E-11	6E-12	6E-12

a: $S = d^2/4$, where d is the furnace diameter in cm.
b: $Q/N =$ /S is the theoretical peak area sensitivity.
c: Weight in grams of element which gives a peak absorbance of 0.0044.

documented in the literature. This would eliminate interferences arising from matrix-induced changes in τ_1 and improve precision.

3. Alternate Designs for Pulse-Heated Electrothermal Atomizers

The remainder of this chapter is devoted to recent changes in pulse-heated furnaces designed specifically for the elimination of matrix-induced alterations in peak and integrated absorbances. The most difficult interference to remove has been the formation of gas-phase analyte molecules which leave the furnace volume before decomposing to atoms. This is the result of inadequate heat transfer to the analyte species during its residence in the furnace. However, this is unavoidable with the furnace designs just mentioned. When the sample is deposited on a cold furnace wall then heated at the low rates now used, (0.1 - 2.0K/ms) thermodynamically stable analyte molecules are formed and vaporized as the temperature is scanned across their volatilization range. In the case of lead in a chloride salt matrix, the time required to reach the atomization temperature is important in determining the distribution of lead among various lead compounds (45). The most recent changes in atomizer design have therefore been made to increase the heating rate, increase heat transfer rates or subject the analyte vapors to temperatures higher than the surface they left before leaving the furnace.

3.1 The L'vov Platform

L'vov, Pelieva and Sharnopolsky (64) first proposed the use of a graphite platform installed inside a furnace from which samples were vaporized rather than the furnace wall. This delayed vaporization until the furnace wall was somewhat hotter than the platform. The magnitude of this difference depended on the heating rate of the wall and the rate of heat transfer to the platform. As a means of minimizing heating due to heat conduction from the furnace walls, the platform was constructed of anisotropic pyrolytic graphite due to its low heat conductivity in the direction perpendicular to the plane of deposition. The platform was a rectangular plate 4 mm x 5 mm and 1 mm thick with sections along two opposite edges cut out to reduce contact with the walls. The platform slid into an HGA-2100 furnace which was operated in the usual manner except that longer drying times were necessary. The peak absorbances of high volatility elements were shifted to higher furnace temperatures more than low volatility elements. Peak heights were increased an average of 1.5 times when high and mid-volatility elements were vaporized from the platform whereas no increase was observed for low volatility elements. L'vov (44) explained these results as a consequence of the more rapid heating rate of the platform compared to the rate of change of the wall temperature. Since part of the platform heating is due to radiation from the walls, its heating

rate is proportional to the fourth power of the wall temperature:

$$\frac{dT_p}{dt} \propto T_w^4 - T_p^4 \qquad (2.1)$$

where T_p is the platform temperature and T_w is the wall temperature. For low volatility elements, the temperature difference between platform and wall becomes so small that the platform heating rate is that of the wall. Therefore no changes in peak height are observed

Slavin and Manning (65,55) studied the effects of the platform on matrix interferences. They modified the platform by placing a depression in the center to allow use of larger sample volumes (up to 50μl). An HGA-2200 was used to allow temperature control during the atomization stage by means of the temperature feedback circuit. Interferences on Cu, Mn, Cd, Pb and Tl from chloride, phosphate and sulfate salts were also reduced using the platform. Twenty times more NaCl could be tolerated when determining lead with the platform than without. When the temperatures of the wall and platform had equilibrated, a temperature difference between wall and platform of $\sim 150^{o}C$ was present when the wall was at $2050^{o}C$.

3.2 Capacitive Discharge Heating

L'vov also first suggested the use of a condenser bank as a large energy source to perform the initial heating of a furnace up to the final temperature (44). After that, a low output power supply could

maintain the final temperature. As mentioned earlier, Chakrabarti, et. al. have studied the effects of capacitive discharge heating on peak height sensitivity (56) and matrix interferences (67). The advantages of very high heating rates (up to 100K/ms) as a means of reducing matrix interferences are twofold. (1) The results of a high-temperature equilibrium model used by French and Cedergren(45) indicated that the time required to reach the final atomization temperature is very important for the distribution of various lead compounds. The formation of volatile lead chlorides is less probable at higher heating rates. (2) In most cases, Chakrabarti et. al. (56) were able to reach a final pre-set temperature before any atomic absorbance signal could be detected. The sample is then vaporized under constant temperature conditions which assures sufficient thermal energy to decompose analyte compounds before leaving the furnace (68). Lead was detected in a 30,000-fold excess of NaCl, 3600-fold excess of $MgCl_2$ and 1200-fold excess of $CaCl_2$ (which simulated a sea water composition) without loss of signal.

Another significant improvement observed with this technique was the absence of background absorbance at the matrix levels studied ($\sim 10\mu g$ NaCl, $1\mu g$ $MgCl_2$ and $0.4\mu g$ $CaCl_2$). Larger sample sizes can therefore be used without overloading the capabilities of the background correction system. This also indicates that vaporization occurs

at temperatures higher than possibly using ordinary heating rates (0.1-2.0K/ms) where a background absorbance of 0.6 is often observed with these salts. The capacitive discharge heating technique appears to offer a good compromise between the existing pulse-heated atomizers and the constant temperature furnaces of L'vov and Woodriff.

3.3 Combination Atomizers

This class of atomizers utilize both an electrothermal heating element and a flame. They have been in use for over a decade (69) but never caught on in popularity. A general arrangement consists of either an open graphite rod (69) or semi-enclosed cup (11) placed in a high temperature flame (eg. methane - air, air-acetylene or hydrogen-entrained air). The analytical light beam is passed through the flame slightly above the atomizer. The purpose of the flame is to normalize the residence time, temperature and chemistry of the analyte for any type of sample matrix. Thus matrix-induced shifts in the analyte appearance time and/or atomization rate will not alter the integrated absorbance signal. However, the effect of such systems on gas-phase interferences has not been studied sufficiently to determine their usefulness.

3.4 The Fastac Autosampler

The Fastac autosampler is a patented sample introduction device

developed by Instrumentation Laboratory, Inc. A solution of the sample is deposited onto the inside of the hot (~450K) graphite furnace as an aerosol which dries on contact. Although studies have not been performed which show this, but presumably a much finer and more uniform layer of sample crystals is thereby formed. There is also less seepage of the solution into porous graphite although the IL, CRA and HGA furnaces all now use non-porous pyrolytically coated graphite. The fact that this change in sample deposition could reduce matrix interferences was discovered accidently. Complete recovery of lead absorbance was obtained in 0.5% NaCl solutions using the Fastac when the absorbance previously had been 50% less using manual pipetting (10). More severe interferences, such as that of $MgCl_2$ on lead, were improved but not eliminated. 0.02% $MgCl_2$ produced about the same interference with Fastac deposition as did 0.005%/ $MgCl_2$ using manual pipetting. The authors of this study did not try to determine the mechanism of the improvements. A reasonable postulation is the greater surface contact between furnace wall and sample increases the heat transfer rate to the sample. Analyte compounds are thereby more completely decomposed before entering the gas phase. The "carrier effect" should also be a less significant factor in causing earlier appearance temperatures of some elements in chloride salt matrices. Looking for shifts to later appearance temperatures when changing from manual to Fastac deposition would therefore be a useful experiment to try.

3.5 Forked Supports

The Varian CTA-63 atomizer is the smallest (9mm length, 3 mm i.d.) among the commercial electrothermal atomizers currently available. From the viewpoint of selective volatilization, this is advantageous. However, when this is not applicable, some of the most severe matrix interferences are seen, especially for the chlorides. Due to its small internal diameter, it is difficult to utilize a L'vov platform or some modification of it. This prompted a search for an alternate modification of the Varian design which would incorporate the simplicity and effectiveness of the L'vov platform. The result is a 2-pronged support by which current passes across the ends of the atomizer tube as illustrated in Fig. 1. The emphasis of this study is on the effects of 'end' heating an atomizer and how these effects vary with increasing tube length and applied power. The interference of six different chlorides and one sulfate matrix on the AA signal of Pb is used throughout the study. Finally conclusions are drawn as to what additional modifications are required for a completely matrix interference free pulsed atomizer.

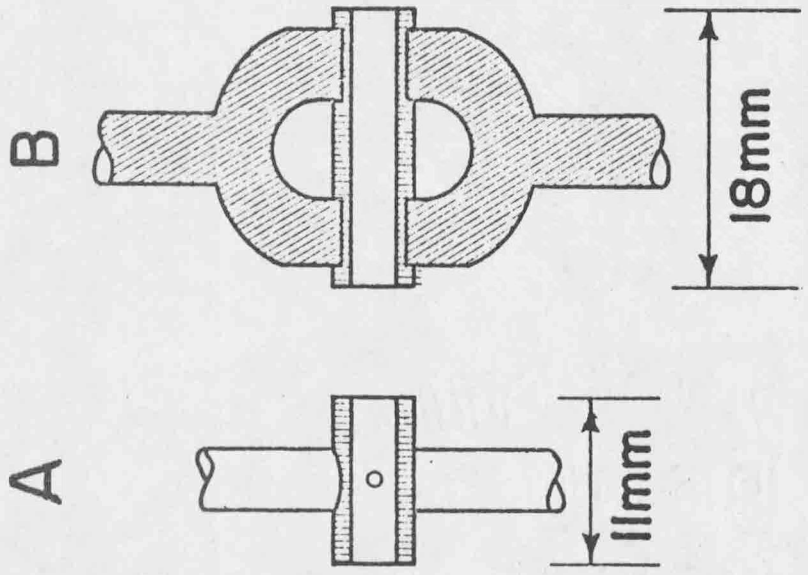
3.5.1 Apparatus and Techniques

Two Pronged Supported Atomizer.

Interference studies were performed on the Varian CRA-63 atomizer with the standard pyrolytically coated 9mm tube heated from the center

Figure 1

(A) CRA-63 atomizer with center heating supports. Furnace tube dimensions are: 9 mm length, 3 mm i.d., 5 mm o.d.
(B) 18 mm tube with two-pronged supports which pass current across each end of the atomizer for end heating. Internal dimensions are identical to the CRA-63.


B
18mm
A
11mm

using the standard supports. For comparison, an identical 9mm tube (3mm i.d., 5mm o.d) was machined from Poco (Decatur, Texas) AXF-5Q grade graphite. No significant difference in recoveries was noted with and without the pyrolytic coating. All tubes were therefore machined from the AXF-5Q graphite in the following lengths: 9 mm, 11mm, 16mm, and 18 mm. All tubes were 3mm i.d. and 5mm o.d. Each atomizer was heated from the ends by allowing the current to flow only across the ends of the tube. This was accomplished by machining 2-pronged graphite supports from 3/8" (for 9mm and 11 mm tubes) and 5/8" (for 16mm and 18mm tubes) graphite rods. Figure 1(A) illustrates the 5/8" support for the 18mm tube. 18mm is the practical upper limit for atomizer lengths which can be shielded by the inert gas sheath from below.

Power Supply

A Varian CRA-63 atomizer head and power supply was used for all measurements except those made at high power levels, where a 5 KW transformer was connected in a parallel with the Varian power supply. This allowed the dry and ash steps to still be performed with the Varian supply while the atomization was initiated with a manually thrown double pole switch connected to a high voltage (208 V) variable transformer. The variable transformer controlled the voltage on the primary windings of a step-down transformer. Up to 140 amperes

at 14V could be used to heat the larger mass of the 18mm tube with the 5/8" 2-pronged supports. This was necessary since the highest "atomize" setting on the CRA-63 power supply was insufficient to provide heating rates comparable to the 9mm and 11mm tubes operated at an atomize setting of 8.5. Significant improvements were obtained with the higher power levels.

Optics and Electronics

A Westinghouse Pb hollow-cathode lamp operated at 65ma was the light source. A dual channel monochromator constructed in this laboratory (70) was operated at the 282.3nm lead resonance line and a bandpass of 0.45nm for all measurements. The 283.3nm lead line was chosen because the background absorbance there is lower than at 217.0nm.

The detector was a IP128 photomultiplier operated at 890V. The PMT signal was fed into an Ithaco (Ithaca, NY) lock-in amplifier with a time constant set at 10 ms. This output was connected in parallel to an Onmiscribe (Austin, Texas) strip chart recorder (for peak height measurement) a logarithmic amplifier followed by a V-F converter and counter (for peak area recording) and a Tektronic 564 dual trace stage oscilloscope (to record peak shapes and positions and measure τ_1 and τ_2). The oscilloscope trace was triggered by the voltage level produced at the onset of the atomization stage. No background corrector was used. This allowed separate measurement of the background signal and

comparison of its magnitude among the various atomizer designs studied.

Temperature Measurements

The temperature of the outside surface of the atomizer was monitored with a phototransistor. The transistor output was fed to the inverting input of a 741 operational amplifier with a diode in feedback. This output was then recorded simultaneously with the absorption curves on the oscilloscope. In order to obtain separate recordings for the temperature ramps generated at the center and ends of the atomizers, the phototransistor was placed in a blackened metal tube and light from a region 3mm in diameter was focused on the transistor base through a lens. It was also necessary to use a graphite baffle placed over the top of the atomizer head when temperature measurements at the center were recorded. This prevented light from the hotter tube ends from reaching the phototransistor. A measureable temperature difference between the center and ends of an atomizer was discernable only for 16mm and 18mm tubes. Temperature ramps given for 9mm and 11 mm tubes are for the entire atomizer.

Reagents and Operating Conditions

Simple matrix solutions were prepared from analytical reagent grade interferent salts and deionized water. A 1000μg/ml lead reference standard was prepared by dissolving the metal in distilled

reagent grade nitric acid. A 200 ppb lead solution was used in the interference studies shown in Tables 2 and 3. 2.4μl aliquots, delivered from a Unimetrics variable micropipet, were used for all solutions. The micropipet was calibrated and found to consistently deliver 2.4 + 0.1μl of solution.

Solutions analyzed in the 9mm and 11mm atomizers were dried at a setting of 3.0 (dry stage) for 25 seconds and ashed at a setting of 6.0 (ash stage) for 15 seconds. Although ashing was not necessary for the synthetic solutions used, an ash step was carried out to simulate conditions often used in an ETAAS analysis. Atomization was run at a setting of 8.5 for 3 seconds which corresponded to a temperature ramp of 1.5 ^{o}K/ms. Line power to the CRA-63 supply was 115V.

Due to their higher mass, 16mm and 18mm atomizers were dried at a setting of 3.5 for 30 seconds and ashed at a setting of 6.5 for 15 seconds. Atomization using the CRA-63 power supply was carried out at a setting of 10 which corresponded to a temperature ramp of 0.23 ^{o}K/ms at both the center and ends of the tube. Atomization using the 5.0 KW transformer produced temperature ramps of 1.1 ^{o}K/ms at the center and 1.9 ^{o}K/ms at the ends using approximately 120 amperes. Higher power was tested but temperature ramps were not recorded. A flow of 10 l/min of nitrogen was used to shield the graphite parts in all measurements.

3.5.2 Results and Discussion

Changes in Peak Shape and Atomization Rate

Tables 2 and 3 list the percent recovery for a fixed amount of Pb in six chloride and one sulfate matrices. Greater recoveries were often obtained by using peak areas rather than peak heights. The largest differences (up to 20%) resulted when NaCl, $FeCl_3$, $CuCl_2$, or $CaCl_2$ were the added interferent. Observation of peak shapes on the storage oscilloscope revealed peak broadening, double peaks, and decreases in τ_1 as the cause. Iron (III) chloride produced a broadened peak while $CuCl_2$ and $CaCl_2$ gave double peaks. The double peaks persisted in all cases for $CuCl_2$; however, only a single peak was observed for $CaCl_2$ in longer (16mm and 18mm) end-heated atomizers. Similarly, a sharp peak with a reduced τ_1 (which produces an increased peak height) observed for NaCl in the 9mm CRA-63 atomizer became a slower rising peak identical to pure lead nitrate in the 16mm and 18mm end heated atomizers.

Studies of τ_1, τ_2 and appearance temperatures must be interpreted with caution since many factors are operating simultaneously. For example, the atomization time, τ_1, is shorter for Pb in the presence of any of the matrices studied that pure $Pb(NO_3)_2$ when atomization occurs in the standard CRA-63 9mm atomizer (e.g. Pb with $ZnSO_4$; τ_1 = 270ms Pb; τ_1 = 470 ms heating rate of 1.5^{o}K/ms). In contrast, when atomizing in

Table 2

Percent Recovery Obtained for 480 pg Pb in Three Chloride Matrices

	24µg NaCl	2.4µg $MgCl_2$	0.48µg $MgCl_2$	2.4µg $ZnCl_2$	0.48µg $ZnCl_2$
9mm[b] center	68 ± 6	0	5	47 ± 6	68 ± 5
9mm[b] end	69 ± 6	0	5	49 ± 6	82 ± 9
11mm[b] end	78 ± 7	4	12	56 ± 7	86 ± 8
16mm[c] end	92 ± 6	46 ± 6	73 ± 6	75 ± 6	87 ± 6
18mm[c] end	100 ± 5	48 ± 6	88 ± 7	82 ± 6	92 ± 6
18mm[d] end	102 ± 5	87 ± 6	100 ± 5	90 ± 5	103 ± 6

a: Peak area measurements.
b: Heating rate of 1.5°K/ms. 'Center' refers to current passed across center of atomizer by commercial CRA-63 supports. 'End' refers to current passed across ends of atomizer by 2-pronged supports.
c: Heating rate of 0.23°K/ms at atomizer center.
d: Heating rate of 1.1°K/ms at atomizer center.

Table 3

Percent Recovery Obtained for 480 pg Pb in Four Different Matrices

	1.41µg $FeCl_3$	2.4µg $CuCl_2$	0.48µg $CaCl_2$	2.4µg $CaCl_2$	0.48µg $CaCl_2$	2.4µg $ZnSO_4$
9mm[b] center	0	2	17 ± 5	10 ± 8	69 ± 9	27 ± 8
9mm[b] end	0	2	18 ± 5	20 ± 5	68 ± 8	80 ± 8
11mm[b] end	0	2	18 ± 5	56 ± 7	74 ± 8	75 ± 8
16mm[c] end	33 ± 8	35 ± 8	65 ± 6	65 ± 6	80 ± 6	73 ± 8
18mm[c] end	45 ± 9	42 ± 8	100 ± 5	75 ± 6	88 ± 6	71 ± 9
18mm[d] end	70 ± 8	67 ± 8	98 ± 5	113 ± 4	100 ± 4	90 ± 7

a: Peak area measurements.
b: Heating rate of 1.5°K/ms. 'Center' refers to current passed across center of atomizer by commercial CRA-63 supports. 'End' refers to current passed across ends of atomizer by 2-pronged supports.
c: Heating rate of 0.23°K/ms at atomizer center.
d: Heating rate of 1.1°K/ms at atomizer center.

the 18mm end-heated tube ($1.1^{o}K/ms$ at center) τ_1 is nearly equal for Pb with and without an interferent matrix present (e.g. Pb with $ZnSO_4$; τ_1 = 490ms Pb; τ_1 = 480ms). Since the measured heating rate is slightly lower for the 18mm atomizer, a comparison was made to the lower heating rate ($0.23^{o}K/ms$) of the same tube powered by the CRA-63 supply: Pb with $ZnSO_4$; τ_1 = 450mn, Pb; τ_1 = 480 ms.

The agreement between the τ_1 values obtained in the 18mm end-heated atomizer at two different heating rates suggests that the small changes in heating rates used in this study are not the source of the atomization time changes. Since τ_1 is constant for an element with a given set of atomization parameters (i.e. atomizer surface, heating rate and chemical environment) independent of the amount atomized (12, 60), the changes observed seem to reflect a change in the chemistry of atomization. The consistent τ_1 values for lead nitrate in all three cases indicated that heating the ends of an atomizer first affects the analyte-matrix chemistry. The details of this change are unknown and beyond the scope of this paper; however, temperature is the key factor. It may be related to the higher gas temperature above the sample. The expanding hot gas at the atomizer ends might rapidly heat the gas throughout the tube. How this would alter the atomization rate of the volatile lead chloride formed in the presence of chloride matrices is uncertain.

The Role of Matrix Properties

The nature of the chloride compound is important to consider as seen from the data in Table 2 and 3 and in previous studies (35,68,71). Several effects must be considered: (1) The atomization temperature of Pb in the presence of a particular matrix. Temperature differences between the center and the ends of the 18mm atomizer with heating rates of 1.1^{o}K/ms at the center and 1.9^{o}K/ms at the end were measured at the point where the Pb peak reached a maximum (the phototransistor responds more accurately at higher temperatures). Figure 3 illustrates the difference between lead nitrate and lead in 2.4 g $ZnSO_4$ (5000 fold excess). Table 4 lists the ΔT's for five chloride matrices in order of increasing recovery. A good correlation between ΔT and recovery was observed: recovery increased with increasing difference in temperature. This is what one would expect for a gas phase interference. Any analyte still bound in molecular form upon leaving the atomizer center must encounter a hotter region before leaving the atomizer. The higher temperature tube ends provide the necessary energy for decomposition of analyte-matrix molecules (e.g. lead chloride). This is what L'vov observed using a platform in the HGA-74 atomizer where the atomizer walls were 500^{o}K hotter than the platform when a volatile element such as Pb peaked (44). Reductions in interferences from a 10,000 fold excess of NaCl were observed.

Figure 2

Oscilloscope traces of the temperature profiles of end-heated 18 mm atomizers heated at two different power levels. The set of fast rising curves at the left represent the atomizer temperature at the ends (upper curve; 1.9^{o}K/ms and at the center (lower curve; 1.1^{o}K/ms) which is heated by conduction from the ends. The set of slow rising curves at the right represent the end temperature (upper curve; 1.23^{o}K/ms) and the center temperature (lower curve: 0.23^{o}K/ms) obtained with the highest atomizer setting on the CRA-63 power supply. A baffle was utilized for increased resolution of center and end temperature curves.

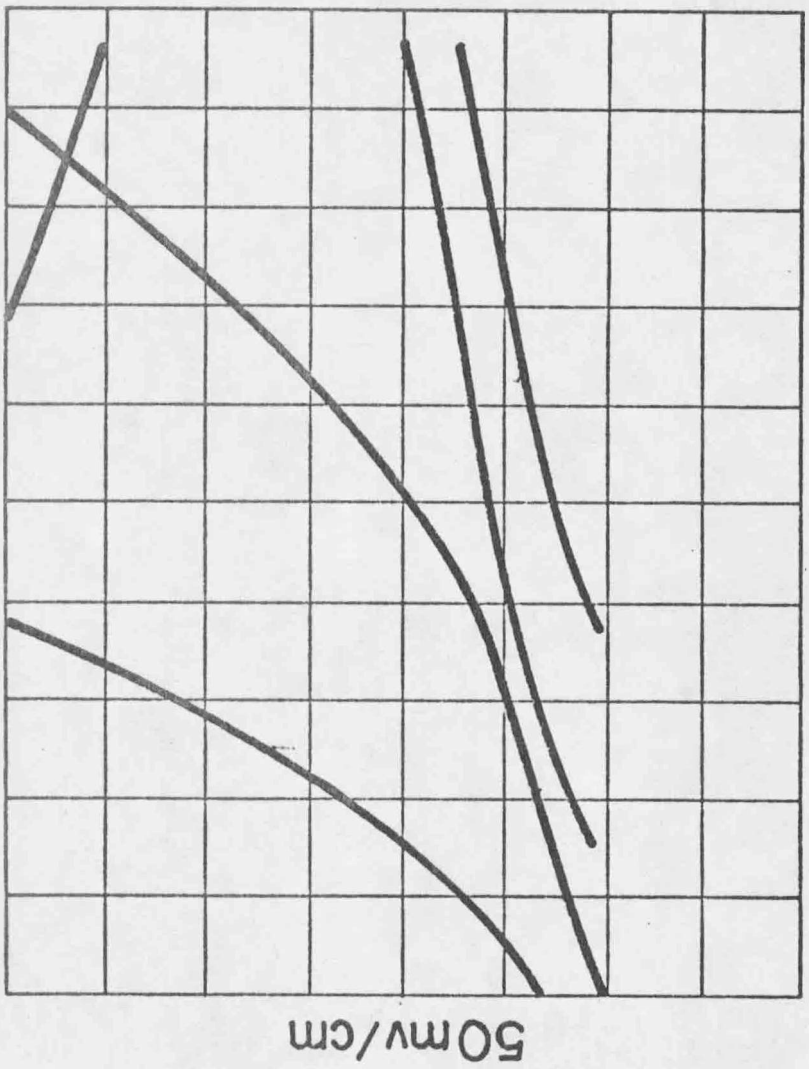

50mv/cm
200ms/cm

Figure 3

Oscilloscope traces of the Pb absorption curves for 480pg Pb with 2.4 µg $ZnSO_4$ (earlier peak at left) and 480 pg Pb as $Pb(nO_3)_2$ (later peak at right). Superimposed are the temperature curves for the center (lower curve; 1.1°K/ms) and the end (upper curve; 1.9°K/ms) of the atomizer. A baffle was not used. Note the decreased resolution of the temperature traces compared to Figure 2. The dependence of the center-end temperature difference on appearance temperature is still apparent.

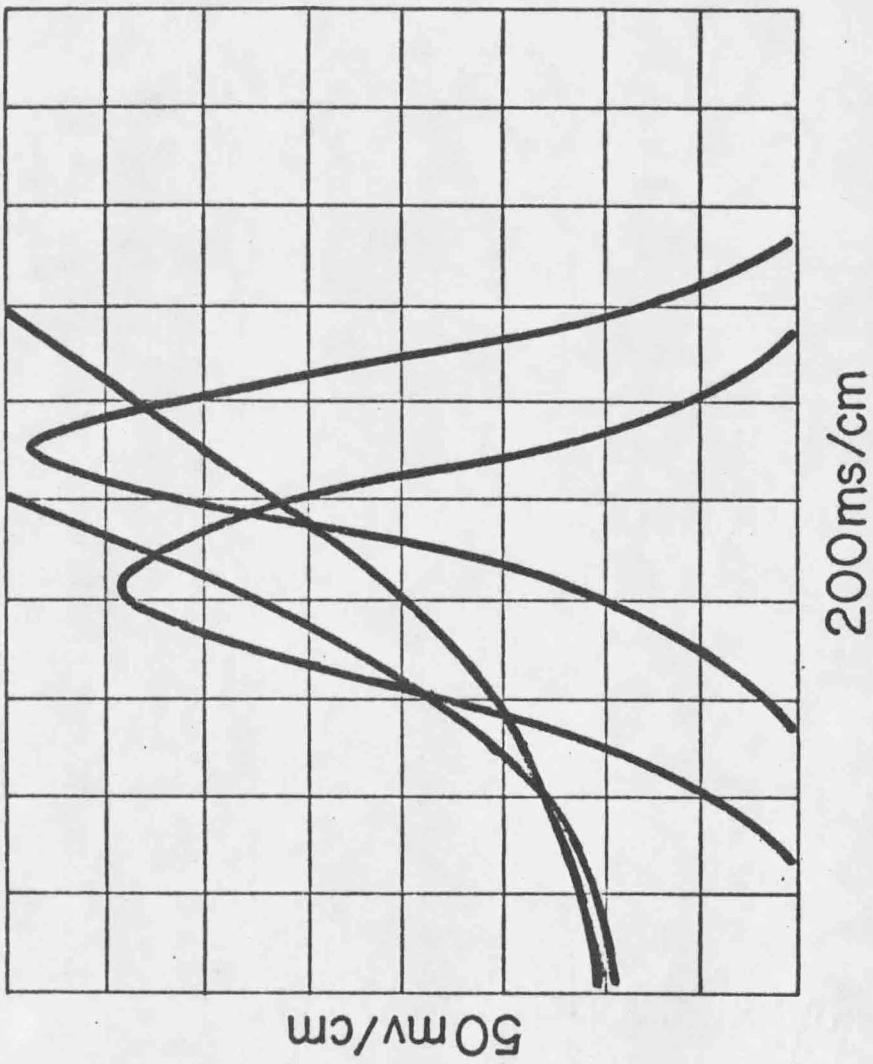

50 mv/cm
200 ms/cm

Table 4

Summary of Data for 480 pg Pb in Several Chloride Matrices

Interferent	ΔT at peak max(^{o}K)	M-Cl Dissociation energy (kcal/m)	τ_2 (ms)	Recovery (%)
1.41µg $FeCl_3$	250	83	360	70
2.4 µg $CuCl_2$	300	90 ± 3	360	67
2.4 µg $MgCl_2$	400	75 ± 3	250	87
2.4 µg $ZnCl_2$	700	53 ± 2	200	90
2.4 µg $CaCl_2$	800	94 ± 2	200	113
0.48 ng Pb	750-900	71 ± 6	200	100

a: 18mm atomizer, end-heated with 2-pronged supports at $1.1^{o}K$/ms at center; $1.9^{o}K$/ms at the ends.

(2) The bond dissociation energy of the interferent molecules and the number of interferent species produced by a given molecule (e.g. $CuCl_2$ decomposes to release two chlorine atoms) must be considered. L'vov listed dissociation energies of halides of 38 elements (44). He found good agreement between the degree of interference and the strength of the interferent M-X bond. At a given temperature, molecules with lower bond dissociation energies produce a higher concentration of chlorine atoms that those with stronger bonds. On the basis of M - Cl dissociation energies alone, the chloride matrices used in this study would be ranked in order of severity of Pb signal depression as: Zn > Mg>Fe>Cu>Ca>Na. However, on the basis of recoveries obtained in this study the actual order is: Fe>Cu>Mg>Ca>Zn>Na.

Why zinc does not produce as severe a signal depression as predicted is uncertain. It may be due to significant expulsion of the decomposition products from the furnace before Pb begins to atomize. This appears reasonable when the large difference in dissociation energies between $ZnCl_2$ (53 kcal/m) and the next highest in the series, $MgCl_2$ (75 kcal/m) is considered. Also, the small size of the CRA-63 would contribute to this separation of matrix from analyte. The small relative improvement in recovery obtained, in progressing from the 9mm CRA furnace to the high power 18mm end-heated case for lead in zinc chloride, suggests that the longer atomizers may decrease the temporal

resolution. However, a solid conclusion is hard to reach from this data alone, considering the other influences such as center-end temperature differences.

The more severe interference observed for $FeCl_3$ than predicted from its dissociation energy may be due to the greater number of chloride atoms per molecule involved. At a specified temperature $FeCl_3$ should produce a 33% greater chlorine concentration than a divalent $MgCl_2$ molecule of comparable bond dissociation energy. As seen from the recovery data in Table 3, 1.41μg of $FeCl_3$ produces an interference on lead comparable to 2.4μg $CuCl_2$ despite the small difference (7 kcal/m) in M-Cl dissociation energies.

(3) The kinetics of the atomization process and the analyte-matrix reactions should be included among the matrix influences on the atomic absorption signal of the analyte. Holcombe, et. al. demonstrated the important role kinetics could play in determining the extent of gas phase metal-oxygen reactions above a West-type filament atomizer (72). Chemical equilibrium is not always attained for slow reactions, low concentrations, and/or atomizers with short residence times. The matrix, atomizer surface and the gas and wall temperatures determine the reactions possible and the relative rates of competing reactions.

Comparison of τ_2 values of the Pb absorption profile in $FeCl_3$, $CuCl_2$, $MgCl_2$, $ZnCl_2$, and $CaCl_2$ revealed a difference in τ_2 between the

chlorides which produce the most severe interferences ($FeCl_3$ and $CuCl_2$) and those for which good recovery was obtained in the 18mm end-heated furnace ($MgCl_2$, $ZnCl_2$ and $CaCl_2$). The τ_2 data in Table 4 show an increase in τ_2 for those matrices which continue to produce low recoveries (70%) in the end-heated 18mm atomizer. Oscilloscopic traces revealed symmetrical peaks almost identical to pure lead nitrate for Pb in $MgCl_2$, $CaCl_2$, and $ZnCl_2$ (18mm tube, 1.1 K/ms at center). In contrast, Pb in $FeCl_3$ and $CuCl_2$ produced unsymmetrical peaks. In both cases, the leading edge had a smooth, fast rise similar in shape and τ_1 to lead nitrate. The tailing side of the $FeCl_3$ was longer with a shallow slope, while a double peak was apparent for $CaCl_2$. This may indicate gradual volatilization of PbCl as successive chlorine atoms are released from the interferent at the surface. For $CaCl_2$ this process is sufficiently separated in time that two distinct peaks are observed. The first peak occurs earlier than Pb alone and is probably due to the more volatile PbCl. The second peak occurs at the same time $Pb(NO_3)_2$ peaks. Thus, it is difficult to say whether this peak is due to the volatization of additional PbCl or Pb metal.

Another interesting observation is that at a heating ramp of 1.1 K/ms at the atomizer center, the first peak is slightly larger and almost no valley separates the two peaks; while, at a center heating rate of 0.23 K/ms, the first peak is much smaller and a distinct

valley is apparent. A shift in the relative importance of the two processes seems to occur with a change in the heating rates. The valley indicates the specific temperature dependence of each step which were arrived at more gradually at the lower heating rate. Further study is needed to elucidate the theromdynamic and/or kinetic controls involved.

(4) The ratio of interferent to analyte can affect the recovery obtained. This point is often overlooked and can lead to errors when the standard additions method is used. Table 5 shows the results obtained when the amount of $MgCl_2$ is held constant and the amount of Pb is varied. For 0.48μg $MgCl_2$, the recovery varies considerably with increasing Pb (ratios of 2000 to 333). However, the change is much less, although noticeable for smaller amounts of Pb, when 2.4μg $MgCl_2$ is used (ratios of 10,000 to 2500). This suggests that constant recovery should be obtained at some (lower) ratios but not at others (higher). Table 6 lists the recoveries obtained for $MgCl_2$/Pb ratios of 1000 and 5000. The recoveries at a ratio of 1000 are surprisingly constant, while considerable variations occur at a ratio of 5000. This illustrates the case where an apparent 'excess' of 1000/1 does not provide a sufficient excess of free chlorine to chemically bind a constant fraction of analyte. This ratio is insufficient for $MgCl_2$; however, it may be sufficient for other chlorides. It will depend on

Table 5

Effect of Increasing the Amount of Pb at a Constant Interferent Level

Pb (ng)	Ratio[b] $MgCl_2$/Pb	Recovery (%)	Pb (ng)	Ratio[c] $MgCl_2$/Pb	Recovery (%)
0.24	2000	58 ± 5	.24	10,000	38 ± 5
0.48	1000	74 ± 5	.48	5000	46 ± 5
0.96	500	83 ± 4	.72	3333	55 ± 6
1.44	333	92 ± 5	.96	2500	55 ± 6

a: 16mm atomizer end heated; heating rate at center 1.1°K/ms.
b: 0.48µg $MgCl_2$
c: 2.4µg $MgCl_2$

Table 6

Effect of Constant Interferent/Analyte Ratios

Pb (ng)	$MgCl_2$/Pb	Recovery (%)	Pb (ng)	$MgCl_2$/Pb	Recovery (%)
0.24	5000	30 ± 5	0.24	1000	70 ± 5
0.48	5000	47 ± 5	0.48	1000	74 ± 5
0.72	5000	46 ± 6	0.72	1000	72 ± 5
0.96	5000	50 ± 5	0.92	1000	72 ± 6

a: 16mm atomizer end heated; heating rate at center 1.1°K/ms.

Table 7

Effect of Atomizer Length on Peak Height

Length (mm)	Peak Ht. (abs. units)
9	.280 ± .014[b]
11	.371 ± .019[b]
16	.540 ± .004[c]
18	.617 ± .020[c]

a: All tubes heated with 2-pronged supports. Peak height values for 480pg Pb.
b: Heating rate of 1.5°K/ms.
c: Heating rate at center of 1.1°K/ms.

the concentration of vapor phase decomposition products present when the analyte vaporizes (which is also a function of the matrix). As observed in the case of $ZnCl_2$, a large fraction of the matrix may have decomposed by the time the analyte vaporizes but only a fraction of the chlorine generated remained in the atomizer.

An important consequence of this ratio dependence is the variation in success of the method of standard addition which might occur from one sample to another of only slightly different composition. It also demonstrates the importance of studying the effect of changing the analyte as well as the interferent amount before reaching conclusions in a matrix interference study.

Sensitivity

In addition to maintaining a greater temperature difference between the atomizer center and ends, longer atomizers also provide increased sensitivity. Table 7 shows the increase in peak height as atomizer length increases. Peak area, however, did not increase significantly for comparable heating rates in changing from a 9mm to an 18mm atomizer. This may be due to the higher heating rate at the atomizer end which causes a more rapid expansion of the gas within the furnace than would be expected from center heating rate alone.

Peak area and residence time increased for the 18mm atomizer heated at 0.23 K/ms. For the 9mm atomizers, τ_2 = 200ms which increased

to 280ms for the 18mm tubes at lower heating rates. Upon increasing the heating rate, however, it decreased to 200ms.

3.3.3 Conclusions

This study demonstrated that by heating a pulsed electrothermal atomizer at the ends and allowing the center to heat by conduction, enough thermal energy could be imparted to the vaporized sample for effective decomposition of the analyte-matrix vapor phase molecules. The data on the more severe interferents ($FeCl_3$ and $CuCl_2$) indicate that a combination of greater temperature differences and longer atomizers are needed for complete elimination of gas phase interference reactions. Studies at power levels beyond those mentioned thus far, resulted in no further increases in the signal obtained for Pb in $FeCl_3$ or $CuCl_2$. The peak area and height for lead nitrate decreased with increasing power, indicating smaller residence times. The fact that the analyte-matrix interference leveled off, instead of decreasing, indicates that the effect of increased temperature was offset by the decreased time spent in this high temperature environment. Simply increasing the residence time without higher temperature might also be sufficient.

Unfortunately there is an upper limit on the atomizer length if the center is heated by conduction from the ends. Eventually, heat is

lost more rapidly to the surrounding inert gas than can be conducted from the ends. The 18mm atomizer, for example, has a 400 K difference between center and ends after seven seconds of applied power. This limits the atomizer to low and medium volatility samples. To prevent this limitation, a power supply arrangement which utilizes both end and center heating in proportions which can be independently controlled was developed. The design is given on page 103. Adjustable electrical contacts allow the use of atomizer lengths between 25mm and 150mm. The shortest constant temperature furnace studied in this laboratory for matrix interferences was a 150mm tube which proved to be equally resistant to interferences as the longer ones (73). The increased residence time produced by a longer furnace not only allows more time for matrix-bound analyte decomposition but also provides the necessary increase in the τ_1/τ_2 ratio to prevent interferences due to matrix induced shifts in τ_1 and/or τ_2. Length also determines the sample size which can be used. Larger samples decrease sampling errors; this is of particular importance with solid sample.

Although this study has narrowed the performance gap between the commercially available pulsed-heated ET atomizers and CTF atomizers,

this lab continues to stress the advantages (including versatility of sampling) inherent to large constant temperature furnaces. The present course of research on end-heated atomizers is toward a pulse-heated furnace which is isothermal in space but not time. Comparatively, for a given length, a CTF (spatial and temporal) will provide a longer residence time and enhance sensitivity. Capacitive discharge heating may offer a useful combination of pulsed-heating and constant temperature (spatial and temporal) sampling provided the desired temperature can be reached and stabilized prior to analyte vaporization. This requirement is most difficult for low volatility elements. Chakrabarti, et. al. (56) have recently demonstrated the sensitivity enhancements obtained by this technique. The next step will be to determine its resistance to interferences. From our experience with a constant temperature furnace (68), matrix independent signals will be obtained as long as the temperature is sufficiently high.

3.6 Double-Walled Furnace

The purpose of this study was to test an alternate design for heating the ends of a graphite furnace first. The two-pronged arrangement was limited to medium and high volatility elements because the center was only heated by end conduction. At higher temperatures, the rate of heat loss from the center by radiation and conduction to the flowing inert gas sheath became competitive with the heat input by

conduction through the graphite walls. The center lagged behind the ends by 700 K when the ends were at 2500 K. A more direct source of heat input to the center was needed.

The two-pronged supports were also less convenient to install on the CRA-63 atomizer head than the standard supports because one of the support holders had to be removed. This necessitates partially dismaneling the atomizer. Good electrical contact between the furnace and supports requires rotating the furnace tube by hand while pressure is applied from the forked holders. This procedure grinds off any irregularities on the graphite which would allow space for arcing to occur. Once operational, this system has a lifetime equal to the CRA-63 furnace and requires adjustment to maintain good electrical contact about once in every 15-20 firings. The recoveries for lead in several chloride matrices were far superior to those obtained with the CRA-63 (7).

A double-walled furnace in which electrical current can cross only at the edges of an outer sleeve (see Figure 4) has been constructed and characterized. The above mechanical problems encountered with the two-pronged supports were overcome with this design; however, both higher and lower recoveries were obtained among the matrices studied. The standard CRA supports are used, therefore no changes in operating procedures are required other than slightly higher voltage settings for a

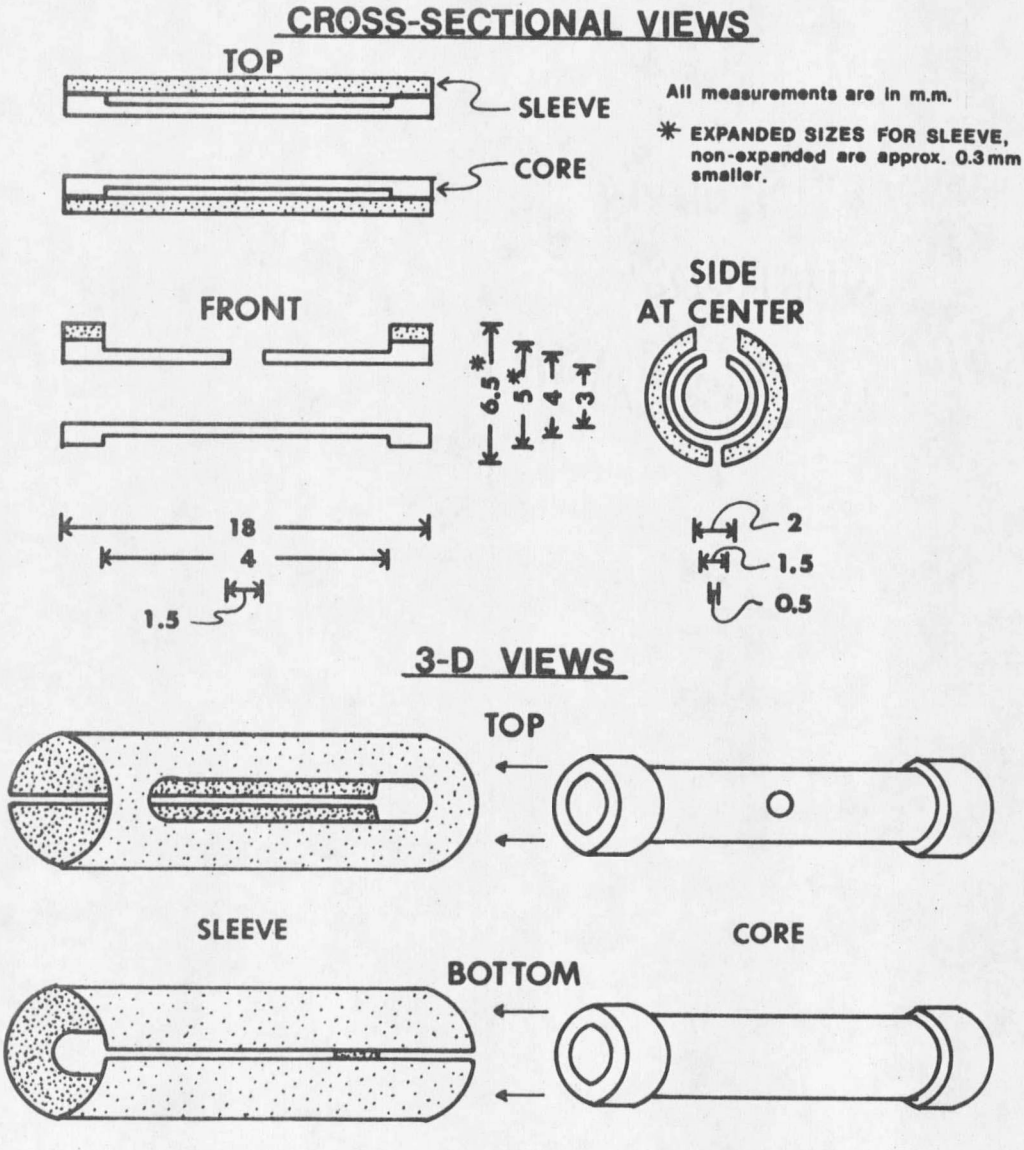


Figure 4

Cross-sectional views of double-walled furnace

given temperature due to the increased mass and resistance. It is much closer to a spatially constant temperature furnace. The furnace center and ends attain the same temperature within 200-500ms depending on the applied power. Studies were conducted on Co as well as Pb in the presence of NaCl, $MgCl_2$, $CaCl_2$, $CuCl_2$, $FeCl_3$, $ZnCl_2$ and $ZnSO_4$. Recoveries obtained for the CRA-63 and both design modifications are presented and compared. We have found the most informative approach to characterizing the double-walled furnace to be a comparison between furnaces. Primarily, the end-heated and double-walled furnaces are extensively compared in the following discussion. We have therefore included any data on the end-heated furnace necessary for this discussion.

3.6.1 Apparatus and Procedure

Double-Wall Furnace

Interference studies were performed on the Varian CRA-63 atomizer with the standard pyrolytically coated 9mm tube heated from the center using the standard supports. For comparison, an identical 9mm tube (3mm i.d., 5mm o.d.) was machined from Poco (Decatur, Texas) AXF-5Q grade graphite. No difference in recoveries was noted with and without the pyrolytic coating. Eleven mm and 18mm furnaces were therefore machined from the AXF-5Q graphite. Details of the 18mm double-wall furnace are provided in Figure 4. The resistance of the double-walled furnace (0.14Ω) was greater than both the end-heated (0.10Ω) and CRA

(0.07Ω) furnaces due to the pressure contact between the tube and outer sleeve. This region did not, however, cause any problems with arcing.

A light baffle containing a 1.5 mm diameter hole was used in all measurements to prevent excessive amounts of furnace light from reaching the photomultiplier. Another baffle (4mm diameter hole) was placed on the opposite side of the atomizer head. This formed a box around the furnace which significantly reduced the amount of oxidation experienced by the ends of the longer 18mm furnaces.

Power Supply

A Varian CRA-63 power supply was used for all recovery measurements on lead. A 5KW transformer was connected in parallel with the CRA power supply for Co recovery measurements and to test the effect of rapid heating rates on Pb recoveries. The parallel connection allowed the dry and ash steps to still be performed with the CRA supply while the atomization was initiated with a manually thrown double pole switch connected to a high voltage (208 V) variable transformer. The variable transformer controlled the voltage on the primary windings of the 5KW step-down transformer. Atomization voltages up to 18 V and maximum currents of 180 and 130 amperes were recorded on the end-heated and double-walled furnaces respectively.

Optics and Electronics

The light source was a Westinghouse lead hollow-cathode lamp operated at 6 ma. A dual channel monochromator constructed in this laboratory was operated at the 283.3 nm lead resonance line and a bandpass of 0.45 nm for all lead measurements. The cobalt 240.7 nm line at a bandpass of 0.45 nm was used for all cobalt measurements.

The detector was a Hamamatsu R212 photomultiplier operated at 890 V. The PMT signal was fed into an Ithaco (Ithaca, New York) lock-in amplifier with a time constant of 10 ms. This output was connected in parallel to an Omniscribe (Austin, Texas) strip chart recorder (for peak height measurements), a logarithmic amplifier followed by a V-F converter and counter (for peak area recording) and a Tektronic 564 dual trace storage oscilloscope (to record peak shapes and measure τ_1 and τ_2). The oscilloscope trace was triggered by the power supply voltage level produced at the onset of the atomization stage. No background corrector was used. This allowed separate measurements of the background absorbance and peak shape so a comparison among the various atomizer designs could be studied.

Temperature Measurements

The temperature of the inner surface of the atomizer was monitored with a phototransistor. Measurements at the furnace center was made by focusing through the sample port. Temperatures at the furnace ends

were measured over an equal area of the inside wall. Details of the electronics and focusing optics have been described in an earlier paper (7). The pyrometer system was calibrated by focusing on the tungsten filament of a General Electric ribbon filament pyrometer (#431-P-732) calibrated between 1300° and 2100°C at 0.664 microns. Additional measurements below 1300° were obtained from optical pyrometer (Leeds & Northrup, #1858692, Philadelphia) readings on the tungsten filament. The temperature vs. voltage plot obtained by this procedure was useful for heating rates and center-end temperature differences in a furnace. Absolute temperatures had a greater uncertainty and were not required for the information sought. The voltage traces produced by the photo-transitor in Figure 5 and therefore labelled as relative temperature curves. The important information was the difference between the two traces over time. Dry and ash temperatures were measured with a Chromel-Alumel (type K) thermocouple.

Reagents and Operating Conditions

Standard matrix solutions were prepared from reagent grade salts and doubly distilled water. The 1000 μg/ml lead and cobalt reference standards were prepared by dissolving the metal in distilled reagent grade nitric acid. 2.4 μl aliquots of either a 200 ng/ml lead solution or a 400 ng/ml cobalt solution were used for all measurements.

Solutions were dried for 30 sec at 420 K and ashed for 15 sec at

Figure 5

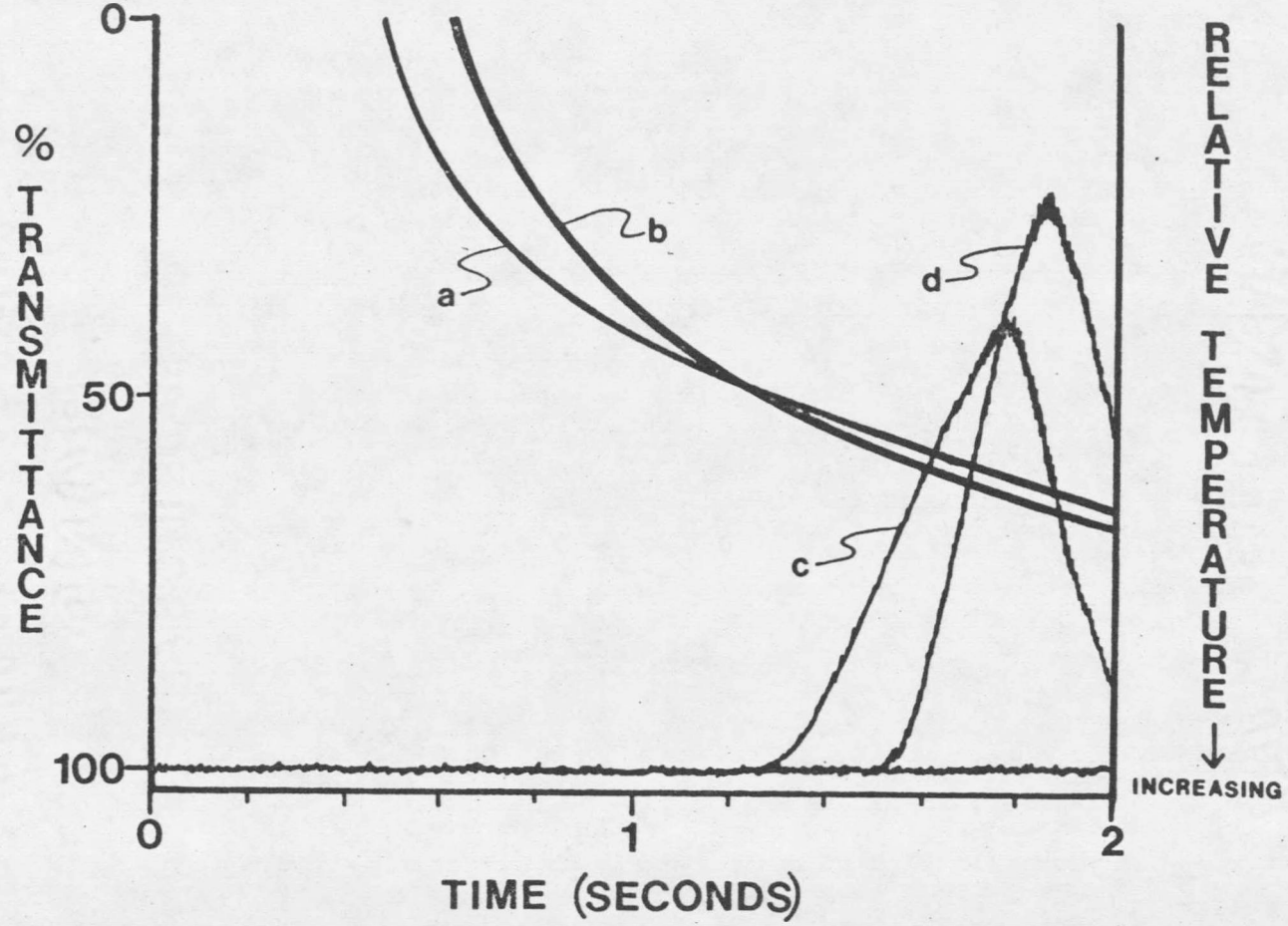
Relative temperature profiles of double-walled furnace operated at 0.4K/ms.

(a) output of pyrometer focused on the inside wall at one end of the furnace.

(b) output of pyrometer focused through sample port.

(c) 480 pg Pb + 0.48 μg $ZnCl_2$

(d) 480 pg Pb


0
50
100
% TRANSMITTANCE
a
b
c
d
0
1
2
TIME (SECONDS)
RELATIVE TEMPERATURE →
INCREASING

680 K.

3.6.2 Results and Discussion

The spatial temperature distribution throughout the double-walled furnace was far more uniform than observed with the two-pronged support configuration. The temperature curves in Figure 5 illustrate the small (~450 K) temperature difference between the furnace center and the ends 600 ms after power was applied (0.4 K/ms). This difference did not appreciably increase at an applied power of 2.4 KW (1.7 K/ms). In either case, the furnace becomes spatially isothermal before a volatile element such as lead enters the light path.

The center 14mm of the 18mm inner tube is heated primarily by radiation from the outside sleeve. This was confirmed from temperature measurements taken at several positions along this central portion. A 6mm region to each side of the sample port heated with temporal and sptaial uniformity at all power levels studied. The mode of heating of this sample-containing central portion resembles that of a L'vov Platform. However, upon leaving the atomizer surface, atoms encounter a region which is isothermal with the surface it left rather than hotter. Despite the absence of a higher temperature region through which atoms must diffuse before leaving the optical path, the double-walled furnace reduces chloride interferences to a slightly greater degree, in some cases, than the end-heated furnace.

The only sizeable differences in recovery between the two furnaces (see Table 8) occurred when $FeCl_3$ or $ZnSO_4$ were added to the lead nitrate. In the presence of 0.06% $FeCl_3$, 94% recovery was obtained using the double-walled furnace compared to 70% with the end-heated furnace. The best correlation which might account for this improvement was between the differences in delay times, $\Delta\tau d$ (τd is the time from onset of applied power for atomization until a signal first appears), for lead in the presence of a chloride matrix (i.e., $FeCl_3$) and lead as nitrate. τd was always smaller for lead in the presence of a chloride matrix. Atomization of 480 pg lead with 1.41 μg $FeCl_3$ (0.06%) produced a $\Delta\tau d$ = 100 ms using the double-walled furnace. In contrast, $\Delta\tau d$ = 280 ms in the end-heated furnace. The later appearance time of lead in 0.06% $FeCl_3$ observed in the double-walled furnace results in a higher appearance temperature for equal heating rates. This produces more complete dissociation of $PbCl_2$ and/or PbCl molecules. At the heating rates utilized, 1.0 K/ms, this corresponds to a 200^{o} K higher tube temperature. Although the end-heated furnace was observed to be 250 K hotter at the ends compared to the center at the moment the lead (in $FeCl_3$) signal reached a maximum (7), this was true only over a 5mm region centered about the contact area of each prong. This leaves a cooler 8mm region centered about the sample port. The sample is therefore not in a higher temperature environment for as long a time

Table 8

Comparison of Recoveries Obtained for 480 pg Pb Measured in Three Different Furnaces

	24 µg NaCl	2.4 µg $MgCl_2$	0.48 µg $MgCl_2$	2.4 µg $ZnCl_2$	0.48 µg $ZnCl_2$	1.41 µg $FeCl_3$
11 mm (double-walled)	62±5	12	78±5	54±5	88±4	14
18 mm (double-walled)	94±6	76±5	100±4	80±5	98±4	94±6
CRA-63	68±6	0	5	47±6	68±5	0
18 mm (end-heated)†	102±5	87±6	100±5	90±5	103±6	70±8

	2.4 µg $CuCl_2$	0.48 µg $CuCl_2$	2.4 µg $CaCl_2$	0.48 µg $CaCl_2$	2.4 µg $ZnSO_4$
11 mm (double-walled)	2	75±6	77±5	78±5	66±6
18 mm (double-walled)	78±6	100±4	100±4	100±3	67±5
CRA-63	2	17±5	10±8	69±9	27±8
18 mm (end-heated)†	67±8	98±5	113±4	100±4	90±7

*Peak Area Measurements

†Best recoveries obtained for end-heated furnace. 1.1°K/ms at center; 1.9°K/ms at the ends.

as is possible with the double-walled furnace. An effect of greater importance may be an increase in temporal overlap between matrix-generated free chlorine and lead vapor vaused by the shift to an earlier appearance time. Czobik and Matousek (35) reported the importance of this overlap to the severity of chloride interferences several years ago. We also obtained comparative interference data from ordinary and pyrolytic graphite furnaces which supports the importance of this overlap shift to the differences in recovery of lead in 0.06% $FeCl_3$ between the two furnaces. This will be discussed in detail later. First we must address the issue of why there are differences in ΔT_d's between the furnaces at all. Our best hypothesis is that heated gas and radiation from the hot furance ends of the end-heated furnace heat the center surface slow enough to cause significant decomposition of the $FeCl_3$ to $FeCl_2$ at 688K (26) and thereby convert much of the lead to $PbCl_2$ on the furnace surface. The more volatile $PbCl_2$ (B.P. =1250K) vaporizes earlier than Pb (B.P. = 2040K) (26). This may be the cause of the larger ΔT_d observed for this furnace compared to the double-walled furnace. From temperature measurements made during our initial work with this furnace (7), the ends are at most 150-200 K hotter than the center when the lead with 0.06% $FeCl_3$ signal first appears. Whether this is sufficiently higher is uncertain. However, this "early" heating is unlikely to occur in the double-walled

furnace since the temperature difference is smaller, rapidly disappears before any signal appears, and has a greater spatial separation between the hot ends and center than the end-heated furnace. The sample would therefore heat as rapidly as the furnace wall which, if the $2FeCl_3$ (s) + Pb (s) $\rightarrow 2FeCl_2$ (s) + $PbCl_2$ (s) reaction were kinetically limited, would restrict the formation of $PbCl_2$ on the surface. Covolatilization (42) of the lead with $FeCl_2$ would then be the predominate mechanism of the early appearance of lead in this furance. Formation of $PbCl_2$ and PbCl would occur predominately in the gas phase to an extent dependent on temporal overlap of matrix and analyte. Whether it is the earlier lead appearance temperature or formation of $PbCl_2$ before entering the gas phase which causes lower recoveries of lead in the end-heated furnace remains unknown at this time.

As we observed in our earlier study of the end-heated furnace, lead volatilized in the presence of $CuCl_2$ and $FeCl_3$ produced distorted, unsymmetrical peaks. The average residence times for lead atoms was increased from τ_2 = 200 ms for lead as nitrate to τ_2 = 360 ms for lead in $CuCl_2$ or $FeCl_3$ matrices. Here τ_2 is defined as the time required for the absorbance to fall form its peak value to a value e times smaller. This assumes $\tau_1 < \tau_2$ and that the maximum absorbance is representative of the total number of atoms introduced into the furnace. However, Broek and Galen (4) have proven this assumption to be invalid

for the CRA-63. They found the vaporization of atoms into the furnace, not their diffusive removal, dominated the observed absorption curve and concluded that only 5 to 10% of the analyte atoms introduced are contained in the furnace at the moment of maximum absorbance. Although this fraction is somewhat larger for 18mm furnaces used in this study (as evidenced by increased peak heights) the diffusive time constant for removal of atoms is still less than the supply time (450 ms vs 1 sec). Broek and Galen (4) measured the supply of analyte vapor to persist for 1 sec at heating rates up to 1.0K/ms. The diffusive removal time constant was calculated from the expression of L'vov (3) using a tube length of 1.8 cm and a diffusivity of 0.9 cm^2/sec for Pb in Ar at 1000K. Thus our use of τ_2 as measured from the tailing portion of the absorption curve was for comparative purposes only. The change observed in this value verifies that atom supply dominates the absorbance curve for this furnace. $CuCl_2$ and $FeCl_2$ apparently alter the atomization process of lead through reactions at the graphite surface. This change in signal shape was not observed for other matrices which continued to give less than full recovery (i.e. 0.1% $MgCl_2$) even in the optimized end-heated and double-walled furnaces. Since a difference in recovery between the two furnaces occurred for only one of the two chlorides ($FeCl_3$), we thought it would be informative to compare this interaction in each furnace. Figure 6 shows the differences observed for lead in 0.06% $FeCl_3$ when atomized in each

Figure 6

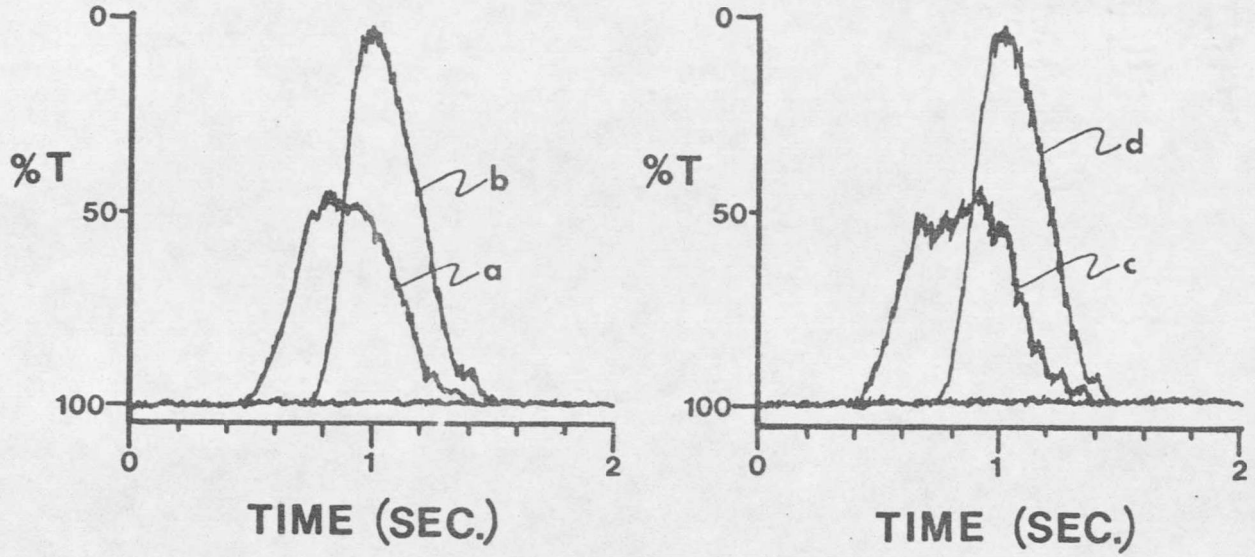
Comparison of Pb signals with and without $FeCl_3$ present in 18 mm ordinary graphite double-walled and end-heated furnaces.

(a) 480 pg Pb + 1.41 µg $FeCl_3$ in double-walled furnace

(b) 480 pg Pb as nitrate in double-walled furnace

(c) 480 pg Pb + 1.41 µg $FeCl_3$ in end-heated furnace

(d) 480 pg Pb as nitrate in end-heated furnace


0
%T
50
100
b
a
0
1
2
TIME (SEC.)
0
%T
50
100
d
c
0
1
2
TIME (SEC.)

furnace. We attributed this difference to the earlier appearance time and the more pronounced multiple vaporization and recondensation at the wall associated with an initially cooler graphite surface. To see what contribution the ordinary porous graphite made to the signals observed, we pyrolytically coated both furnaces (only the inner tube was coated on the double-walled furnace) as described by Siemer et. al. (37). The dealy time, τ_d, was decreased by 100-200 ms for lead as nitrate and in the presence of the chloride matrices in both furnaces. This is to be expected since the aqueous solutions used in this study soak into the porous layers of ordinary graphite which slightly delays the appearance of atoms in the light path. Although the shift in d was about equivalent in each furnace, a further shift toward even earlier appearances times in the end-heated furnace should cause additional decreased in recovery for lead in $FeCl_3$. As shown in Table 9, not only does this recovery decrease, but the interference from $CuCl_2$ increased by a factor of three. Pyrolytically coating the double-walled furnace, however, produces no change from either matrix. The shift in d values for this furnace were not sufficient to noticeably alter the atomization efficiency. The large increase in interference observed using $CuCl_2$ in the end-heated furance is probably due to an increased temporal

Table 9

Correlation of $\Delta\tau_d$ Values with Percent Recovery

	18 mm double-walled furnace		18 mm end-heated furnace	
	Δ_T d (ms)	% Recovery	Δ_T d (ms)	% Recovery
480 pg Pb + 1.41 µg $FeCl_3$ (graphite)	100	94	280	70
480 pg Pb + 1.41 µg $FeCl_3$ (pyrolytic coating)	240	94	320	55
480 pg Pb + 2.4 µg $CuCl_2$ (graphite)	280	78	260	67
480 pg Pb + 2.4 µg $CuCl_2$ (pyrolytic coating)	380	75	360	21

overlap between the decomposition products of $CuCl_2$ and atomic lead. The increased overlap observed between the CuCl background peak and the absorbance trace for lead in 0.1% $CuCl_2$ when switching from a graphite to a pyrolytic graphite tube supports this hypothesis.

The increase in slope on the rising side of the lead in 0.06% $FeCl_3$ peak which occurs upon changing to a pyrolytic graphite surface in the end-heated furnace (see Figure 7) indicates a large degree of condensation and reevaporation within the layers of ordinary graphite below the immediate surface. The lead vaporizes over a shorter period of time on a non-porous pyrolytic graphite surface. Multiple condensation and evaporation still occur but within a much thinner layer on the immediate surface.

Although a pyrolytic surface was not useful in terms of interference reduction, we were able to demonstrate through the above comparison that interactions on and within the furance wall do occur, but they are not the source of the differences in recovery between furnaces.

No significant differences in ΔT_d values were observed between the two furnaces for the atomization of lead in 0.1% $ZnCl_2$ and $MgCl_2$. This reflects the greater stability of these molecules relative to $FeCl_3$ which decomposes to $FeCl_2$ and Cl at 688 K. However, in the double-walled furnace, $ZnCl_2$ and $MgCl_2$ (along with $CuCl_2$) were the most troublesome chlorides studied. The combination of the relative

Figure 7

Comparison of Pb signals with and without $FeCl_3$ in 18 mm pyrolytically coated graphite double-walled and end-heated furnaces.

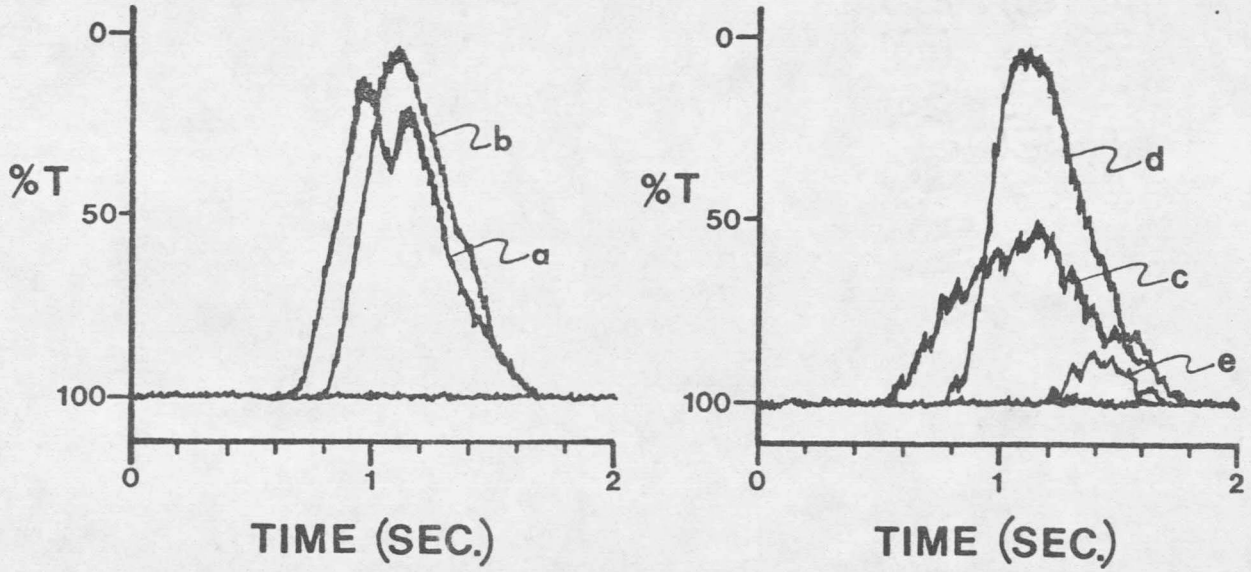
(a) 480 pg Pb + 1.41 μg $FeCl_3$ in double-walled furnace

(b) 480 pg Pb as nitrate in double-walled furnace

(c) 480 pg Pb + 1.41 μg $FeCl_3$ in end-heated furnace

(d) 480 pg Pb as nitrate in end-heated furnace

(e) 1.41 μg $FeCl_3$


0
%T
50
100
b
a
0
1
2
TIME (SEC.)
0
%T
50
100
d
c
e
0
1
2
TIME (SEC.)

degree of temporal overlap and relatively low monochloride dissociation energies, particularly $ZnCl_2$ (288 and 377 kJ/m for $ZnCl_2$ and $MgCl_2$, respectively (46), give the end-heated furnace a slight advantage (10-11% better recoveries) over the double-walled furnace. When other variables are equivalent in both furnaces, the higher temperatures at the ends (400-700 K (7)) drive the PbCl reaction further toward dissociation than can be achieved in the double-walled furnace.

A similar situation exists with the Pb-$ZnSO_4$ system. Vaporization of a solution of 200 ppb lead in 0.1% $ZnSO_4$ in the end-heated furnace yeilds a 90% recovery, while only 67% of the lead signal is recovered from the double-walled furnace. This can be attributed to the 700 K difference in temperature between the hot ends and cooler center at the moment the lead absorbance reaches a maximum. Using 1040 K as the lead appearance temperature (20), this corresponds to ~1700 K at the furnace ends when the absorbance maximizes. Hageman et. al.(68) obtained a 96% recovery in a CTF at 1900 K for lead in 1% Na_2SO_4. This indicates that higher temperatures should remove the remaining interference. Longer residence times probably are not required. French et. al. (74) using a theoretical treatment on the Pb-Na_2SO_4 system in a HGA-74 furnace under isothermal conditions concluded that the reactions which formed PbS were rapid enough to reach equilibrium (τ_2=200-300ms). The equilibrium partial pressure of oxygen was reached at 1800 K but

not at 1500 K.

Manning and Slavin (66) recently noticed the same persistence of interference effects from sulfates, phosphates, and perchlorates using the L'vov Platform. The difference in temperature between the platform and the wall was at most 300-400 K which explains the lack of full recovery.

Achieving higher atomization temperatures is straightforward with a constant temperature furnace but can become a difficult problem in pulse-type furnaces especially with high volatility elements. Both the L'vov Platform and end-heated furnace, in their present forms, are limited in the magnitude of the sample-furnace temperature difference obtainable by their heating rates. The delay in sample heating inherent in their design realizes the required rates somewhat from those needed by Chakrabarti et. al. (67) who deposits the sample on the furnace wall then reaches a steady state temperature of 2570 K before a lead signal appears. Heating rates up to 63 K/ms were studied, but 14 K/ms eliminated the interference of 2.5 μg $MgCl_2$ on 1.0 ng Pb.

In contrast to the end-heated furnace, recoveries in the double-walled furnace did not improve with an increased heating rate over the range of rates available: 0.4-1.8 K/ms. This is because of the nearly isothermal condition developed over the length of the furnace. Thus, heating rates closer to those used in the capacitive discharge techniques may be required to eliminate some matrix interferences. In order

to do this, the outer sleeve on the double-walled furnace would have to be increased from the 0.5mm thickness currently used to 1.0mm to withstand the additional stress from faster heating. At rates of 1.0 to 1.8 K/ms, the heat and pressure exerted on this section during the atomization cycle causes it to gradually bend inward. The curvature remains after cooling and eventually becomes large enough to allow arcing between the inner and outer walls at the furnace center. The sample heats first and interferences suddenly become severe. Increasing the wall thickness to 1.0 mm increases the useful life of the sleeve from 5-6 cycles to about 20 at 1.5 K/ms. The inner tube has a life of twice this due to the additional shielding from oxygen that the outer sleeve provides.

Determination of cobalt in the presence of the same matrices as used in the lead study offers a comparative evaluation of the two furnaces at a higher analyte appearance temperature. Cobalt has an appearance temperature of 1430 K (20). As shown in Table 10, the recoveries of cobalt in 0.1% $MgCl_2$ are the same in both furnaces. The double-walled furnace becomes sufficiently hot by the time cobalt atomizes to provide comparable decomposition of the gas phase chloride. However, this furnace still produces better recoveries in a 0.06% $FeCl_3$ matrix than the end-heated furnace. This case, like that of lead, may be due to premature heating of the sample on the surface of the wall

Table 10

Comparison of Recoveries Obtained for 960 pg Co Measured in Three Different Furnaces

18 mm end-heated	CRA-63	18 mm double-walled	Inteferent
81±7	50±7	101±5	$FeCl_3$
30±8	25±7	68±5	$CuCl_2$
82±6	32±7	85±5	$MgCl_2$
100±5	88±6	100±4	$CaCl_2$

by heated gases and radiation from the hot ends. This leads to a time shift of the analyte atom population and/or increased reactions at the surface between analyte and matrix due to the more gradual heating and increased reaction time. It is interesting that the absolute magnitude of the differences in recovery are the same for both cobalt and lead. Both the average furnace temperature and the center-end temperature difference are higher when the cobalt signal appears compared to lead, but so is the Co-Cl bond dissociation energy (46). The difference in analyte-matrix temporal overlap between furnaces may be comparable in both cases and/or the premature heating decomposes $FeCl_3$ to $FeCl_2$ and forms large amounts of $PbCl_2$ or $CoCl_2$ on the surface. Both elements than vaporize predominantly as the chlorides, not all of which decomposes before leaving the light path. Relative temporal overlap between analyte and matrix would not be so important for this mechanism as with a stable molecule such as $MgCl_2$. A similar difference in recoveries between furnaces for other elements in the $FeCl_3$ matrix would lend support to the formation of chlorides on the surface.

The severe interference of $CuCl_2$ on cobalt in all three furnaces (Table 10) is probably due to a large temporal overlap. However, the large difference in recovery between the end-heated and double-walled furnaces indicates a difference in the degree of overlap between furnaces and/or an increase in the formation of CoCl on the surface.

At 1263 K $CuCl_2$ decomposes to CuCl (26) giving rise to a situation similar to that observed for $FeCl_3$. This is past the appearance temperature of lead (1040 K) so the interference in that case is probably predominantly gas phase and relatively easier to correct. Almost no improvement over the CRA-63 is obtained with the end-heated furnace despite the higher temperature. Thus, the introduction of an additional interference mechanism, not previously predominant in the CRA-63 furnace, or a shift toward an increased temporal overlap, would help account for the lack of change observed with the end-heated furnace.

Difference in appearance times were difficult to observe for cobalt because the atomization rate is slower that that of lead at the heating rates used. A new furnace, described on page 100, will provide better data to either support or disprove the hypotheses presented in this paper. The furnace should combine the advantages of both the double-walled and end-heated furnaces. I hope to selectively simulate the conditions of each furnace in the same system to provide a better comparison. Finally, it should be a better pulsed furnace for AAS which approaches constant temperature conditions.

3.6.3 Conclusion

This study of a double-walled furnace demonstrated the reduction in gas phase interferences which can be obtained by simply increasing

the residence time and maintaining a spatially uniform temperature. The CRA-63 is close to a spatially isothermal furnace due to its' short length (9mm). Therefore, the large differences in recoveries between the CRA and double-walled furnaces are apparently due to kinetically limited decomposition of the gas phase chloride. Despite the possible increase in temporal overlap between matrix and analyte, increasing the path length was always advantageous in the cases studied. Heating the ends first should decrease any temperature lag of the gas within the furnace. Although this factor is considered small (50-100^{o}) in the CRA due to the small internal diameter (21), it might contribute to the gas phase reactions considered here.

Comparison of the double-walled furnace to the end-heated design also demonstrated the advantage of delaying atomization until the furnace is hotter than the appearance temperature. However, even in the absence of such a delay, use of the double-walled furnace in combination with matrix vaporization in the ash cycle and use of H_2 in the sheath gas during atomization can significantly extend the range of interference-free operation of a GFAAS system.

3.7 Dual-Pulse Heated Furnace

INTRODUCTION

A third possible means of increasing the thermal energy available to the analyte before it is diffusively lost from the furnace is illustrated in Figures 8 and 9. A graphite tube is held by four electrically isolated supports. The current can be changed from a flow across both ends of the furance to a lengthwise flow by switching the polarity of two diagonally opposite supports. This allows the furance ends to heat first, as in the two-pronged support furnace, while still providing power to directly heat the center. Two advantages are thereby gained: (1) the furnace can be made longer which gives both longer residence times and a higher temperature at the ends when the analyte vaporizes. (2) directly heating the center eliminates the limitations on heating rate and final atomization temperature at the center imposed by heating with two-pronged supports. Reductions in gas-phase interferences beyond those obtained with the two-pronged support furance and the double-walled furnace should therefore be possible.

3.7.1 Experimental

The electronic switching circuit is illustrated and described in Figure 8. Five SC 260 M triacs, rated at 25A and 600 V (Newwark Electronics, Shaumburg, Ill.), were used to control current to the furnace. The triac gates were controlled by MOC 3030 optical couples

(Newwark Electronics) rated at 250 V peak blocking voltage and 7500 V isolation voltage. They were also designed with zero-crossing detection so that the triacs were only switched on and off at the low voltage portion of the AC 120 V RMS cycle. This provides less distortion in the triac operation. Not shown in Figure 8 was an RC snubber network connected in parallel across each triac. This is necessary when switching large inductive loads (eg., transformers) to avoid false triggering after the triac gate is turned off. The values used here were R = 22Ω and C = 22 pf. The purpose of monostable C in Figure 8, which provided a 50 ms delay between switching the polarity of two of the four furnace supports, was to give additional protection against a short circuit caused by false triggering. However, as of the time of this writing, one of the two triacs controlled by monostable B does not always switch off on time to prevent a short. The system, therefore, is still under development.

The furnace is a laboratory-constructed model designed for research rather than commercial use. A wide range of furnace diameters and lengths can be accommodated for study in order to find an optimum design. Internal diameters between 3 and 8 mm and lengths from 20 to 100 mm can be used. However, I anticipate that the concept of dual-pulse heating will be adapted to commercial instrumentation because of the relatively simple alteration in power supply design required.

Figure 8

Schematic drawing of the electrical switching network used to change current direction in the dual-pulse heated furnace. Components A - D are 555 monostable oscillators used to time the duration and sequence of each triac 'on' time. Monostables A and B are triggered by a negative pulse from a toggle switch. A, which controls power to the transformer at the top of the drawing, remains on throughout the entire atomization cycle. B controls two of the four triacs at the center of the diagram which supply power to the lower transformer. After a preset time period, B switches off which turns on monostable C. B and C (also C and D) are AC coupled but this is not shown for clarity. C is on for a fixed 50 ms period. This provides a time delay of several AC cycles before monostable D turns on the two crossed triacs. This changes the polarity of two of the four electrical furnace contacts as indicated by the sign changes in parenthesis next to opposite sides of the furnace. Component E is a MOC 3030 optical coupler with zero-crossing switching. Each one shown is connected to - VDC but this was omitted for clarity as were all power supply connections.

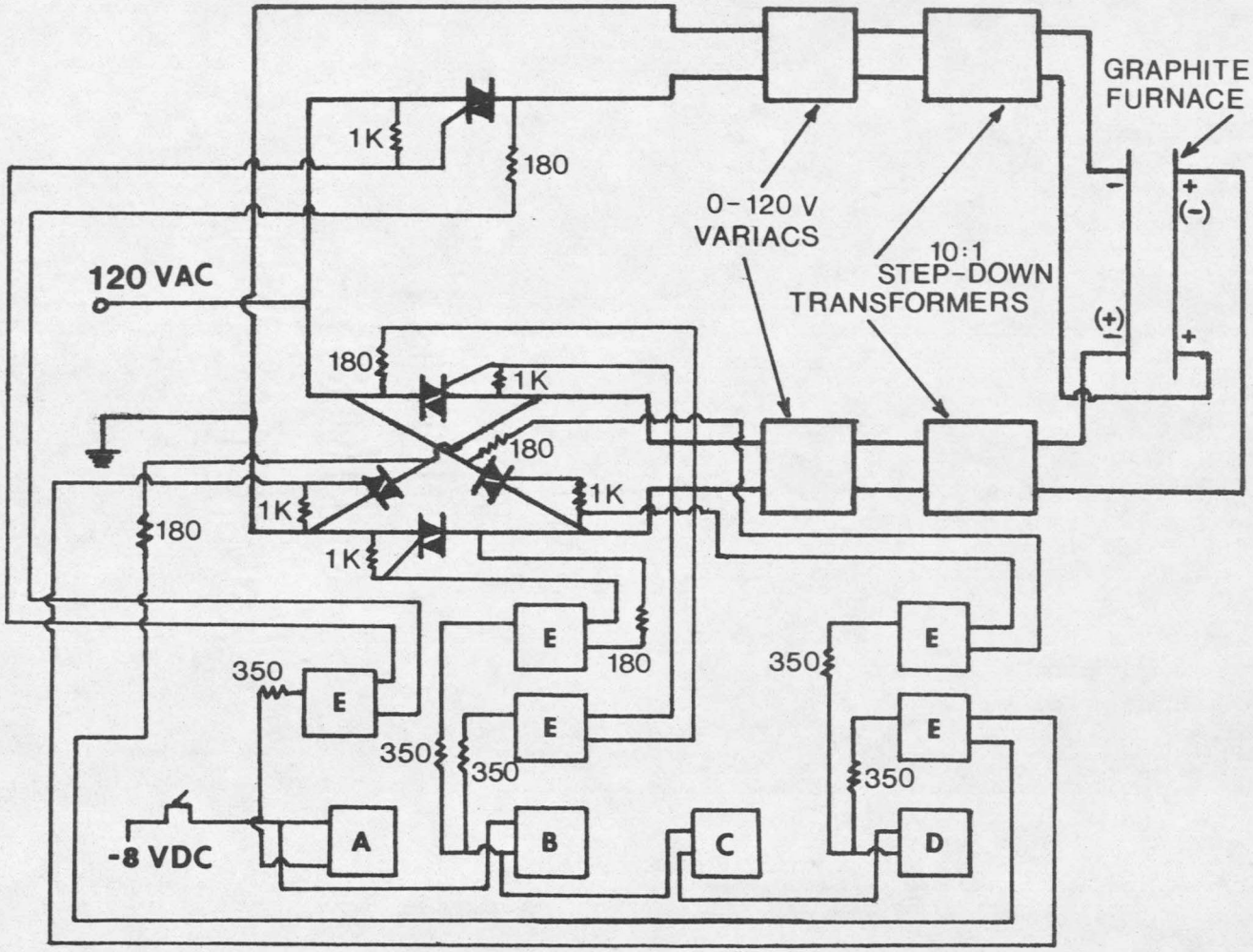
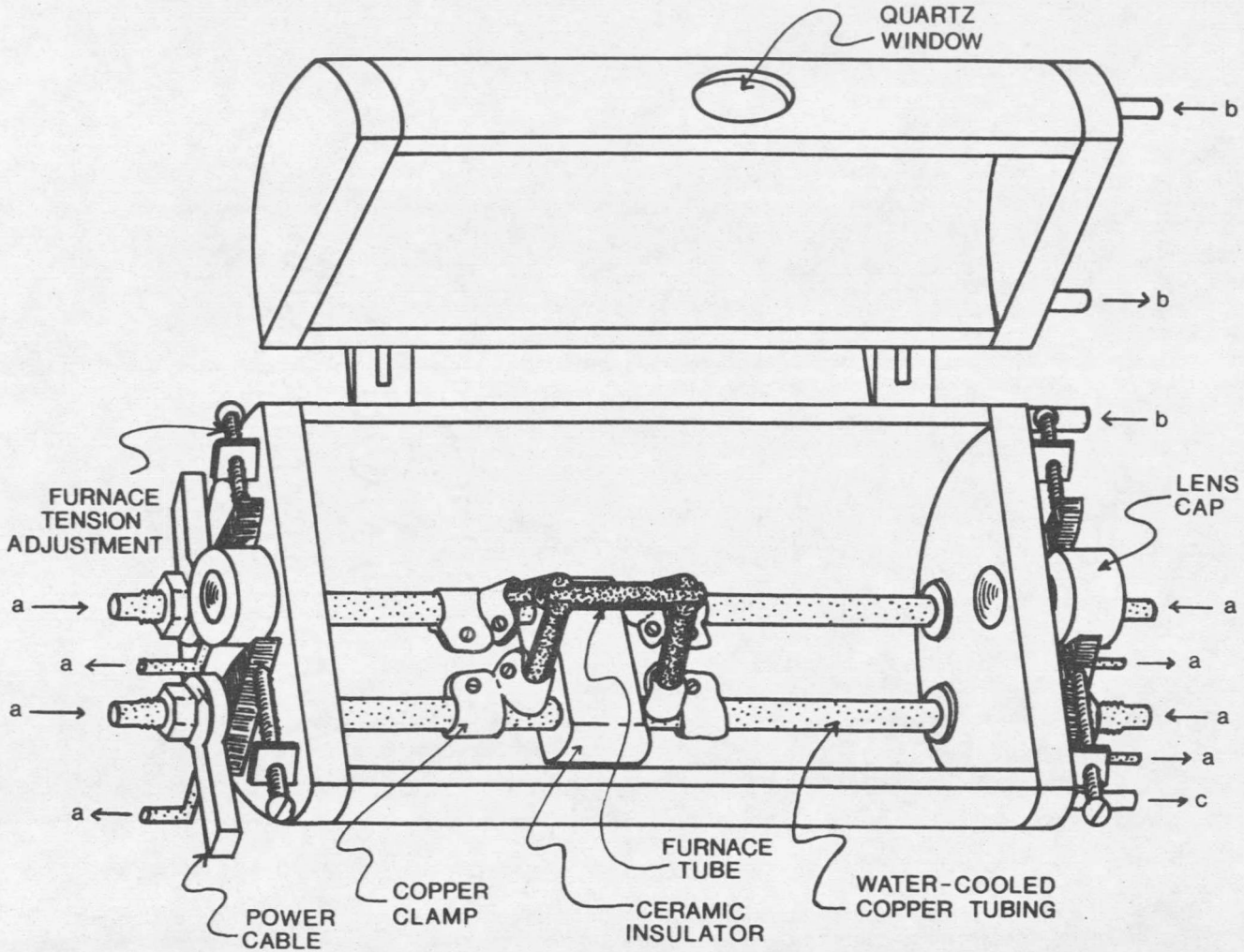

GRAPHITE
FURNACE
0-120 V
VARIACS
10:1
STEP-DOWN
TRANSFORMERS
120 VAC
1K
180
180
1K
180
1K
1K
1K
180
350
350
350
350
E
E
E
E
E
E
A
B
C
D
-8 VDC
-
+
(-)
(+)
+

Figure 9

Diagram of the dual-pulse heated furnace. Length of the water-cooled aluminum shell is 16 cm. The graphite furnace depicted is 25 mm long although lengths up to 100 mm can be accommodated. (a) Water ports for cooling copper support rods. (b) Water ports for cooling aluminum shell. (c) Argon inlet.


QUARTZ WINDOW
b
b
b
FURNACE TENSION ADJUSTMENT
LENS CAP
a
a
a
a
a
a
a
a
c
FURNACE TUBE
COPPER CLAMP
CERAMIC INSULATOR
WATER-COOLED COPPER TUBING
POWER CABLE

Conclusions

It must be emphasized that although improvements in gas-phase interferences were achieved with these alternate furnace designs, the forked-support furnace, double-walled furnace and dual-pulse heated furnace do not eliminate interferences due to shifts in atomization temperature and rate. Fast heating rates coupled with a temperature feedback control system would improve both matrix-induced τ_1 and τ_2 changes and gas-phase interferences. It is advised, therefore, that further development of these furnaces should include temperature control.

CHAPTER 2

1. INTRODUCTION

Multielement Atomic Absorption Spectroscopy

During the last 25 years, atomic absorption spectroscopy has become a widespread and highly practical analytical tool. Combined with electrothermal atomization, AAS makes ultra-trace element analyses and direct solid sampling accessible to even budget-limited laboratories. Thus the chance to even double the number of elements that can be determined at one time with minimum additional cost led many workers in the field to attempt development of a practical multi-element atomic absorption spectrometer (75-78). This interest led to the development of a commercial dual channel AAS system (Instrumentation Labs). Workers who desire more elements usually employ modified direct readers, which is a practical route for labs that acquired them as part of an emission setup. Hollow cathode lamps are available which contain up to 6 or 7 elements, although line intensities tend to decrease as the number of elements increases. Alder, et. al., (78) used an array of 9 hollow cathode lamps to analyze up to 9 elements and still retain GFAA detection limits comparable to commercially available AA instruments using single element HCL's and electrothermal atomization.

O'Haver and coworkers (79) have recently provided the best demonstration of a practical simultaneous multielement atomic

absorption system which they dubbed SIMAAC. A Xenon arc continum lamp was the primary source and wavelength modulation provided background vorrection at each analytical line for up to 16 elements. Instrumentally, it appears that simultaneous multielement analyses are equally feasible using AAS or AES. However, the use and growth of multielement AAS has in fact been quite slow. Two main factors have contributed to this slow growth: (1) some electrothermal atomizers have been prone to chemical interferences and/or preatomization losses; (2) AAS typically has a limited working range in contrast to the wide linear dynamic range for AES, particularly ICP-AES. These problems tend to force the analyst to provide custom-tailored atomization conditions and dilution factors for each sample-analyte combination (63,80). When several elements must be considered simultaneously, the search for a chemical pre-treatment to resolve all possible interferences become insurmountable. A matrix interference free atomizer is, therefore, as essential to a multielement AAS system as the light source and polychromator. This becomes especially evident when we go beyond the synthetic solutions which have thus far been the primary focus of multielement AAS instrument development studies.

2. EXPERIMENTAL

2.1 Apparatus

The monochomrator is a variable-wavelength, dual-channel, single grating model built in this lab. Construction details have been described previously (63). It is exceptionally versatile since two photomultiplier tubes pivot around the Rowland circle by mechanical drive while still allowing room for 5-10 fixed channels.

An Ithaco model 353 DL lock-in amplifier system consisting of two independent linear lock-in amplifiers sharing a common power supply was connected to a dual pen omniscribe strip chart recorder for peak height measurements (Houston Instruments). A logarithmic amplifier, V-F converter and counter were used for peak area measurements. This setup provided simultaneous readout from both channels on the same chart paper and thereby produced a permanent time history of the relative appearance time of each analyte species.

One power supply was used for both photomultiplier tubes to assure that any slight voltage variations would cause similar changes in their responses. Both photomultiplier tubes have approximately the same response characteristics.

A Varian CRA-63 graphite cup electrothermal atomizer was used for pulse-type atomization. Dry and ash temperatures were measured with a Chromel-alumel thermocouple. A 30 ms time constant was used for all graphite cup work.

A constant temperature Woodriff furnace was used for all measure-

ments except the blood analysis. It is an ideal furnace for multi-element AAS due to its freedom from matrix interferences (68,71) and the ability to run solid samples without pretreatment (81).

Hollow cathode lamps were the primary source for all measurements. Either multielement or single element lamps combined with a half-silvered mirror were utilized.

2.2 Procedure

NBS Orchard Leaves SRM 1571, bovine liver SRM 1577, Coal SRM 1632 and coal fly ash SRM 1633 were analyzed in the Woodriff furnace. The coal and coalfly ash were run without pretreatment in closed graphite cups(81). Large samples (>5 mg) of orchard leaves and bovine liver were ashed prior to introduction into the furnace as described by Nichols, et. al. (81) to reduce particulate scattering and molecular background.

Blood samples were obtained from the Montana State University Health Center and Bozeman Deaconess Hospital. The samples were 1-5 days old at the time of analysis. 2.3 μl of whole blood were pipetted into a Varian CRA-63 cup along with 2.3 μl of 6N nitric acid. The mixture was dried at 410 K for 30 seconds then increased to 450 K for an additional 30 seconds. This allowed complete and even drying of the viscous sample without loss due to splattering. Ashing was performed in air at 950 K for 55 seconds. Finally, the sample was atomized to a

final atomization temperature of 2600°C for 6 seconds.

3. RESULTS AND DISCUSSION

3.1 Dual Element Analysis in Solids

Many workers have stated that compromise conditions of atomization in multielement AAS are not a problem because one can simply use the atomization temperature of the least volatile analyte (79). This lab has found that complex samples can make it more difficult to find compromise conditions. This is especially true with solid sampling which eliminates sample digestion and pre-treatment. In general, we have found that solid biological tissue samples can be run successfully under a wider variety of conditions than siliceous materials. One reason for difficulties with glasses and rock samples is the high background (0.25 abs unit at 2670 K in a CTF for less than 1 mg of NBS S. R.M. 616 glass) which appears due to vapor of silica if the atomization temperature must exceed 2470 K for any of the analytes sought (82). Thus sample weight may be excessively restricted if the maximum temperature desired for one or more elements produces uncorrectably high background. Here the sequential volatilization available with pulsed atomization would be advantageous provided complete recoveries are obtained.

For more volatile elements, samples such as coal fly ash may show

poor recovery under atomization conditions which work well for standard solutions and some biological samples (Table 11). Cadmium and zinc give good recoveries (Cd 95 ± 5%, Zn 105 ± 10%) in orchard leaves and bovine liver using closed sample crucibles (81) at 1800 K. However, in NBS coal fly ash, good recoveries were obtained only for Cd at this temperature (see Table 12). It was necessary to work at 2100 K in order to obtain good recoveries of Zn without compromising cadmium.

3.1.1 Analysis of Major and Minor Constituents in Unweighed Samples

A multielement spectrometer provides AAS with a unique opportunity for use of an internal standard by which analysis of unweighed samples or solutions diluted to an unmeasured volume (a desirable practice when performing ultratrace analysis, where each transfer to volumetric glassware brings further possible contamination) can become additional standard methods in AAS analysis.

1. Determination of Trace Zinc in Cadmium Samples

The following study of zinc contamination levels in reagent-grade cadmium compounds illustrates some typical problems and possible solutions in the use of the second channel of the spectrometer to weigh the cadmium content of a solid sample of reagent. In this case the internal standard is not a separate, deliberate addition; knowledge of the stoichiometry of the compound and the assumption that it is at

Table 11

Sample Results for Simultaneous Determination of
Cu and Zn in Mineral Feed and NBS Orchard Leaves

Sample*	Cu, ug/ml		Zn, ug/ml	
	found	actual	found	actual
Orchard Leaves	0.103	0.10	0.25	0.21
Mineral Feed	13.0	12.8	12.7	11.5

*microwave digested with HNO_3

(results read vs simple aqueous standards)

Table 12

Simultaneous Determination of Zinc and Cadmium In NBS Coal Fly Ash (SRM 1633)

Sample Size mg	Zinc/ng			Cadmium/ng		
	Observed	Expected	Percent Recovery	Observed	Expected	Percent Recovery
0.9	100	189	52.9	4.3	1.3	340[b]
3.8	285	800	35.6	6.4	5.5	116
8.6	590	1800	32.8	10.8	12.5	86
9.7	710	2035	34.9	11.6	14.0	83
18.5	1345	3880	34.7	24.0	26.8	90

[a] Atomization temperature: 1770K

λ_{Zn} = 307.6 nm λ_{Cd}=326.1 nm

[b] High Cd recovery due to inhomogeneity effects encountered at small sample sizes.

least 95-99% pure compound, allow us to calculate the gross sample weight from the measured amount of cadmium.

The zinc analyses were performed using the 307.6 nm line instead of the excessively sensitive 213.9 nm zinc line. This permitted use of convenient sample sizes of the reagents being analyzed (on the order of 1 mg). However, such sample sizes also produced extremely large responses for cadmium line at 326.1 nm. The response pegged in excess of 0.8 absorbance unit for at least 40 seconds due to 0.5 mg cadmium.

Fortunately, the diffusion controlled loss of sample vapor from a constant temperature furance can be expressed as one or a sum of exponential terms containing time constants related to residence time and the time required to attain a particular absorbance value (15). The length of time that the response is above a fixed peak height (in this case, 0.8) can thereby be related to the logarithm of the analyte quantity. Normally, a linear relationship between these two parameters can be obtained over a concentration range for cadmium of one thousand times higher than the concentration at which the response first exceeds the chosen height (0.8 absorbance unit).

Some of our responses were in excess of this linear range and so it was necessary to establish empirically the curvature of the relationship at higher concentrations. Onset of curvature appeared to vary from compound to compound as shown in Figure 10.

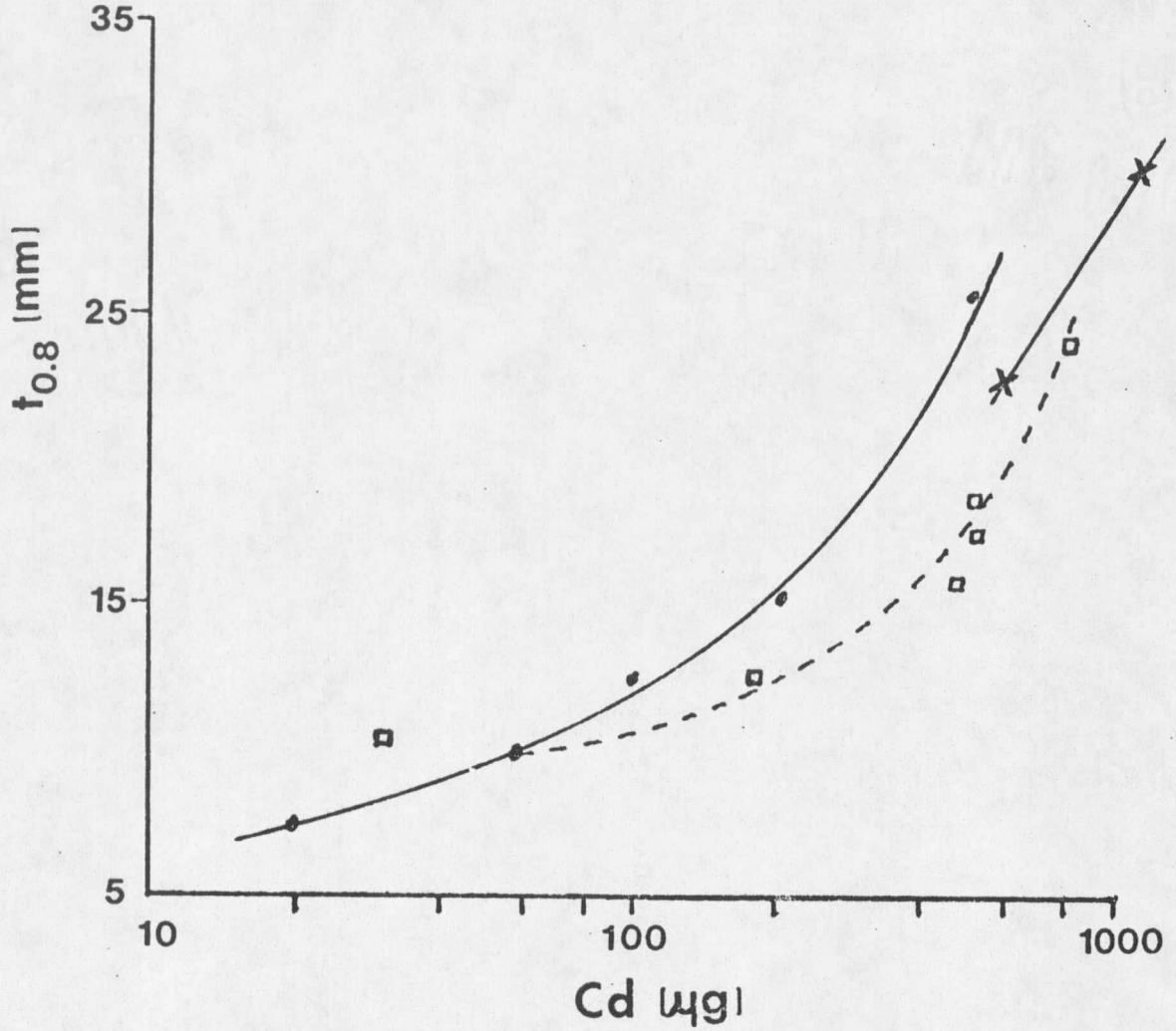
Figure 10

Plot of the peak width in millimeters measured at a fixed absorbance level (0.8 absorbance units) versus the weight of cadmium as:

(O) solution of nitrate salt

(□) solid chloride salt

(X) solid sulfate salt


35
25
15
5
$t_{0.8}$ (mm)
10
100
1000
Cd µg/l

On the ability to weigh these samples by use of the 326.1 nm cadmium line was established, it was quite straight forward to measure simultaneously the zinc responses with the other channel of the spectrometer set at 307.6 nm. An example of the data obtained is shown in Table 13.

An alternative to solid sampling, in the above case, would be to dissolve the reagent and pipet small enough aliquots to avoid part of the difficulties of calibration for cadmium. However, certain samples may be insoluble or difficult to dissolve completely (for example, analysis of arsenic in some samples of antimony oxides), and solid sampling may be appreciably faster and simpler.

2. Use of Iron In Hemoglobin as the Internal Standard in Blood

The same technique was applied to the determination of lead in human whole blood analyses using the iron in hemoglobin as the internal standard. The lead levels of nine different blood samples were determined by standard additions. A plot of lead concentration against the ratio of iron to lead absorbance (peak areas) produced a linar graph from 25 to 90 pb Pb (Figure 11). The range of lead concentration in the samples studied was between 25 and 45 ppb. 30 ppb Pb is considered average and 80 ppb or above is toxic (83). Data at higher lead concentrations were obtained by addition of standard lead nitrate solutions to several blood samples. This produced a graph which

Table 13

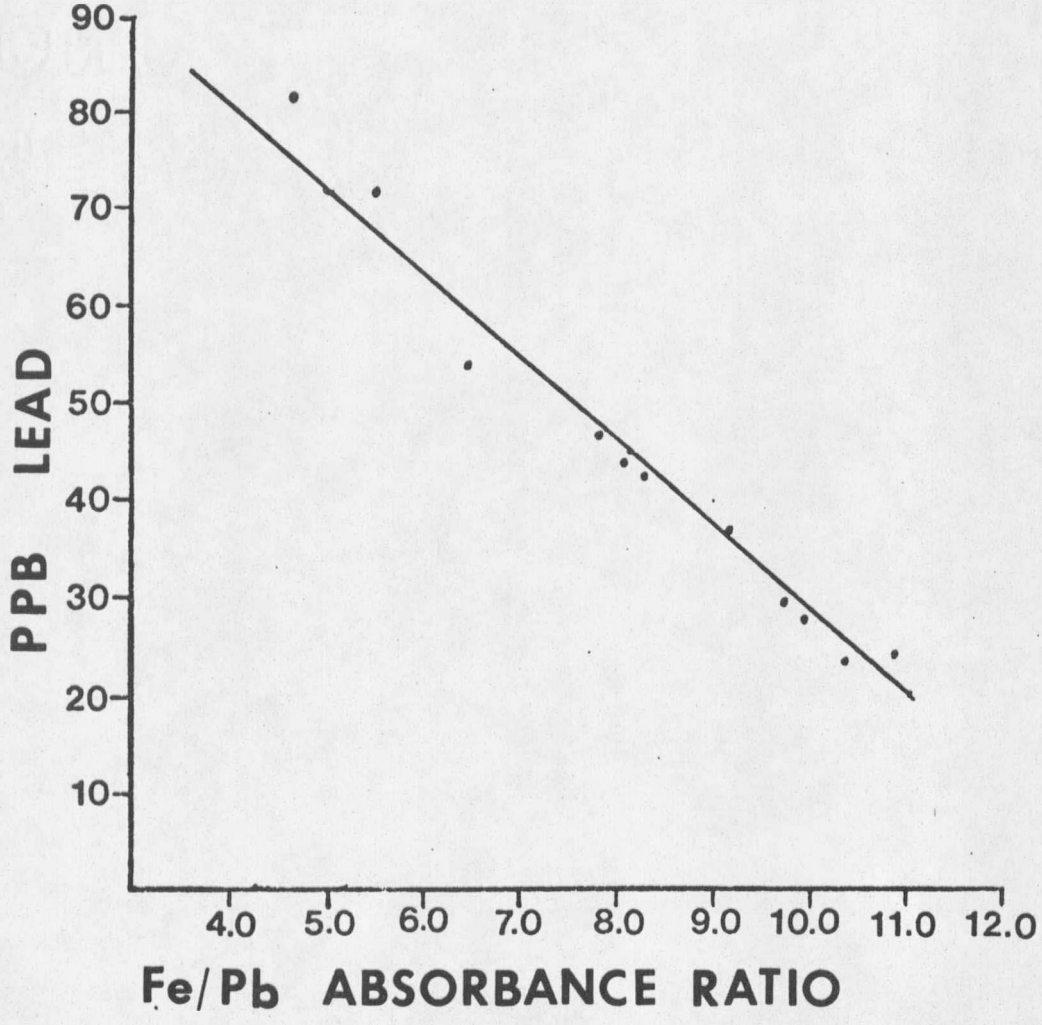
Calculation of Zinc Concentration in an Unweighed Sample

Zinc Absorbance	0.12
Amount of Zinc from Calibration Curve	0.47 g
PWAFH of Cd Signal*	21.2 div
Amount of Cd from Calibration Curve	560µg
Amount of $CdCl_2 \cdot 2.5\ H_2O$ Corresponsing to Cd found	1.09mg
Concentration of Zn in the Unweighed Sample	0.43µg/mg
Concentration of Zn According to Baker's Analysis	0.3µg/mg
Concentration of Zn on the Basis of a Weighed Sample	0.31µg/mg

*PWAFH: Peak Width at Fixed Height

Figure 11

Plot of the weight of lead against the ratio of absorbances measured simultaneously for iron and lead in each of nine blood samples.


90
80
70
60
50
40
30
20
10
PPB LEAD
4.0
5.0
6.0
7.0
8.0
9.0
10.0
11.0
12.0
Fe/Pb ABSORBANCE RATIO

covered the range of lead concentrations usually found in clinical laboratories with a standard deviation representative of the natural fluctuations in iron levels for a small number of people.

Hemoglobin levels can vary from 12 (anemic) to 16 (high altitudes) hemoglobin/100 ml whole blood (both males and female ranges included) (84). This corresponds to a range of 408 to 544 ppm iron. The average iron concentration among the nine samples used in this study was 460 $\pm$ 13 ppm. Using a lead absorbance which corresponds to 44 ppb Pb and the Pb vs Fe/Pb plot, values from 35 to 50 ppb lead are possible due to the iron related fluctuations in the Fe/Pb absorbance ratio. Thus a 14-18% error is possible at these extremes. However, general screening tests are usually designed to distinguish between a 44 ppb and an 80 ppb lead level. An anemic person might be misinterpreted to have a high lead level but this would trigger further tests to determine whether the problem was the iron or lead level. A high altitude area would be calibrated for higher iron levels to avoid erroneously low lead readings. Thus the effectiveness of ratioing Fe to Pb (or other trace metals), which avoids the need for accurate blood volume readings, should be sufficient for mass screening programs or any situation where speed is important.

3.2 General Analysis

It is always desirable in a high volume analytical laboratory to

obtain two or more determinations with a negligible increase over the labor required for one. In this lab, we have made extensive use of multielement AAS in analyzing trace elements in metals with both CTF and CRA and generally group elements by voltility to minimize degradation of the graphite. For the refractory elements in particular, lifetime of HGA furnace tube is an important limiting factor on productivity of automated sequential analyses, as well as an expensive replacement factor. Combinations such as Pb-Cu, Mn-Cu, Mn-Co, Cr-Ni, Al-Si and Cr-Si are typical examples of dual-element determinations performed in this lab.

Element ratioing has proven useful in saving time and labor when seeking to establish that two metal items are of the same composition. This obviates the need for standards and simplifies range finding through use of random dilutions. Another approach to range finding is to set each monochromator channel on a different wavelength of the same element but with different sensitivities. High and low concentrations samples can be run together and one or both wavelengths will give a useful response. If a computer is available and a suitable algorithm to fit the curve can be found, non-linear portion may be useable.

CHAPTER 3

INTRODUCTION

Graphite Furnaces As Sources For Atomic Emission Spectroscopy

1. Electrical Plasmas for Emission Spectroscopy

Analytical uses of plasmas for emission spectroscopy require several properties in an excitation source. (1) Capability of exciting lines of a large number of elements. (2) High sensitivity. (3) Minimum fluctuation in intensity arising from instability of the source. (4) Freedom from interferences. These include spectroscopic, chemical and ionization interferences. Spectroscopic interferences arise from the inability to resolve the line of interest from a line or lines of one or more other elements or from a band of a molecular spectrum. Chemical interferences arise from a reduction in the population of free atoms due to the formation of molecules or radicals. Ionization interferences are the result of the presence of easily ionized elements which can cause a significant change in the electron density of the source thereby shifting the ionization equilibrium. Interferences due to contamination from the construction materials of the source (eg. electrodes) must also be considered. (5) Reproducibility in the introduction of samples. This is a function of both the sample introduction system itself and the stability of the source toward the introduction of foreign matter. This property of an excitation source was a major focus of the plasma design studies presented in this chapter. Satisfactory attainment of each requirement in a single source is usually

difficult since they are not necessarily compatible. Therefore a brief review of the current status of three types of electrical plasmas developed for elemental analyses is presented below. It has been developed to provide a background on the technical difficulties still remaining when I began studies on confined plasmas. The discussion has been limited to D. C. arcs and radio and microwave frequency plasmas because they are the types of plasmas which were used in the studies. The area of flame sources alone is enormous and certainly still a viable means of excitation despite the recent decline in interest. In fact, the first source used for qualitative analyses was the flame of a Bunsen burner (85). Although the work of Kirchhoff and Bunsen led to development of the modern spectroscope (86), it soon became clear that this source did not have sufficient energy for universal application to most samples. High temperature flames have since been developed: acetylene - oxygen; 3400 K, carbon subnitride - ozone; 5516 K, cyanogen ozone; 5200 K, atomic hydrogen; 4000 K and the ozone decomposition flame; 2677 K to mention a few (87). However, some of these are difficult and/or dangerous to use. More fundamentally, the temperature of the gas in flame sources is limited by the heat of combustion of the fuel. Electric discharges have no such fundamental limitation and therefore their use has grown from the belief that excitation capability, sensitivity and freedom from matrix interference increase with temperature.

Although this is true, unless other parameters of the source design are carefully considered the full potential of a high temperature plasma is never realized.

Two parameters which are often neglected in characterizing a plasma but which also exert a strong influence on the desired properties of analytical plasmas are: (1) the presence of local thermodynamic equilibrium (LTE) and (2) the residence time of analytes in the observation zone. LTE refers to systems where the energy distribution of particles is subject to the laws of thermodynamic equilibrium but where the radiation is not. Thus the dominating mode of energy transfer is by collision between particles rather than by absorption or emission of radiation. All three types of temperature measurement give equivalent temperatures for a system in LTE and the relative populations of various excited states are given by Boltzmann's law (88):

$$N_i / N_j = g_i / g_j \exp\left[-(E_i - E_j)/kT\right]$$

where N is the population, g the statistical weight and E the energy of the ith and jth energy levels. The practical importance of LTE to an analytical plasma is that: (1) a high kinetic temperature is most likely to be achieved with a system in LTE since energy transfer is dominated by collisions. (2) In LTE, the ratio N_i/N depends essentially only on temperature (although electron density influences the partition function through the drop in ionization potential (88)).

ated without interference. The chance to increase the sensitivity of atomic emission, which currently is lower than atomic absorption, should be worth the effort.

1.1 D. C. Arcs

The wide range of devices which fall into this category all have the common characteristics of relatively high currents (~1-200A) and the need for at least two electrodes. Beyond these similarities, two distinctive categories must be recognized: (1) arc devices in which observations are made in the current - carrying portion of the plasma, and (2) plasma jet devices in which observations are made in the flame-like plume which does not carry the discharge current.

(1) The basic two-electrode D. C. arc has been in use since the early 1920's. Since then, numerous modifications have been made in an effort to stabilize the position and intensity of the arc which tends to wander. This emission source is also subject to fairly severe ionization interferences due to its moderate degree of ionization. Morrison et. al. noted that an optimum current of 28 A resulted in higher sensitivities than the commonly used 6-12 A range (90). Marinkovic and Dimitrijevic (91) stabilized an arc with a series of water cooled brass segments and added potassium chloride as a buffer to lower the arc temperature to 3100 K. They found that lowering the arc temperature in this manner permitted the use of a low-dispersion

monochromator (fewer lines). The greater stability allowed the use of non-integrating photoelectric detectors (as opposed to film). Vukanovic et. al. (92,93) demonstrated that external magnetic fields stabilize a d.c. arc and increase sensitivities. The magnetic fields made the plasma more diffuse thereby increasing the plasma volume. The authors postulated that this volume increase was the cause of an observed increase in the residence time of particles in the plasma. This in turn results in higher sensitivities. Another interesting finding of this study was the optimum shape for the electrodes: rather than a pointed cathode, as is commonly used, the authors found that a flat anode and cathode (the anode being about twice as wide) were optimum for plasma stability. Marinkovic and Antonijevic (94) stabilized an arc and increased the residence time of analytes in the observation zone by using a U-shaped d.c. arc. A fairly long horizontal part of the arc column made possible 'end-on' observation along the column. A potassium chloride buffer was necessary to suppress ionization interferences.

(2) A plasma jet is formed when the current density to be dissipated on the surface of an electrode is greater than can be removed by radiation and conduction alone. Maecker (95) showed that any constriction of an arc gives rise to a jet by forcing an arc to burn in a narrow water pipe. When the periphery of the arc column is deliberately cooled or constricted by any means the ionization, and

therefore the conductivity of the outer gases, lowers. The current then concentrates in the central region which increases the temperature and hence the conductivity. This increase in current density caused by a thermal pinch can become high enough to form a magnetic pinch due to the attraction of streams of flowing charged particles. The advantages of a constricted arc are greater stability, higher energy concentration and higher temperatures. There are also several disadvantages of plasma jets. Their analytical application was hindered due to random wandering of the arc streamer over the surface of the cathode which perturbed the jet (96). Owen (96) stabilized the jet by using a third electrode. Three electrode plasma jets of slightly different design are now commercially made by Spex Industries. Another means of stabilizing the plasma column is to place it in the center of a gas vortex which cools the outer column thereby constricting a d.c. arc to a plasma jet (97). Plasma jets have electrodes (often thoriated tungsten) which operate at high temperatures and produce their own spectroscopic contamination of the sample. It is difficult to inject aerosols into the plasma jet other than direct injectors which pass the whole aerosol of the nebulized sample into the plasma. Many of the larger droplets leave the plasma without being atomized and consequently simply cool the plasma (98). Temperatures between 5000 K and 15000 K (98) have been reported. However, the hottest portions also have extremely

intense background. The cooler plume above the current dense region is therefore utilized. Despite these drawbacks, plasma jets are relatively inexpensive and offer greater sensitivities than conventional d.c. arcs.

No mention of LTE conditions has been mentioned for either d.c. plasma. This is because few authors attempt to determine such parameters which is by no means easy or reliable. However, in general atmospheric pressure plasmas are more likely to be in LTE than low pressure (~ few torr) plasmas due to the greater collision frequency. Higher current densities also tend to improve attainment of LTE. Thus the plasmas just reviewed can be assumed to be in LTE (temperature measurements made on these sources depend on the presence of LTE for their validity).

1.2 Radiofrequency Plasmas

This class of emission source involved generation of a plasma in an electromagnetic field oscillating between 1 and 300 MHZ using two, one or no electrodes (99). Badarau et. al. (100) utilized a high-frequency plasma generated between a circular plate and a hollow cyclinder for spectrochemical analysis in 1957. Mavrodineanu and Hughes (101) analyzed solutions by passing the sample aerosol through a single hollow conductor which formed both a central electrode and a coaxial coil surrounding it. The plasma was thus both capacitively

and inductively coupled. A large variety of configurations have evolved over the years but most can be characterized by capacitive coupling and powers less than 1000 W. The low currents ($<$ 1A) and presence of only one or no electrode reduced background emission considerably compared to the direct current arcs but the low powers and sometimes low pressures often used made these rf plasmas very susceptible to matrix interferences and unstable toward sample introduction. They were also susceptible to ionization interferences. Greenfield et. al. stated that the chemical interferences observed with these plasmas was direct evidence that the kinetic gas temperature was not sufficiently high (99). This coupled with reported electron temperatures between 10,000 and 100,000 K (102) indicated that these plasmas were not in LTE. Low pressure plasmas were likely to deviate even more from LTE.

The most successful of the rf plasmas has been the inductively coupled plasma now known as the ICP. The basic design consists of two turns of a heavy, water-cooled copper tubing wrapped around a quartz tube. Radio-frequency (27 MHZ) current between 1 and 2 A is passed down the copper tubing. Argon (or in some cases nitrogen or argon/nitrogen) gas at 15-18 /min is forced through the quartz tube as a vortex. The argon inductively couples to the rf field (as in a transformer) which causes sufficient ionization to produce a plasma.

Powers between 0.4 and 10KW have been studied but ~1.2KW has become the standard operating power in commercial instruments. Samples are introduced as nebulized solutions into the center of the plasma vortex. The analytical viewing zone is generally 15-25 mm above the copper load coil. Because of the popularity of this excitation source, it is probably one of the most thoroughly studied (103-109). As a consequence, a bewildering array 'optimum' conditions for various groups of elements appeared. Sensitivity, matrix interferences and ionization interferences depend in a complex manner on rf power, gas flow, observation height in the plasma and size of the observation zone (106). Several groups have intensively studied temperature distributions, electron densities and the existence of LTE conditions in the ICP with respect to these operating parameters (103-105). Kalnicky, Fassel and Kniseley (103) concluded that LTE depended on the operating parameters of the ICP and therefore many ICP's reported in the literature did not attain LTE (107). They also found that LTE was more likely to exist at lower observation heights in the plasma near the load coil, at higher power levels and lower gas flows. This was in good agreement with the studies of Boumans and De Boer (106) who found that matrix interferences decreased with higher powers, lower gas flows and lower observation heights. They also concluded in a comparative study between the ICP and capacitively-coupled microwave plasmas (CMP,

which will be covered in the next section) that the ICP was 'superior in all respects' to the CMP (108). Many of the interferences which were observed were attributed to 'nebulizer - desolvation' effects. The aqueous sample aerosol was passed through a desolvation apparatus which consists of a heating tube to vaporize the solvent followed by a condenser to remove the solvent. Apparently, some matrix salts selectively trapped out certain analytes in the condenser thereby causing a signal depression. A desolvator was required for their ICP because of the low power used (0.7 KW). Later ICP's using 1 KW or greater power were able to directly introduce the aerosol into the plasma without perturbation. The remaining interferences are due to changes in electron density when an easily ionized element is introduced in large amounts. The magnitude of this effect varied widely from author to author until Horlick (109) found that the size of the observation zone used had a large influence on the line intensity changes observed. Observation over a large area of the plasma resulted in a much lower, averaged ionization interference than small areas.

The ICP is currently one of the best emission sources available. It's main disadvantages are short residence times, analyte dilution by the high gas volumes used (both factors result in sensitivities one to three orders of magnitude higher than flameless AA), problems with solid sample introduction systems which are reliable and non-perturbing,

and some ionization interferences the exact magnitude of which is still debated.

1.3 Microwave Plasmas

Microwave plasmas are in some ways similar to the rf plasmas. However, because of their shorter wavelength, microwaves deliver more of their total energy to the plasma. They can also be more difficult to couple to a gas and the coupling is usually sensitive to temperature fluctuations of the system. There are two basic types of microwave plasmas: (1) the microwaves generated from a magnetron and conducted through a coaxial cable to the tip of a coaxial electrode where a flame-like plasma is formed. They are capacitively coupled systems and are often referred to CMP's. (2) Electrodeless systems where the microwave energy is coupled to a gas stream contained in a nonconductive tube (eg., quartz) placed in a resonant cavity (110). The microwaves are radiated into the cavity where standing waves are set up. The quartz tube is placed in the cavity at a point where the field intensity is greatest thereby causing breakdown of the gas to a plasma (111). These systems are known as microwave induced plasmas (MIP). Powers less than 200 W are commonly used because medical diathermy units operating at 2450 MHZ and $\sim$100 W are widely available. Some microwave plasmas are also operated at low pressures ($\sim$ 25 torr) because gas breakdown can be difficult at low powers unless coupling is

efficient (111). As a consequence, these plasmas are not in LTE, cannot handle large amounts of sample without extinguishing, have fairly severe ionization interferences and interferences from radical and molecule formation in the plasma (108). Such problems are the result of insufficient kinetic gas temperatures which, coupled with high excitation temperatures, is indicative of the absence of LTE. The most useful application of microwave plasmas has been as element specific detectors for gas chromatography (112).

2. Stabilization of Plasmas by Confinement in a Constant Temperature Furnace.

In light of the problems encountered with the three classes of plasmas reviewed (ie. residence time, sample introduction stability, interelement effects and intensity fluctuations) I considered the use of a constant temperature graphite tube as an emission source. The thermal energy provided by a hot graphite tube has been utilized as an emission source by Hutton et. al. (113). Useful sensitivities were obtained for a few elements with low-lying excited states otherwise the energy available was insufficient for most elements. However, if a plasma discharge were generated within a hot graphite tube, then sufficient excitation energy would be available for a useful emission source and the hot graphite would provide the thermal energy necessary for sample decomposition (both liquid and solid). This combination

would bring the whole system closer to LTE. The hot graphite (which has a fairly low work function) also generates a moderate electron pressure within the tube through thermionic emission. Sturgeon, Berman and Kashyap (114) made direct measurements of the electron concentration in an HGA-2200 furnace by microwave attenuation experiments. They obtained a value of 7.8×10^{12} cm $^{-3}$ at 3000 K. This value may be compared to values of 10^{11} cm^{-3} for a clean air-acetylene flame (115), 1×10^{13} cm $^{-3}$ for the same flame in which 1M $Cs(NO_3)$ was aspirated (116) and $10^{15} - 10^{16}$ cm $^{-3}$ for the ICP (103). This electron pressure should have two effects: (1) provide 'seed' electrons to initiate a plasma and maintain it at greater stabilities. (2) reduce ionization interferences to some extent by suppressing ionization which is the purpose of adding KCl as a buffer to d.c. arcs.

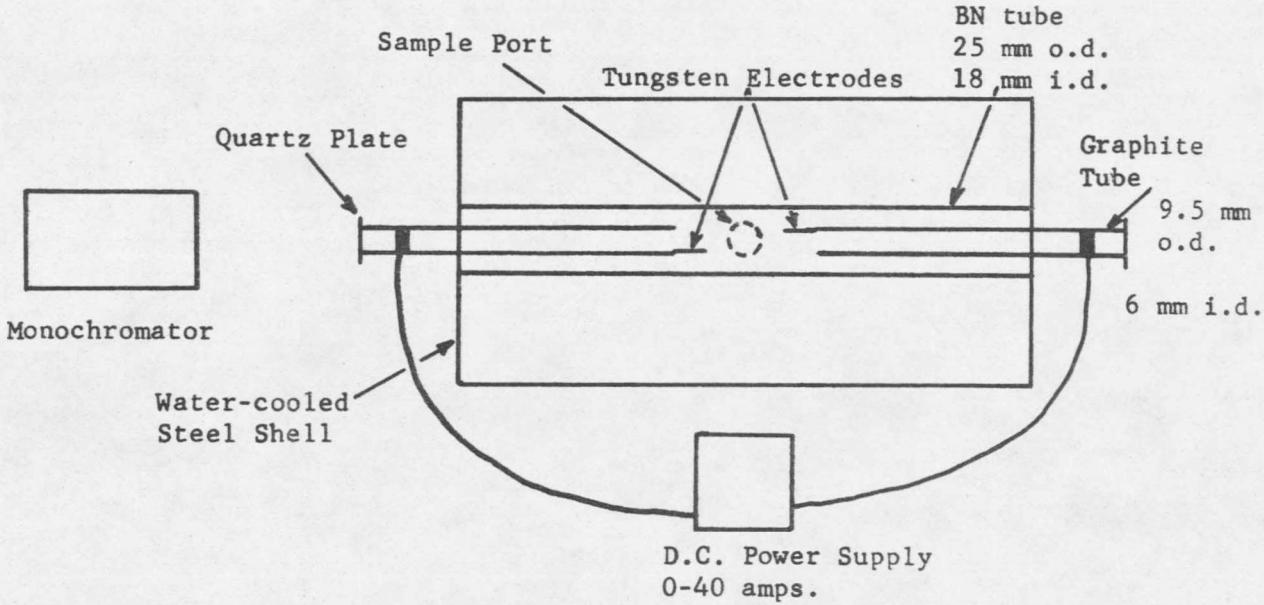
2.1 D.C. Arc in a Closed Tube

Experimental and Results

The first plasma tried was a high current (10-45 A) d.c. arc. Since sufficient thermal energy is available in these plasmas for sample volatilization and atomization, the discharge was merely confined in a cold graphite tube. The plasma quickly heated the tube to a steady temperature (1400 - 3000 K depending on the current). Otherwise the sample introduction system and furnace design were the same as in a constant temperature Woodriff furnace (2). Figure 12

Figure 12

Top view of the d.c. arc confined in a boron nitride tube. The entire apparatus is contained in a water-cooled shell identical to a constant temperature Woodriff furnace for AAS. The shell is shown with the top half removed. Samples are introduced through a side tube attached to the bottom of the steel shell.


Sample Port
BN tube
25 mm o.d.
18 mm i.d.
Tungsten Electrodes
Quartz Plate
Graphite
Tube
9.5 mm
o.d.
6 mm i.d.
Monochromator
Water-cooled
Steel Shell
D.C. Power Supply
0-40 amps.

illustrates the electrode arrangement inside a boron nitride tube which was tried as an alternate, non-conducting material. The tungsten electrodes were simply fitted into holes drilled into the walls of the smaller graphite tubes. Tungsten rods were used for the electrode tips rather than graphite because of their greater resistance to wear at high discharge currents. Observation of the plasma emission was made through one of the graphite tubes which hold the tungsten electrodes. This arrangement greatly reduced the intensity of tungsten lines and bremsstrahlung continuum which are more intense when the electrodes are viewed directly.

The purpose of confining the plasma inside a tube was to stabilize the emission. It was though that once the plasma expanded to the walls, it would stabilize. By viewing down the length of plasma and forcing a flow of argon gas to exit through the graphite electrode holders, the residence time of analyte atoms would be increased. Mercury salts, deposited as dried aqueous solutions in a graphite cup were introduced into the furance on a pedastle as in the Woodriff furnace. Although the plasma did expand to the walls at currents greater than 35 A, it did not do so uniformly. A concentrated discharge usually arced to the wall over a small area eventually burning a hole in it. A high temperature material which was non-conducting was tried instead. Boron nitride was chosen as the most suitable material. Although no

direct arcing to wall occurred, the emission intensity remained too erratic to be analytically useful for periods of more than a few minutes. The signals measured for a given amount of mercury (the 253.6 nm line was used) varied by 30%. Examination of the tube and electrodes after fifteen minutes of operation revealed significant shortening of the electrodes due to melting and oxidation. The tube walls were also unevenly pitted. Apparently, the position of the arc drifted as these materials changed with wear. The amount of sample which entered the plasma changed with time as a consequence.

Other designs could have been tested but it became apparent that a continuous operation emission source would require lower currents to reduce materials wear. Thus, the low current, high frequency plasmas were tried instead.

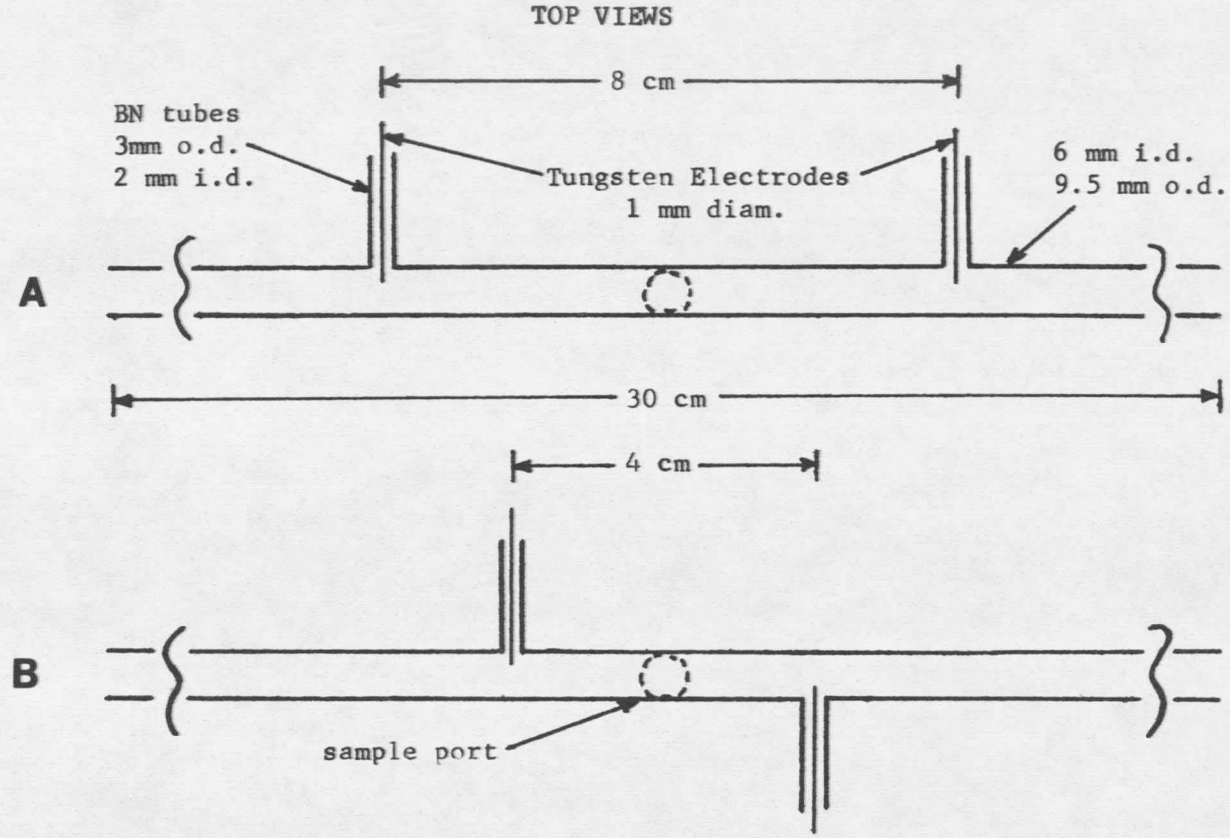
2.2 Radio-Frequency Plasma in a Constant Temperature Furnace

Experimental

An rf plasma was generated in a constant temperature Woodriff furnace by coupling the output of a radio-frequency diathermy unit to the hot graphite heater tube via two tungsten wire electrodes. The diathermy unit output a rich spectrum (numerous harmonics) between $\sim$ 10 and 50 MHZ. No impedance matching network was initially used and later attempts were not useful. Figures 13 and 14 illustrate the various electrode configurations which were tested.

Figure 13

Top views of two electrode arrangements used to couple rf power to a constant temperature graphite furnace. Except for the electrodes, the furnace configuration and sample introduction system are identical to a single-phase heated Woodriff furnace.


TOP VIEWS
8 cm
BN tubes
3mm o.d.
2 mm i.d.
Tungsten Electrodes
1 mm diam.
6 mm i.d.
9.5 mm o.d.
A
30 cm
4 cm
B
sample port

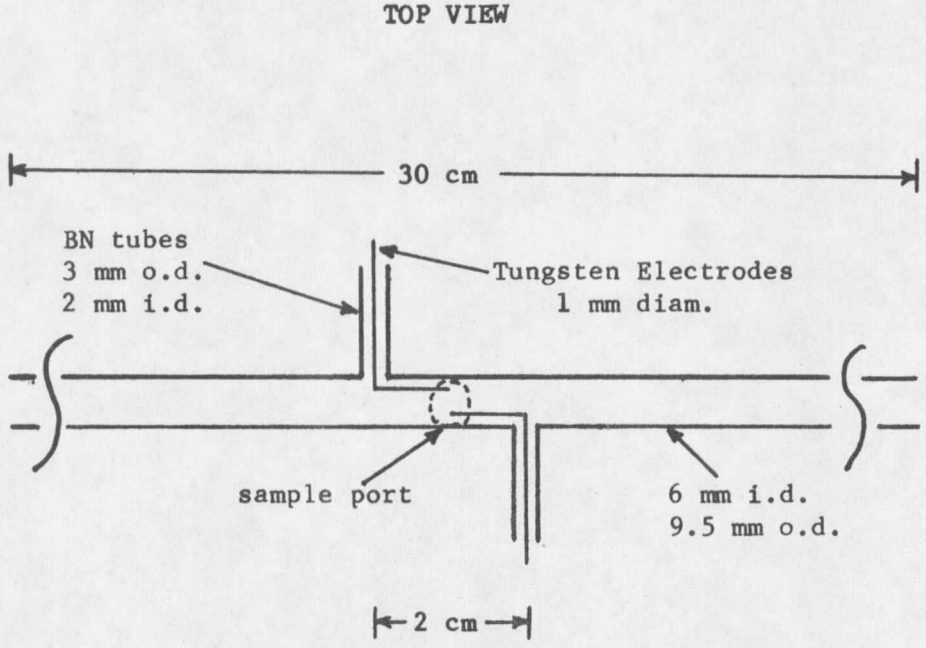


Figure 14

Illustration of an overlapping electrode arrangement used to couple rf power to a constant temperature graphite furnace. The discharge formed along the length of both electrodes. Other furnace details are the same as those given in Figure 13.

The furnace itself was run the same as in atomic absorption analyses. An argon flow of 150 ml /min was used throughout the experiments except when the effect of using helium was tested. The gas flow through the furnace tube is normally stopped when the sample pedastle seals to the furnace tube entrance port. This perturbed the plasma stability so slits were later cut in the sides of the pedastle to allow gas flow during same introduction. Furnace temperatures were recorded with a Leeds and Northrup optical pyrometer, a Beckman DU monochromator operated at a spectral resolution of 2.0A^{o}, an IP 128 photomultiplier tube operated at 900 V and an omniscribe strip chart recorded (Houston Instruments, Inc.) were used to record spectra.

Solutions of cadmium nitrate diluted from a 100 $\mu g/ml$ stock solution were used to characterize the plasma's analytical capabilities. The cadmium 228.8 nm line was used throughout the study because no modulation system was utilized to reject the intense plasma and furnace wall continuum which were emitted along with the atomic lines. The continuum was acceptably low in the UV.

Results and Discussion

Two trends were observed in the coupling of power to the plasma: (1) coupling improved with decreasing distance between electrodes and (2) increasing furnace temperatures. The relative changes in coupling were determined by monitoring the forward output current meter (0-500

ma) on the diathermy unit. Line intensities also increased with higher currents and coupling efficiencies. Table 14 lists the peak areas obtained for varying amounts of cadmium using three different electrode configurations. When the electrodes were far apart, local discharges around each electrode occurred due to arcing to the furnace wall. Moving the electrodes closer together (four centimeters apart or closer) produced a continuous discharge between them. Placing them on opposite sides of the furnace tube increased the plasma stability and volume.

The discharge could not be initiated when the furnace tube was less than 1200K even with a Tesla coil. This, along with the increased plasma currents measured at higher temperatures, supported the importance of thermionic emission from the furnace walls that was initially postulated. Potassium chloride is often used as a buffer and a stabilizer especially in low power ($\lesssim$ 1000W) plasmas. Due to the age of the diathermy unit, the exact power rating was not available but it appeared to output approximately 400W at the best coupling obtained ($\sim$400 ma). To roughly test the buffering capacity of the hot graphite, 1 mg of potassium chloride were added to the graphite sample cup along with 1 ng of cadmium. There was no signal increase when potassium chloride was added. The 228.8 nm resonance line was monitored which would not be as sensitive to electron density changes

TABLE 14.

Summary of Peak Areas Obtained for Various Electrode Configurations

Nanograms Cd	0.250	2.5	25	50
		Peak Area		
Electrode separation; 8 cm same side of furnace			32± 3	
Electrode separation; 4 cm opposite sides of furnace				
a) Argon flow 150 ml/min.		66± 4	236± 22	
b) Helium flow 150 ml/min.			61± 12	
Electrode separation; 2 cm opposite sides of furnace	69± 9	255± 12		831± 11

Conditions: Argon flow 150 ml/min. Furnace temperature 1850 K.

as an ionic line. However, no ionic lines of sufficient intensity could be found. Although the degree of ionization depends on the plasma temperature, high-frequency plasmas have specifically been exploited for their high excitation temperatures. The problem with the low power discharges commonly used has been the low gas temperatures not low electron temperatures. Thus it appears that thermionic emission from hot (~1500K) graphite provides a resonably effective ionization buffer. Other, more easily ionizable elements need to be tested to determine the system's full capabilities.

The plasma did become more diffuse and filled the volume between electrodes when potassium chloride was added. This increased the intensity of the background continuum slightly. Also an exponential increase in intensity was observed for cadmium at high concentrations (Figure 15). Why this occurred is unknown. More severe problems with plasma stability had to be dealt with first before this could be investigated. Although the data in Table 14 shows a relative standard deviation of 12%, the agreement between values obtained on different days often varied by 500%. Once operational, the plasma could remain stable for over an hour of continuous use. If then extinguished and the furnace cooled down, intensities of analyte lines and plasma stability could be several times higher or lower upon reignition. Coupling and stability were too dependent on changes in furnace

conditions. Changes in the electrode chemistry also altered the plasma conditions. Oxidation, carbide formation and heat changed the surface of the tungsten electrodes and reduced the coupling efficiency with age. The background continuum was also unacceptably high above 290nm. Even with a quartz refractor plate and lock-in amplifier, background to signal ratios greater than 1000 became too difficult to extract a signal from without high noise levels. The intense background was largely due to the bright bremsstrahlung radiation from the electrodes.

Higher powers, one electrode coupling and a power supply with a narrower frequency range would improve the system. The broad frequency range of the rf oscillator used made coupling at a fixed power level more difficult. Higher powers would lessen the effects of furnace wear on plasma stability. Therefore, magnetrons, which oscillate at very specific frequencies, were tried next since no other rf source was available.

Figure 15

Plot of emission intensity versus concentration of cadmium. 20 µl aliquots were used for all samples.

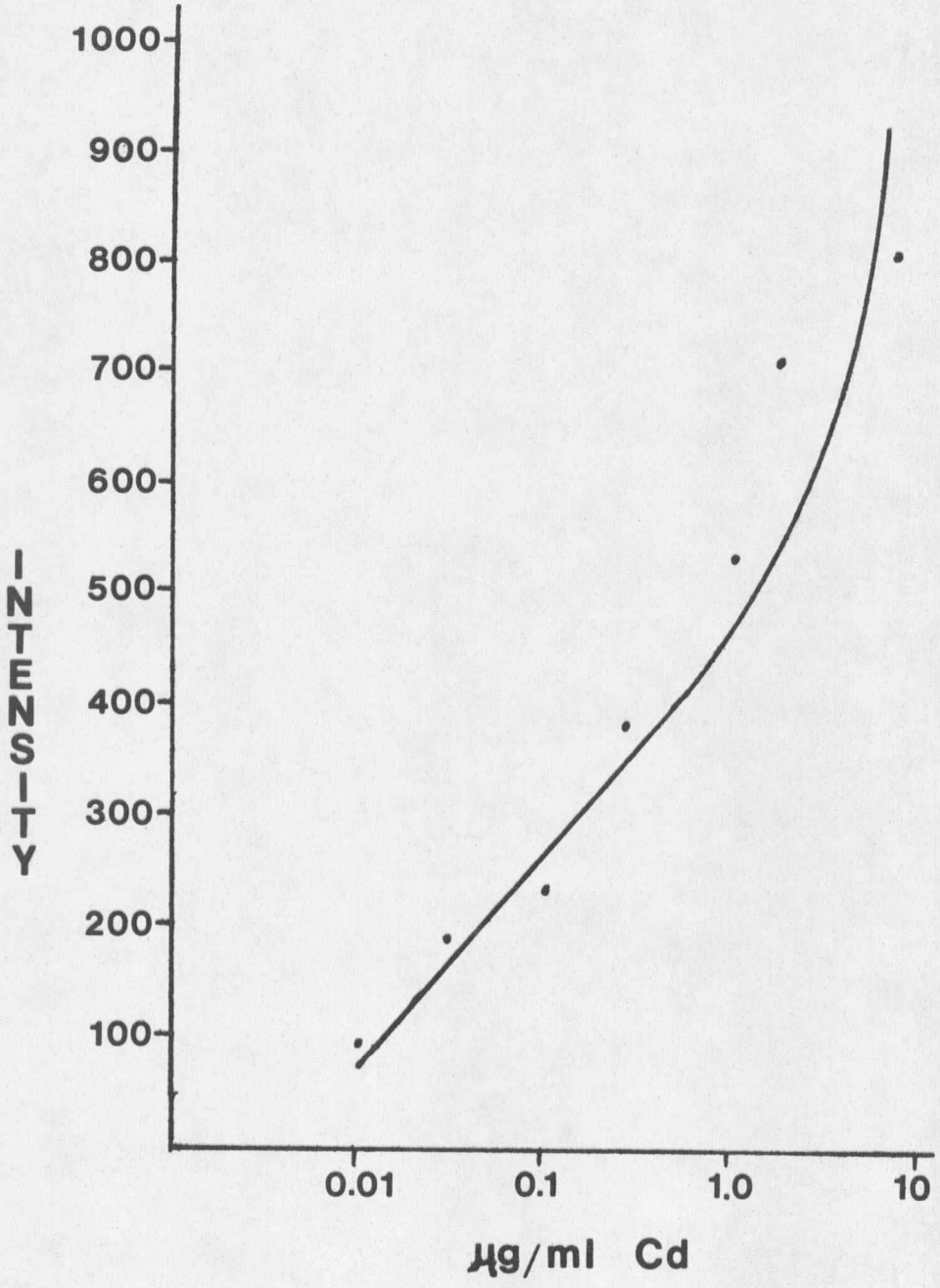
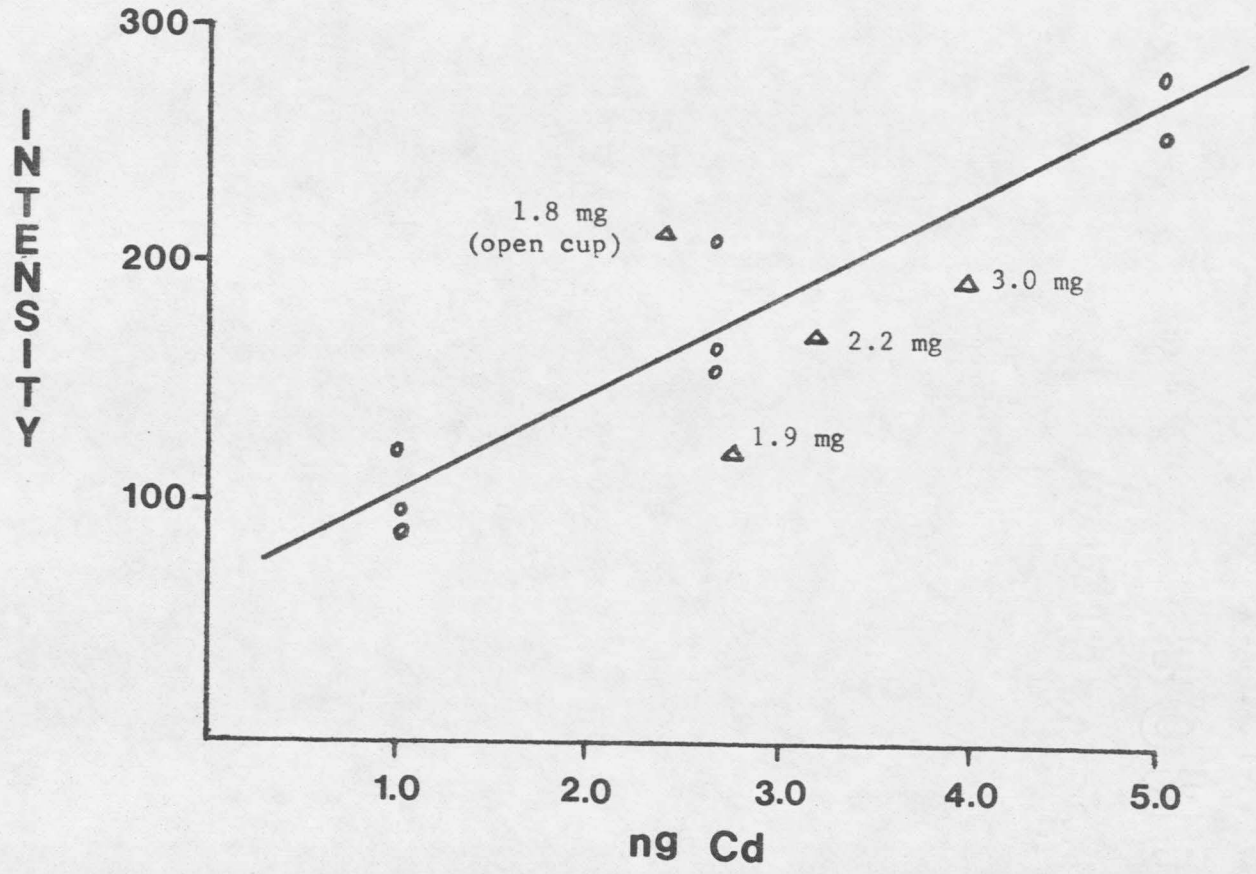

1000
900
800
700
600
500
400
300
200
100
INTENSITY
0.01
0.1
1.0
10
µg/ml Cd

Figure 16

Plot of emission intensity versus weight of cadmium.

(O) indicates aqueous solution of cadmium nitrate.

(△) indicates solid NBS 1633 fly ash sample atomized in closed graphite cups.


300
200
100
INTENSITY
1.8 mg
(open cup)
3.0 mg
2.2 mg
1.9 mg
1.0
2.0
3.0
4.0
5.0
ng Cd

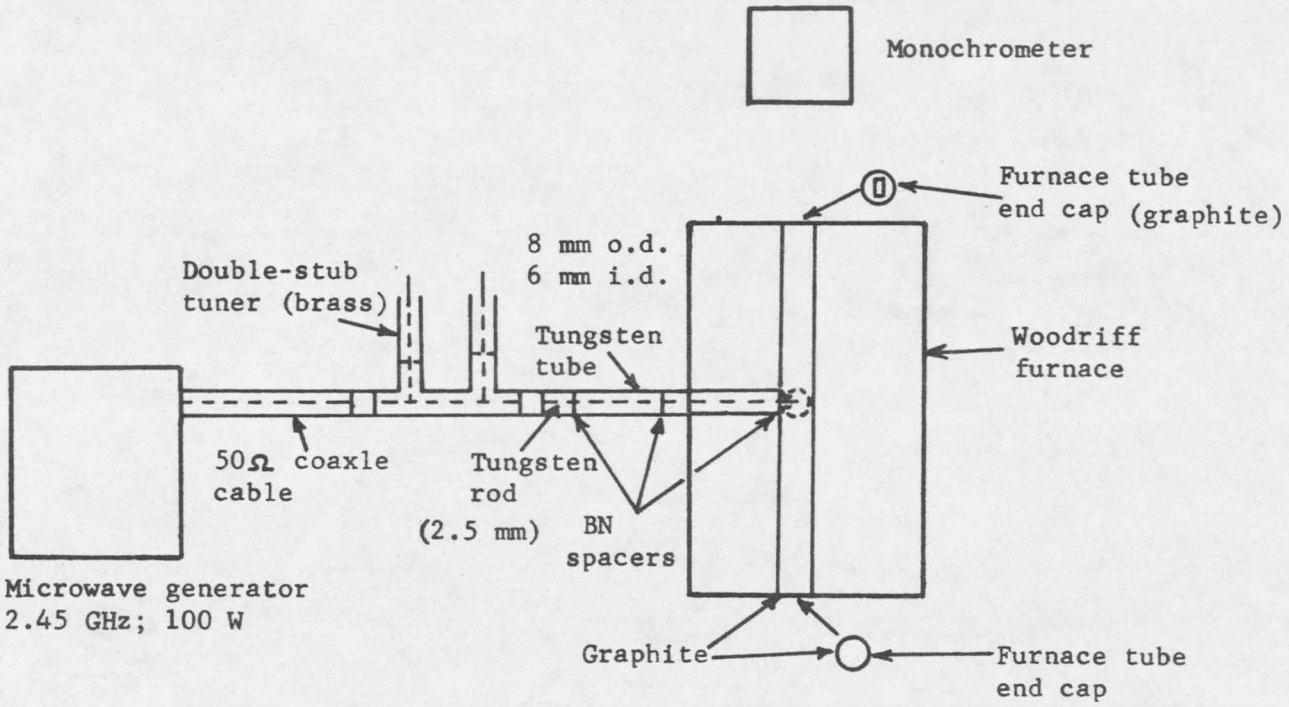
2.3 Microwave Plasma Confined in a Constant Temperature Furnace

EXPERIMENTAL

A 100 W, 2450 MHZ Raytheon microwave diathermy power supply was coupled to a constant temperature graphite furnace as illustrated in Figure 13. Coupling was more difficult and exacting at this higher frequency. A standard 50Ω coaxle cable transferred power from the power supply to a laboratory-constructed double-stub tuner for impedance matching. The tuner was constructed of brass rods and tubing. The brass rod center conductor was silver soldered to a tungsten rod which formed the center conductor of a 50Ω coaxle line constructed of tungsten tubing and rod. Boron nitride spacers were used to center the tungsten rod. The spacers change the impedance of the line insignificantly as long as their width is small (.2cm) compared to the radiation wavelength (4 cm) (117). The center conductor projected approximately 3 mm into the center of the furnace directly above the sample port. A final boron nitride spacer, fitting into the hole made in the side of the furnace for coupling, prevented direct electrical contact between the coaxle line and furnace tube. This probe-coupled circuit was designed to transfer power from the magnetron power supply to the graphite furnace even at high temperatures.

Figure 17

Schematic drawing of the apparatus used to couple 2.45 GHZ microwaves to a constant temperature graphite furnace. The furnace is viewed from the top without the upper half of the water-cooled shell. Operating conditions of the furnace are the same as a single-phase heated Woodriff furnace.


Monochrometer
Furnace tube
end cap (graphite)
8 mm o.d.
6 mm i.d.
Double-stub
tuner (brass)
Tungsten
tube
Woodriff
furnace
50Ω coaxle
cable
Tungsten
rod
(2.5 mm)
BN
spacers
Microwave generator
2.45 GHz; 100 W
Graphite
Furnace tube
end cap

A standard Woodriff furnace heater tube, 30 mm long, 9 mm i.d., was used. However, since this was used as the resonant cavity for the 2450 MHZ microwaves, both ends were fitted with threaded graphite caps. In order to view the plasma, the cap on one end had a slit 2 mm x 4 mm. A hole this small (relative to the radiation wavelength) does not leak significant amounts of radiation. From the wavelength and furnace dimensions that were used, a TE_{111} resonant mode should have been established (117, 118).

Results and Discussions

Two primary requirements had to be fulfilled: (1) Using the double stub tuner, the magnetron-transfer line impedance had to be matched to the furnace impedance to prevent most of the power from being reflected back into the magnetron. (2) A resonant mode of standing waves had to be established and sustained within the hot graphite tube in order to create a high-frequency electric field sufficiently intense to cause breakdown of the argon gas which fills the furnace. These requirements are often difficult to fulfill in systems where high conductivity metals (eg. silver) are plated onto the cavity and cavity configurations have been carefully designed. The system used in this study utilized tungsten coaxle line and a graphite cavity of non-ideal dimensions. The lower electrical conductivity of graphite compared to metals ($\sim$ 100 times lower) also considerably lowers the efficiency of

the cavity (the Q value). Thus, even when efficiently coupled, a larger fraction of the total input power is wasted as heat. However, efficient coupling was never obtained with this system. So much power was reflected that the magnetron dangerously overheated. Repeated shutdowns of the power supply were required during the tuning procedure. Addition of a directional coupler would have protected the magnetron from the reflected power but so much of the total wattage was lost as heat that there wouldn't be sufficient power remaining to generate a plasma. Thus it appeared that, although the system was far from ideal, higher total powers might still accomplish a breakdown. Unfortunately, I was limited to a 100 W magnetron.

Several months later I learned that Koizumi (119) had also been attempting to couple microwaves to a graphite furnace. Using higher power magnetrons, he also was unable to couple microwave energy to the furnace. The feasibility of this route to plasma generation appears low.

REFERENCES

(1) B. V. L'vov, Spectrochim. Acta 17, 761 (1961).

(2) R. Woodriff and J. Ramelow, Spectrochim. Acta 23B, 665 (1968).

(3) B. V. L'vov, Atomic Absorption Spectrochemical Analysis. Hilger, London (1970).

(4) W. M. G. T. van den Broek and L. de Galan, Anal. Chem. 49, 2176 (1977).

(5) W. Slavin and D. C. Manning, Anal. Chem. 51, 261 (1979).

(6) D. C. Manning, W. Slavin and S. Myers, Anal. Chem. 51, 2375 (1979).

(7) S. R. Lawson and R. Woodriff, Spectrochim. Acta 35B, 753 (1980).

(8) S. R. Lawson and R. Woodriff, submitted to Anal. Chem.

(9) C. L. Chakrabarti, C. C. Wan, H. H. Hamed and P. C. Bertels, Anal. Chem. 53, 444 (1981).

(10) H. L. Kahn, M. K. Conley and J. J. Sotera, Am. Lab. 1980, August, 72.

(11) D. D. Siemer and J. Baldwin, Anal. Chem. 52, 295 (1980).

(12) J. Smeyers-Verbeke, Y. Michotte and D. L. Massart, Anal. Chem. 50, 10 (1978).

(13) J. Smeyers-Verbeke, Y. Michotte, P. Van den Winkel and D. L. Massart, Anal. Chem. 48, 125 (1976).

(14) B. V. L'vov, Pure Appl. Chem. 23, 11 (1970).

(15) R. Woodriff, M. Marinkovic and R. A. Howald, Anal. Chem. 49, 2008 (1977).

(16) C. W. Fuller, Analyst 99, 739 (1974).

(17) G. Torsi and G. Tessari, Anal. Chem. 47, 839 (1975).

(18) G. Tessari and G. Torsi, Anal. Chem. 47, 842 (1975).

(19) G. Torsi and G. Tessari, Anal. Chem. 48, 1318 (1976).

(20) R. E. Sturgeon, C. L. Chakrabarti and C. H. Langford, Anal. Chem. 48, 1972 (1976).

(21) W. M. G. T. van den Broek, L. De Galan, J. P. Matousek and E. J. Czobik, Anal. Chim. Acta 100, 121 (1978).

(22) J. Aggett and A. J. Sprott, Anal. Chim. Acta 72, 49 (1974).

(23) R. E. Sturgeon and C. L. Chakrabarti, Anal. Chem. 49, 1100, (1977).

(24) B. Watne, Ph.D. Dissertation, Montana State University, Bozeman, Montana (1977).

(25) L. R. McCreight, H. W. Rauch, Sr., and W. H. Sutton, Ceramic and Graphite Fibers and Whiskers, p. 136, Vol. 1, Academic Press, New York, 1965.

(26) Handbook of Chemistry and Physics, 54th ed., R. C. Weast, Ed., Chemical Rubber Co., Cleveland, Ohio, 1974.

(27) A. S. Darling, G. L. Selman and A. A. Bourne, Platinum Metals Review, 12, 12 (1968).

(28) J. K. Grime and T. J. Vickers, Anal. Chem. 47, 433 (1975).

(29) E. L. Henn, Anal. Chem. 47, 428 (1975).

(30) D. J. Hodges, Analyst 102, 66 (1977).

(31) V. J. Zatka, Anal. Chem. 50, 538 (1978).

(32) T. Stiefel, K. Schulze, G. Tolg and H. Zorn, Anal. Chim. Acta 87, 67 (1976).

(33) K. C. Thompson, K. Wagstaff and K. C. Wheatstone, Analyst 102, 310 (1977).

(34) A. Andersson, Atom. Absorption Newsl. 15, 71 (1976).

(35) E. J. Czobik and J. P. Matousek, Anal. Chem. 50, 2 (1978).

(36) L. Brewer and D. F. Mastick, J. Chem. Phys. 61, 1980 (1957).

(37) D. D. Siemer, R. Woodriff and B. Watne, Appl. Spectrosc. 28, 582 (1974).

(38) R. E. Sturgeon and C. L. Chakrabarti, Progr. Analyt. Atom. Spectrosc. 1, 78 (1978).

(39) V. A. Phillips, Metallography 6, 362 (1973).

(40) F. C. Cowlard and J. C. Lewis, J. of Materials Science 2, 507 (1967).

(41) V. A. Filimonov, Izv. Akad. Nauk. SSSR, Neorg. Mater 9, 2226 (1973).

(42) E. Schroll, Z. Anal. Chem. 198, 40 (1963).

(43) G. Baudin, Progr. Analyt. Atom. Spectrosc., 3, 6 (1980).

(44) B. V. L'vov, Spectrochim. Acta 33B, 153 (1978).

(45) W. French and A. Cedergren, Anal. Chim. Acta 82, 83 (1976).

(46) B. V. L'vov and L. A. Pelieva, Progr. Analyt. Atom. Spectrosc., 3, 65 (1980).

(47) K. Johansson, W. French and A. Cedergren, Anal. Chim. Acta 94, 245 (1977).

(48) J. E. Poldoski, Anal. Chem. 52, 1147 (1980).

(49) J. P. Matousek and K. G. Brodie, Anal. Chem. 45, 1606 (1973).

(50) S. I. Pardham and J. M. Ottaway, Proc. Analyt. Div. Chem. Soc. 12, 291 (1975).

(51) W. French and A. Cedergren, Anal. Chim. Acta 82, 93 (1976).

(52) D. J. Churella and T. R. Copeland, Anal. Chem. 50, 309 (1978).

(53) D. J. Hydes, Anal. Chem. 52, 959 (1980).

(54) J. G. T. Regan and J. Warren, Analyst (London) 103, 447 (1978).

(55) J. W. McLaren and R. C. Wheeler, Analyst (London) 102, 542 (1977).

(56) C. L. Chakrabarti, H. A. Hamed, C. C. Wan, W. C. Li, P. C. Bertels, D. C. Gregoire and S. Lee, Anal. Chem. 52, 167 (1980).

(57) H. Massmann, Spectrochim. Acta 23B, 215 (1968).

(58) M. J. Adams and G. F. Kirkbright, Anal. Chim. Acta 84, 79 (1976).

(59) R. E. Sturgeon and C. L. Chakrabarti, Spectrochim. Acta 32B, 231 (1977).

(60) R. E. Sturgeon, C. L. Chakrabarti and P. C. Bertels, Anal. Chem. 47, 1250 (1975).

(61) W. F. Findlay, A. Zdrojewski and N. Quickert, Spectrosc. Lett. 7, 63 (1974).

(62) R. E. Sturgeon, C. L. Chakrabarti, I. S. Maines and P. C. Bertels, Anal. Chem. 47, 1240 (1975).

(63) W. Slavin, S. A. Meyers and D. C. Manning, Anal. Chim. Acta 117, 267 (1980).

(64) B. V. L'vov, L. A. Pelieva and A. I. Sharnopolsky, Zh. Prikl. Spectroskopiya 27, 395 (1977).

(65) W. Slavin and D. C. Manning, Anal. Chem. 51, 261 (1979).

(66) W. Slavin and D. C. Manning, Spectrochimica Acta 35B, 701 (1980).

(67) C. L. Chakrabarti, C. C. Wan, H. A. Hamed and P. C. Bertels, Anal. Chem. 53, 444 (1981).

(68) L. R. Hageman, J. A. Nichols, P. Viswanadham and R. Woodriff, Anal. Chem. 51, 1406 (1979).

(69) V. P. Borzov, B. V. L'vov and G. V. Plyushch, Zh. Prikl. Spectroskopiya 11, 217 (1969).

(70) R. Woodriff and D. Shrader, Appl. Spectrosc. 27, 181 (1973).

(71) L. Hageman, A. Mubarak and R. Woodriff, Appl. Spectrosc. 33, 226 (1979).

(72) J. A. Holcombe, R. H. Eklund and J. E. Smith, Anal. Chem. 51, 1205 (1979).

(73) H. Howell, Masters Thesis, Montana State University, Bozeman, Montana (1974).

(74) W. French, J-A. Persson and A. Cedergren, Prog. Analyt. Atom. Spectrosc. 3, 279 (1980).

(75) A. Strasheim and H. G. C. Human, Spectrochim. Acta 23B, 265 (1967).

(76) R. Mavordineanu and R. C. Hughes, Appl. Opt. 7, 1281 (1968).

(77) K. W. Jackson, K. M. Aldous and D. G. Mitchell, Spectrosc. Lett. 6, 315 (1973).

(78) J. F. Alder, D. Alger, A. J. Samuel and T. S. West, Anal. Chim. Acta 87, 301 (1976).

(79) J. M. Harnley, T. C. O'Haver, B. Golden and W. R. Wolfe, Anal. Chem. 51, 2007 (1979).

(80) K. Ohls, J. J. Sotera and H. L. Kahn, paper #429, 1980 Pittsburgh Conference.

(81) J. A. Nichols, R. D. Jones and R. Woodriff, Anal. Chem. 50, 2071 (1978).

(82) D. A. Bath, Ph.D. Thesis, Montana State University, Bozeman, Montana, (1975).

(83) Fundamentals of Clinical Chemistry N. W. Tietz, Ed. (W. B. Saunders Co., New York, 1976) pp. 1123.

(84) Ibid., p. 1214.

(85) G. Kirchhoff, Pogg. Ann. d. Physik 109, 275 (1860).

(86) G. Kirchhoff and R. Bunsen, Pogg. Ann. d. Physik 110, 161 (1860).

(87) R. Mavrodineanu and H. Boiteux, Flame Spectroscopy. John Wiley and Sons Inc., New York, 1965.

(88) H. R. Greim, Plasma Spectroscopy (McGraw Hill, New York, 1964).

(89) K. Fuwa and B. Vallee, Anal. Chem. 35, 942 (1963).

(90) G. H. Morrison, R. K. Shogerboe, and A. J. Bedrosian, Appl. Spectrosc. 23, 349 (1969).

(91) M. Marinkovic and B. Dimitrijevic, Spectrochim. Acta 23B, 257

(92) M. Todorovic, V. Vukanovic and B. Georgijevic, Spectrochim. Acta 24B, 571 (1969).

(93) V. Vukanovic, V. Georgijevic, D. Vukanovic and M. Todorovic, Spectrochim. Acta 24B, 555 (1969).

(94) M. Marinkovic and V. G. Antonijevic, Spectrochim. Acta 35B, 129 (1980).

(95) H. Maecker, Z. Physik 129, 108 (1951).

(96) L. E. Owen, Appl. Spectrosc. 15, 150 (1961).

(97) M. Malinek and H. Massmann, Can. Spect. 15, 77 (1970).

(98) S. Greenfield, H. McD. McGeachin and P. B. Smith, Talanta 22, 1, (1975).

(99) S. Greenfield, H. McD. McGeachin and P. B. Smith, Talanta 22, 553, (1975).

(100) E. Badarau, M. Giurgea, Gh. Giurgea and A. T. H. Trutia, Spectrochim. Acta 11, 441 (1957).

(101) R. Mavrodineanu and R. C. Hughes, Spectrochim. Acta 19, 1309 (1963).

(102) C. I. M. Beenakker, Spectrochim. Acta 32B, 173 (1977).

(103) D. J. Kalnicky, V. A. Fassel and R. N. Kniseley, Appl. Spectrosc.

(104) H. G. C. Human and R. H. Scott, Spectrochim. Acta 31B, 459 (1976).

(105) G. R. Kornblum and L. de Galan, Spectrochim. Acta 32B, 71 (1977).

(106) P. W. J. M. Boumans and F. J. De Boer, Spectrochim. Acta 30B, 449 (1975).

(107) J. M. Mermet, Spectrochim. Acta 30B, 383 (1975).

(108) P. W. J. M. Boumans, F. J. de Boer, F. J. Dahmen, H. Hoelzel and A. Meier, Spectrochim. Acta 30B, 449 (1975).

(109) G. Horlick and M. W. Blades, Appl. Spectrosc. 34, 229 (1980).

(110) R. K. Skogerboe and G. N. Coleman, Anal. Chem. 48, 611A (1976).

(111) C. I. M. Beenakker, Spectrochim. Acta 31B, 483 (1976).

(112) C. I. M. Beenakker, Spectrochim. Acta 32B, 173 (1977).

(113) R. C. Hutton, J. M. Ottaway, T. C. Rains and M. S. Epstein, Analyst 102, 429 (1977).

(114) R. E. Sturgeon, S. S. Berman and S. Kashyap, Anal. Chem. 52, 1049 (1980).

(115) C. T. Alkemade, Ph.D. Thesis, University of Utrecht, The Netherlands (1954).

(116) F. W. Hofmann, H. Kohn and J. Schneider, J. Opt. Soc. Am. 51, 508 (1961).

(117) B. McLeod, Private Communication, Montana State University, Dept. of Electrical Engineering (1979).

(118) S. F. Adam, Microwave Theory and Applications, Prentice-Hall, Inc., Englewood Cliffs, New Jersey (1969).

(119) Hadeiki Koizumi, Private Communication, University of California, Berkeley, California.

MONTANA STATE UNIVERSITY LIBRARIES
stks D378.L447
Effect of furnace design on atomic absor RL
3 1762 00118064 3

[redacted]

D378
L447
cop.2

Lawson, S. R.
Effect of furnace design on atomic absorption and emission..

DATE	ISSUED TO

GAYLORD

D378
L447
Cop 2